Chapter 5
Wigner Function Approach

M. Nedjalkov, D. Querlioz, P. Dollfus, and H. Kosina

Abstract The Wigner function formalism has been introduced with an emphasis on basic theoretical aspects, and recently developed numerical approaches and applications for modeling and simulation of the transport of current carriers in electronic structures. Two alternative ways: the historical introduction of the function on top of the operator mechanics, and an independent formulation of the Wigner theory in phase space which then recovers the operator mechanics, demonstrate that the formalism provides an autonomous description of the quantum world.

The conditions of carrier transport in nano-electronic devices impose to extend this coherent physical picture by processes of interaction with the environment. Relevant becomes the Wigner–Boltzmann equation, derived for the case of interaction with phonons and impurities. The numerical aspects focus on two particle models developed to solve this equation. These models make the analogy between classical and Wigner transport pictures even closer: particles are merely classical, the only characteristics which carries the quantum information is a dimensionless quantity – affinity or sign.

The recent ground-breaking applications of the affinity method for simulation of typical nano-devices as the resonant tunneling diode and the ultra-short DG-MOSFET firmly establish the Wigner–Boltzmann equation as a bridge between coherent and semi-classical transport pictures. It became a basic route to understand the nano-device operation as an interplay between coherent and de-coherence phenomena. The latter, due to the environment: phonon field, contacts or defects, attempts to recover the classical transport picture.

Keywords Wigner function · Wigner-Boltzmann equation · Monte Carlo · Quantum particles · De-coherence

M. Nedjalkov (✉)
Institute of Microelectronics, TU Vienna, Vienna, Austria
e-mail: mixi@iue.tuwien.ac.at

D. Vasileska and S.M. Goodnick (eds.), *Nano-Electronic Devices: Semiclassical and Quantum Transport Modeling*, DOI 10.1007/978-1-4419-8840-9_5,

1 Introduction

The Wigner picture of quantum mechanics constitutes a phase space formulation of the quantum theory. Both states and observables are represented by functions of the phase space coordinates. The Weyl transform attributes to any given operator of the wave mechanics a phase space counterpart which is a c-number. Furthermore, the Wigner function is both the phase space counterpart of the density matrix and the quantum counterpart of the classical distribution function. Basic notions of the classical statistical mechanics are retained in this picture. In particular the usual quantities of interest in operator quantum mechanics, i.e. mean values and probabilities, are evaluated in the phase space by rules resembling the formulae of the classical statistics. It is for these reasons that the Wigner function is often considered as a quasi-distribution. The phase space formulation of quantum mechanics has been established historically on top of the operator mechanics [1–3]. In this respect, it is natural to raise the question of whether the Wigner theory can be considered as an equivalent autonomous alternative of the operator mechanics. What outlines classical from quantum behavior in the phase space? In particular how to determine if a given function of the phase space coordinates is a possible quantum or classical state? These questions have been addressed by the inverse approach, which has been explored later [4, 5]. It provides an independent formulation of the Wigner theory and then recovers the operator mechanics, which completes the proof of the logical equivalence between the two theories.

Device modeling needs a conjunction of Wigner quantum mechanics of carrier – potential interactions with other interactions due to the environment. Physical models of the carrier kinetics taking into account the engineering characteristics of the device structure are developed, which are further approached by corresponding numerical methods. Models, algorithms and applications are mutually developed within the Wigner transport picture. This work is an effort to give a self-contained overview of the basic notions, and to point at some recent results in the field. Further details and a presentation of the recent advances can be found in [66].

We feel that here is the place to acknowledge the work of W. Frensley, D. K. Ferry and co-authors, C. Jacoboni and the Modena group and other important contributions, which are frequently cited in the sequel.

In the next section we will introduce the Wigner quantum mechanics by following the historical approach. Some concepts of statistical mechanics and Hermitian operators are recalled in a way to outline the mutual relationship between the classical and quantum counterparts. The operator ordering is discussed: actually there are alternative phase space formulations of the quantum mechanics which are associated with alternative ordering prescriptions. A particular ordering given by the Weyl transform introduces the Wigner function. The corresponding evolution equation is a central entity in this approach. The presented detailed derivation of the Wigner equation is based on the von Neumann equation for the density matrix. Fundamental concepts of the picture are discussed along with the characteristics of pure and mixed state Wigner functions.

We believe that it is important to introduce in parallel some basic notions of the inverse approach. Conditions determining whether a given phase space function is

a possible quantum state are presented. Explicit expressions exist which associate to given phase space pure or mixed quantum state the corresponding wave function or density matrix. Results which establish the equivalence between the operator and Wigner quantum mechanics are summarized. Behind the abstract mathematical aspects, these results allow to understand and solve practical for semiconductor device community problems, encountered when bound states exist in the physical system.

A strong advantage of the Wigner formalism of quantum transport is its ability to include all relevant scattering mechanisms. Though the full quantum treatment of scattering is difficult to apply to practical situations, namely for the description of transport in realistic devices, it is shown that under some reasonable approximations, such as the fast and weak scattering limits, the Wigner collision operator simplifies into the well-known Boltzmann collision operator. This is demonstrated in Sect. 3 for the case of electron–phonon and electron–ionized impurity interactions. The Wigner transport equation thus reduces to the so-called Wigner–Boltzmann equation. In the latter form, the transport equation becomes very convenient for device simulation. It can benefit from all the knowledge acquired for many years in semi-classical device physics and especially in the physics of scattering.

Furthermore we show that the analogy between classical and Wigner transport pictures become even closer. Particle models are associated with the Wigner-quantum transport in Sect. 4. The Wigner potential is interpreted as a source which, in addition to the common classical parameters, associates to each particle a new dimensionless quantity which, depending on the model, could be affinity or sign. This quantity is the only characteristic carrying the quantum information for the system. It is taken into account in the computation of the physical averages.

Two numerical techniques of Monte Carlo device simulation are described in Sect. 4. They may be seen as a generalization of the well-known Monte Carlo method for semi-classical device simulation.

Finally, in Sect. 5, the device simulation is applied to some typical nano-devices, namely the resonant tunneling diode (RTD) and the ultra-short double-gate (DG) metal-oxide-semiconductor field-effect transistor (MOSFET). Quantum and de-coherence effects taking place in these are emphasized.

The occurrence of quantum de-coherence in devices of a size smaller than the electron wave length and mean free path is becoming an important subject of experimental and theoretical research [6–9]. The theory of de-coherence has shown that the semi-classical behavior of a quantum system may emerge from the interaction with its environment. For electrons in a nano-device, the environment likely to induce de-coherence may be the phonon field, the contacts or defects.

In this final section the theory of de-coherence is briefly introduced through an academic example of the free evolution of a Gaussian wave packet and the phonon scattering-induced de-coherence is investigated in a typical nano-device, the RTD. The Wigner–Boltzmann formalism is proved to be an appropriate framework for such analysis [10]. One of its major advantage lies in the fact that it offers a straightforward access to the off-diagonal elements of the density matrix which provides a clear visualization of de-coherence phenomena.

The Wigner–Boltzmann equation may also become – in establishing a link between semi-classical and quantum transport – a ground-breaking route to understanding nano-device behavior. We focus in particular on the case of the ultra-small DG-MOSFET with gate length of 6 nm through comparison between quantum (Wigner–Boltzmann) and semi-classical simulations. Beyond the analysis of direct source-drain tunneling and quantum reflections on the steep potential drop at the drain-end of the channel, the results emphasize the role of scattering which remains surprisingly important in such a small device in spite of significant quantum coherence effects.

2 Wigner Quantum Mechanics

2.1 Classical Distribution Function

A single particle of mass m is considered to move with a potential energy $V(x)$. The phase space is defined by the Cartesian product of the particle position x and momentum p. Physical quantities are dynamical functions $A(x,p)$ of the phase space coordinates, such as the kinetic and potential energies and their sum giving the Hamiltonian $H(x,p)$. The state of the single particle at given time is presented by a point in the phase space. Provided that the initial particle coordinates are known, the novel coordinates $x(t), p(t)$ at time t are obtained from the Hamilton equations

$$\dot{x} = \frac{\partial H(x,p)}{\partial p} = \frac{p}{m}; \qquad \dot{p} = -\frac{\partial H(x,p)}{\partial x} = -\frac{\partial V(x)}{\partial x} \tag{5.1}$$

The function $A(t)$ describes how physical quantities change in time. Two ways are possible: (a) $A(t) = A(x(t), p(t))$ is the old function in the novel coordinates; (b) $A(t) = A(t,x,p)$ is a new function of the old coordinates. In the first case we postulate that the laws of mechanics do not change with time: A remains the same function for the old and the new coordinates. Then, with the help of (5.1) we obtain the equation of evolution for A:

$$\dot{A} = \frac{\partial A(x,p)}{\partial x}\frac{\partial H(x,p)}{\partial p} - \frac{\partial A(x,p)}{\partial p}\frac{\partial H(x,p)}{\partial x} = [A,H]_P; \qquad [x,p]_P = 1 \tag{5.2}$$

A basic notion between the dynamical functions is endowed with the Poisson bracket $[\cdot,\cdot]_P$. It gives rise to an automorphic (conserving the algebraic structure) mapping of the set of such functions.

Alternatively, in the second case we have to postulate a law for the evolution of $A(t,x,p)$. If it is imposed according to (5.2), the automorphism consistently leads to the conservation of the mechanical laws: the new function in the old coordinates is the old function in the novel coordinates: $A(t,x,p) = A(x(t), p(t))$!

A statistical description is introduced if the coordinates of the point cannot be stated exactly, but with some probability. According to the basic postulate of

classical statistical mechanics, the state of the particle system is completely specified by a function $f(x,p)$, with the following properties:

$$f(x,p) \geq 0 \qquad \int dxdpf(x,p) = 1 \tag{5.3}$$

Physical quantities A are then described by the corresponding mean values:

$$\langle A \rangle(t) = \int dxdpA(t,x,p)f(x,p) \tag{5.4}$$

This equation is not convenient since it requires calculation of the evolution of any particular quantity A. However, due to the automorphism of the Poisson bracket, it is possible to change the variables so that time is transferred to the distribution function f [11]. Equation (5.4) modifies to:

$$\langle A \rangle(t) = \int dxdpA(x,p)f(x,p,t) \tag{5.5}$$

The evolution equation for f can be derived with the help of (5.1) and (5.2):

$$\left(\frac{\partial}{\partial t} + \frac{p}{m}.\frac{\partial}{\partial x} + F(x)\frac{\partial}{\partial p}\right) f(x,p,t) = \left(\frac{\partial f}{\partial t}\right)_c \tag{5.6}$$

Here the force $F = -\nabla_x V$ is given by the derivative of the potential energy V. The characteristics of the differential operator in the brackets, called Liouville operator, are classical Newton's trajectories, obtained from (5.1). Over such trajectories the left hand side of (5.6) becomes a total time derivative. In the case of no interaction with the environment, $\left(\frac{\partial f}{\partial t}\right)_c = 0$, i.e. trajectories carry a constant value of f. Otherwise the particles are redistributed between the trajectories and the right hand side of (5.6) is equal to the net change of the particle density due to collisions. In the rest of this section we derive a quantum analog of (5.3), (5.5) and the Boltzmann equation (5.6).

2.2 Quantum Operators

We recall the principles of the operator quantum mechanics, which will be used to reformulate the formalism in the phase space. Physical quantities in quantum mechanics are presented by Hermitian operators $\hat{A}$:

$$\hat{A}|\phi_n\rangle = a_n|\phi_n\rangle; \quad \langle\phi_n|\phi_m\rangle = \delta_{mn} \qquad \sum_n |\phi_n\rangle\langle\phi_n| = \hat{1} \tag{5.7}$$

Such operators have real eigenvalues and a complete system of orthonormal eigenvectors which form an abstract Hilbert space. The states of the system are specified by the elements $|\Psi_t\rangle$ of the Hilbert space $\mathscr{H}$ which are square integrable and normalized with respect to the L_2 norm in $\mathscr{H}$. In wave mechanics it is postulated that the evolution of $|\Psi_t\rangle$ is provided by the Schrödinger equation

$$\hat{H}|\Psi_t\rangle = i\hbar\frac{\partial|\Psi_t\rangle}{\partial t} \qquad \langle\Psi_t|\Psi_t\rangle = 1 \qquad |\Psi_t\rangle = \sum_n c_n(t)|\phi_n\rangle \tag{5.8}$$

The state can be decomposed in the complete basis of an observable A. Also, it can be shown that during the evolution the state remains normalized. This property is often called conservation of probability.

According to the correspondence principle, to classical position and momentum variables correspond the Hermitian operators $\hat{x}$ and $\hat{p}$, satisfying a quantum counterpart of the Poisson bracket:

$$x \rightarrow \hat{x} \qquad p \rightarrow \hat{p} \qquad \hat{x}\hat{p} - \hat{p}\hat{x} = [\hat{x}, \hat{p}]_{-} = i\hbar\hat{1} \tag{5.9}$$

Wave mechanics uses only half of the phase space – coordinate or momentum representation – for the description of the physical system. We assume a coordinate representation; according to (5.7) and (5.9) it holds that

$$\hat{x}|x\rangle = x|x\rangle \qquad \int dx|x\rangle\langle x| = \hat{1} \qquad \hat{p} = -i\hbar\frac{\partial}{\partial x} \tag{5.10}$$

Finally, we recall the equation for the averaged value of a physical quantity:

$$\langle A\rangle(t) = \langle \Psi_t|\hat{A}|\Psi_t\rangle = \int dx\langle \Psi_t|x\rangle\langle x|\hat{A}|\Psi_t\rangle \tag{5.11}$$

The operator formulation of the quantum mechanics looks too abstract when compared to the familiar classical concepts. Nevertheless it is possible to reformulate the ideas of the quantum mechanics in the phase space. The first step is to evaluate the actual number of variables involved in (5.11). With the help of (5.7) and (5.10) it holds:

$$\langle x|\hat{A}|\Psi_t\rangle = \int dx' \sum_n a_n \langle x|\phi_n\rangle\langle\phi_n|x'\rangle\langle x'|\Psi_t\rangle = \int dx' \alpha(x,x')\Psi_t(x')$$

where $\Psi_t(x) = \langle x|\Psi_t\rangle$. A substitution in (5.11) shows that the physical average is actually evaluated in a "double half" of the phase space:

$$\langle A\rangle(t) = \int dx' \int dx \alpha(x,x')\rho_t(x',x) = Tr(\hat{\rho}_t\hat{A}) \tag{5.12}$$

with ρ_t and $\hat{\rho}_t$ the density matrix and density operator:

$$\rho_t(x,x') = \Psi_t^*(x')\Psi_t(x) = \langle x|\Psi_t\rangle\langle\Psi_t|x'\rangle = \langle x|\hat{\rho}_t|x'\rangle \qquad \rho_t = \sum_{m,n} c_m^*(t)c_n(t)|\phi_n\rangle\langle\phi_m| \tag{5.13}$$

2.3 Weyl Transform

Equation (5.12) resembles (5.5) provided that one of the spatial variables is replaced by a momentum variable. A proper transform for such a replacement is needed. The important consequence is that the transformed density matrix can be interpreted as

the quantum counterpart of the classical distribution function. Pursuing a proper rule, we consider how an operator $\hat{A}$ can be associated to a given physical quantity. $\hat{A}$ can be obtained explicitly with the help of (5.9) and the knowledge of $A(x,p)$: the Taylor expansion, for example, can be used to establish the rule:

$$A(x,p)=\sum_{i,j} b_{i,j}x^i p^j \quad \rightarrow \quad A(\hat{x},\hat{p})=\sum_{i,j} b_{i,j}\hat{x}^i\hat{p}^j$$

For the Hamiltonian of a particle in a potential field, $H(x,p)=\frac{p^2}{2m}+V(x)$, this rule leads to a consistent result. However, for general functions A the procedure is not well defined, since the operators $\hat{p}$ and $\hat{x}$ do not commute. First, non-Hermitian operators can appear. Second, even for Hermitian operators there is ambiguity in the correspondence: let us consider two equivalent expressions for the function $A(x,p)$:

$$A_1=px^2p=A_2=\frac{1}{2}(p^2x^2+x^2p^2)$$

The substitution of x and p by $\hat{x}$ and $\hat{p}$ gives rise to the following operators:

$$A_1\rightarrow\hat{A}_1=\hat{p}\hat{x}^2\hat{p} \qquad A_2\rightarrow\hat{A}_2=\frac{1}{2}(\hat{p}^2\hat{x}^2+\hat{x}^2\hat{p}^2)$$

Now, while $A_1=A_2$, the obtained operators differ by $\hbar^2$: $\hat{A}_1=\hat{A}_2+\hbar^2$. The example shows how different operator functions are mapped into the same function of the phase space coordinates: the relation (5.9) is not sufficient to establish a unique correspondence between A and $\hat{A}$. A certain rule must be applied in order to remove this ambiguity. We will make use of the fact that an arbitrary function $f(x,p)$ can be obtained from the generating function $F(s,q)=e^{i(sx+qp)}$ as follows:

$$f(x,p)=f\left(\frac{1}{i}\nabla_s,\frac{1}{i}\nabla_q\right)F(s,q)_{s=0,q=0}=\frac{1}{(2\pi)^2}\int dsdqdldmf(l,m)e^{-i(ls+mq)}F(s,q)$$

It remains to consider possible operator generalizations of F, e.g.

$$\hat{F}_1=e^{i(s\hat{x})}e^{i(q\hat{p})}; \qquad \hat{F}_2=e^{i(q\hat{p})}e^{i(s\hat{x})}; \qquad e^{i(s\hat{x}+q\hat{p})}$$

which represent the standard order where the positions precede the momenta, the anti-standard order, where the momenta come before the positions, and the Weyl order. The fully symmetric Weyl order bears some of the basic properties of a characteristic function of a probability distribution [4] and will be used henceforth to establish the rule of correspondence. The choice of alternative orders leads to alternative quasi-distributions. It should be noted that once postulated, the correspondence rule must be consistently applied to all notions of the operator mechanics in order to ensure conservation of the values of the physical averages (5.11). The Weyl transform reads:

$$A(x,p)=W(\hat{A}(\hat{x},\hat{p}))=\frac{\hbar}{(2\pi)}\int dsdqTr\left(\hat{A}(\hat{x},\hat{p})e^{i(s\hat{x}+q\hat{p})}\right)e^{-i(sx+qp)} \qquad (5.14)$$

Equivalently, as discussed in the appendix, it holds:

$$\hat{A} = \hat{A}(\hat{x},\hat{p}) = \int dsdq\beta(s,q)e^{i(s\hat{x}+q\hat{p})} \tag{5.15}$$

Here β is adjoint to A via the Fourier transform:

$$A(x,p) = \int dsdq\beta(s,q)e^{i(sx+qp)} \qquad \beta(s,q) = \frac{1}{(2\pi)^2}\int dxdpA(x,p)e^{-i(sx+qp)} \tag{5.16}$$

The Wigner function is defined as the transform of the density operator, multiplied by the normalization factor $(2\pi\hbar)^{-1}$. The Weyl map W provides the algebra of phase space functions with a non-commutative *-product defined as:

$$W(\hat{A}) * W(\hat{B}) = A(x,p) * B(x,p) = W(\hat{A}\ \hat{B}) \tag{5.17}$$

Basic notions of the operator quantum mechanics are formulated in the phase space with the help of the *-product.

2.4 Wigner Function for Pure State

Equation (5.8) and its adjoint equation give rise to the von Neumann equation of motion for the pure state density matrix ρ_t (5.13).

$$\begin{aligned} i\hbar\frac{\partial\rho(x,x',t)}{\partial t} &= \langle x|[\hat{H},\hat{\rho}_t]_-|x'\rangle \\ &= \left\{-\frac{\hbar^2}{2m}\left(\frac{\partial^2}{\partial x^2}-\frac{\partial^2}{\partial x'^2}\right)+\big(V(x)-V(x')\big)\right\}\rho(x,x',t) \end{aligned} \tag{5.18}$$

The variables are changed with the help of a center of mass transform:

$$x_1 = (x+x')/2, \quad x_2 = x-x'$$

$$\begin{aligned} &\frac{\partial\rho(x_1+x_2/2,x_1-x_2/2,t)}{\partial t} \\ &= \frac{1}{i\hbar}\left\{-\frac{\hbar^2}{m}\frac{\partial^2}{\partial x_1\partial x_2}+(V(x_1+x_2/2)-V(x_1-x_2/2))\right\}\rho(x_1+x_2/2,x_1-x_2/2,t) \end{aligned} \tag{5.19}$$

As shown in the appendix, the Wigner function is obtained by Fourier transform with respect to x_2:

$$f_w(x_1,p,t) = \frac{1}{(2\pi\hbar)}\int dx_2\rho(x_1+x_2/2,x_1-x_2/2,t)e^{-ix_2.p/\hbar} \tag{5.20}$$

We note that, due to the Wigner transform, x_1 and p are independent variables. It is easy to show that the corresponding operators commute. Thus x_1 and p define a phase space – the Wigner phase space.

The Fourier transform of the right hand side of (5.19) gives rise to two terms which are evaluated as follows. It is convenient to introduce the abbreviation $\rho(+,-,t)$ for $\rho(x_1+x_2/2, x_1-x_2/2, t)$:

$$I = -\frac{1}{i\hbar}\frac{\hbar^2}{m(2\pi\hbar)}\int dx_2 e^{-ix_2.p/\hbar}\frac{\partial^2\rho(+,-,t)}{\partial x_1\partial x_2}$$

$$= -\frac{1}{m(2\pi\hbar)}p.\frac{\partial}{\partial x_1}\int dx_2 e^{-ix_2.p/\hbar}\rho(+,-,t) = -\frac{1}{m}p.\frac{\partial f_w(x_1,p,t)}{\partial x_1}$$

where we have integrated by parts and used the fact that the density matrix tends to zero at infinity: $\rho \to 0$ if $x_2 \to \pm\infty$.

$$II = \frac{1}{i\hbar(2\pi\hbar)}\int dx_2 e^{-ix_2.p/\hbar}(V(x_1+x_2/2)-V(x_1-x_2/2))\rho(+,-,t)$$

$$= \frac{1}{i\hbar(2\pi\hbar)}\int dx_2\int dx' e^{-ix_2.p/\hbar}(V(x_1+x_2/2)-V(x_1-x_2/2))$$

$$\times\,\delta(x_2-x')\rho(x_1+x'/2, x_1-x'/2, t)$$

After a substitution of the delta function with the integral

$$\delta(x_2-x') = \frac{1}{(2\pi\hbar)}\int dp' e^{i(x_2-x')p'/\hbar}. \tag{5.21}$$

the following is obtained:

$$II = \frac{1}{i\hbar(2\pi\hbar)}\int dp'\int dx_2 e^{-ix_2.(p-p')/\hbar}(V(x_1+x_2/2)-V(x_1-x_2/2))$$

$$\times\,\frac{1}{(2\pi\hbar)}\int dx' e^{-ix'p'/\hbar}\rho(x_1+x'/2, x_1-x'/2, t)$$

$$= \int dp' V_w(x_1, p-p') f_w(x_1, p', t)$$

We summarize the results of these transformations. Equation (5.19) gives rise to the Wigner equation:

$$\frac{\partial f_w(x,p,t)}{\partial t} + \frac{p}{m}.\frac{\partial f_w(x,p,t)}{\partial x} = \int dp' V_w(x, p-p') f_w(x, p', t) \tag{5.22}$$

where V_w is the Wigner potential.

$$V_w(x,p) = \frac{1}{i\hbar(2\pi\hbar)} \int dx' e^{-ix'p/\hbar} (V(x+x'/2) - V(x-x'/2)) \tag{5.23}$$

A change of the sign of x' reveals the antisymmetry of the Wigner potential.

2.5 Properties of the Wigner Function

We first outline the equivalence between the Schrödinger equation and the Wigner equation in the case of a pure state. From Ψ_t we can obtain ρ and thus f_w. The opposite is also true: it can be shown that, if we know f_w we can obtain Ψ_t up to a phase factor.

Comparing this with the Boltzmann equation (5.6), we can recognize on the left hand side of the Wigner equation the field-less Liouville operator. Furthermore, it is easy to see that the Wigner potential is a real quantity, $V_w = V_w^*$. It follows that, being a solution of an equation with real coefficients, f_w is real. The Wigner function conserves the probability in time:

$$\int dx \int dp f_w(x,p,t) = \int dx \int dx_2 \rho(x+x_2/2, x_1 - x_2/2, t)\delta(x_2) = \int dx \langle x|\hat{\rho}_t|x\rangle = 1 \tag{5.24}$$

In a similar way it can be demonstrated that the position or momentum probability distributions are obtained after integration over momentum p or position x respectively:

$$\int dp f_w(x,p,t) = |\Psi_t(x)|^2 \qquad \int dx f_w(x,p,t) = |\Psi_t(p)|^2 \tag{5.25}$$

The most important property of the Wigner picture is that the mean value $\langle A\rangle(t)$ of any physical quantity is given by

$$\langle A\rangle(t) = \int dx \int dp f_w(x,p,t) A(x,p) \tag{5.26}$$

where $A(x,p)$ is the classical function (5.16). This is proven in the appendix.

Our goal to derive a quantum analog of (5.3), (5.5) and (5.6) has been attained to a large extent. Equation (5.24) corresponds to the second equation in (5.3) and the Wigner function is real. Equation (5.26) is equivalent to (5.5). The left hand sides of the Wigner equation (5.22) and the Boltzmann equation are given by the Liouville operator. Classical and quantum pictures become very close.

Nevertheless, there are basic differences. The Wigner function allows negative values and thus is not a probability function. It cannot be interpreted as a joint distribution of particle position and momentum. Actually, the Wigner function can have

nonzero values in domains where the particle density is zero. As follows from (5.25), a physical interpretation is possible only after an integration.

The quantum character of the Wigner function is underlined by the following remarkable result. If the spectrum of $\hat{A}$, (5.7), is non-degenerate, then the corresponding to an eigenvector Wigner function $f_{w(n)} = (2\pi\hbar)^{-1}W(|\phi_n\rangle\langle\phi_n|)$ satisfies the following equation:

$$f_{w(n)}(x,p) * A(x,p) = a_n f_{w(n)}(x,p); \quad A(x,p) * f_{w(n)}(x,p) = a_n f_{w(n)}(x,p) \tag{5.27}$$

The probability P that a measurement of the observable corresponding to a given generic operator $\hat{A}$ yields the value a_n in a state $f_w(x,p,t)$ is:

$$P(a_n) = (2\pi\hbar)\int dxdp f_w(x,p,t) f_{w(n)}(x,p) \tag{5.28}$$

2.6 Classical Limit of the Wigner Equation

We discuss the classical limit of (5.22) by considering the case when the potential V is a linear or a quadratic function of the position:

$$V\left(x \pm \frac{x'}{2}\right) = V(x) \pm \frac{\partial V(x)}{\partial x}\frac{x'}{2} + \cdots = V(x) \mp F(x)\frac{x'}{2} + \cdots$$

where the dots stand for the quadratic term. The force F can be at most a linear function of the position. As the even terms of the Taylor expansion of V cancel in (5.23), the Wigner potential becomes:

$$V_w(x,p) = \frac{i}{\hbar(2\pi\hbar)}\int dx' e^{-ix'p/\hbar}F(x)x'$$

The right hand side of (5.22) becomes

$$\begin{aligned}\int dp' V_w(x,p-p')f_w(x,p',t) &= \frac{i}{\hbar(2\pi\hbar)}\int dp'\int dx' e^{-ix'(p-p')/\hbar}F(x)x' f_w(x,p',t)\\ &= \frac{-F(x)}{(2\pi\hbar)}\frac{\partial}{\partial p}\int dp'\int dx' e^{-ix'(p-p')/\hbar} f_w(x,p',t)\\ &= -F(x)\frac{f_w(x,p,t)}{\partial p}\end{aligned} \tag{5.29}$$

where we have used the equality $ix' e^{-ix'(p-p')/\hbar} = -\hbar\frac{\partial}{\partial p}e^{-ix'(p-p')/\hbar}$. Then the Wigner equation reduces to the collisionless Boltzmann equation:

$$\frac{\partial f_w(x,p,t)}{\partial t} + \frac{p}{m}.\frac{\partial f_w(x,p,t)}{\partial x} + F(x)\frac{\partial f_w(x,p,t)}{\partial p} = 0 \tag{5.30}$$

Now consider as an initial condition a minimum uncertainty wave-packet. The Wigner function of such a packet is a Gaussian of both position and momentum [12]. The latter can equally well be interpreted as an initial distribution of classical electrons. Provided that the force is a constant or linear function of the position, the packet evolves according to (5.30). The evolution resembles that of the classical distribution. Despite the spread in the phase space, the Gaussian components determine the general shape of the packet. f_w remains positive during the evolution.

However, stronger variations of the field with position introduce interference effects. Near band offsets the packet rapidly looses its shape and negative values appear.

2.7 Wigner Potential and Fourier Transform

In this section we discuss some properties of the Wigner potential in terms of the Fourier transform. For this purpose we express the momentum p through the wave number k as $p = \hbar k$. We introduce $\hat{V}(q)$, the Fourier transform of the potential. The Fourier transform and its inverse read

$$\hat{V}(q) = \int \mathrm{d}x V(x) \mathrm{e}^{-iqx}, \qquad V(x) = \frac{1}{2\pi} \int \mathrm{d}q \hat{V}(q) \mathrm{e}^{iqx}. \tag{5.31}$$

The result of the Fourier transform is in general a complex function, which can be expressed in polar form by its modulus and phase.

$$\hat{V}(q) = A(q) \mathrm{e}^{i\varphi(q)} \tag{5.32}$$

With the variable substitutions $s = x \pm x'/2$ the integrals in the definition (5.23) of the Wigner potential can be evaluated as

$$\int \mathrm{d}x' V\left(x + \frac{x'}{2}\right) \mathrm{e}^{-ikx'} = 2\mathrm{e}^{2ikx} \int \mathrm{d}s V(s) \mathrm{e}^{-2iks} = 2\mathrm{e}^{2ikx} \hat{V}(2k),$$

$$\int \mathrm{d}x' V\left(x - \frac{x'}{2}\right) \mathrm{e}^{-ikx'} = \left[2\mathrm{e}^{2ikx} \hat{V}(2k)\right]^*,$$

and the following relation between the Wigner potential (5.23) and the Fourier transform of the potential can be established.

$$V_{\mathrm{w}}(x, \hbar k) = \frac{1}{i\hbar(2\pi\hbar)} \left\{ 2\mathrm{e}^{2ikx} \hat{V}(2k) - \left[2\mathrm{e}^{2ikx} \hat{V}(2k)\right]^* \right\}$$

This expression can be simplified using the polar form (5.32).

$$V_{\mathrm{w}}(x, \hbar k) = \frac{2}{\pi\hbar^2} A(2k) \sin[\varphi(2k) + 2kx] \tag{5.33}$$

The x-dependence of the Wigner potential is given analytically by an undamped sine function, independent of the actual shape of the potential. This result also shows, that even for a well localized potential barrier the Wigner potential is fully delocalized in the coordinate space. In any numerical procedure, therefore, the Wigner potential needs to be truncated at some finite x-coordinate.

Another property of the Wigner potential can be derived by considering the function

$$\Delta(x,x') = V\left(x+\frac{x'}{2}\right) - V\left(x-\frac{x'}{2}\right). \tag{5.34}$$

The Wigner potential is defined as the Fourier transform of this function with respect to the argument x'. We note that

$$\Delta(x,-x') = -\Delta(x,x'). \tag{5.35}$$

Due to this antisymmetry, the substitution $\exp(-ikx') = \cos(kx') - i\sin(kx')$ in (5.23) readily yields the Fourier sine transform.

$$\begin{aligned} V_{\mathrm{w}}(x,\hbar k) &= \frac{1}{i\hbar(2\pi\hbar)}\int \mathrm{d}x'\,\Delta(x,x')\mathrm{e}^{-ikx'} \\ &= -\frac{1}{\hbar(2\pi\hbar)}\int \mathrm{d}x'\,\Delta(x,x')\sin(kx') \end{aligned} \tag{5.36}$$

In general the potential $V(x)$ is given within a finite simulation domain, representing, for instance, the active region of an electronic device. Outside of this domain the potential is continued by two constants, say V_L and V_R. This situation represents an active device region connected to semi-infinite leads on both sides, where the leads are assumed to be ideal conductors. Therefore, in practical cases Δ will have the asymptotic behavior,

$$\lim_{x'\to\pm\infty}\Delta(x,x') = \mp(V_L - V_R) \tag{5.37}$$

where $(V_L - V_R)$ is the potential difference between the left and the right lead. Since the integrand in (5.36) does not vanish at infinity, the Fourier integral will diverge at $q = 0$. From the asymptotic behavior of $\Delta(x,x')$ for $x' \to \infty$ we find the asymptotic behavior of $V_{\mathrm{w}}(x,\hbar k)$ for $k \to 0$.

$$\Delta(x,x') \simeq (V_R - V_L)\mathrm{sgn}(x'), \qquad x' \to \infty \tag{5.38}$$

$$V_{\mathrm{w}}(x,\hbar k) \simeq \frac{2(V_L - V_R)}{\hbar(2\pi\hbar)}\mathscr{P}\frac{1}{k}, \qquad k \to 0 \tag{5.39}$$

Here, sgn denotes the signum function and $\mathscr{P}$ the principal value. This consideration shows that if the potential difference is nonzero, there will be a pole in the Wigner potential at $k = 0$. Numerical methods for the Wigner equation generally use a k-space discretization, where the discrete k-points are located symmetrically around the origin and the point $k = 0$ is not included. In this way, no particular treatment of the singularity is needed.

2.8 Classical Force

The potential operator in (5.22) takes the form

$$Qf_{\mathrm{w}}(x,p) = \hbar \int \mathrm{d}q\, V_{\mathrm{w}}(x,\hbar q) f_{\mathrm{w}}(x,p-\hbar q), \tag{5.40}$$

if variables are changed according to $p - p' = \hbar q$. To deal with the singularity of V_{w}, one can define a small neighborhood around $q = 0$ and split the domain of integration as follows [13].

$$Qf_{\mathrm{w}}(x,p) \quad = \int\limits_{|q|\le q_{\mathrm{c}}/2} + \int\limits_{|q|>q_{\mathrm{c}}/2} = Q_{cl} f_{\mathrm{w}} + Q_{qm} f_{\mathrm{w}} \tag{5.41}$$

Here q_{c} is some small wave number. In this way, we have split the potential operator Q in two parts, which we refer to as Q_{cl} and Q_{qm}. A linearization can be introduced in the integral over the small wave numbers.

$$Q_{cl} f_{\mathrm{w}}(x,p,t) = \hbar \int\limits_{|q|\le q_{\mathrm{c}}/2} \mathrm{d}q\, V_{\mathrm{w}}(x,\hbar q) f_{\mathrm{w}}(x,p-\hbar q) \tag{5.42}$$

$$\simeq \hbar \int\limits_{|q|\le q_{\mathrm{c}}/2} \mathrm{d}q\, V_{\mathrm{w}}(x,\hbar q) \left[f_{\mathrm{w}}(x,p) - \hbar q \frac{\partial f_{\mathrm{w}}(x,p)}{\partial p} \right] \tag{5.43}$$

$$= -\frac{\partial f_{\mathrm{w}}(x,p)}{\partial p} \hbar^2 \int\limits_{|q|\le q_{\mathrm{c}}/2} \mathrm{d}q\, q V_{\mathrm{w}}(x,\hbar q) \tag{5.44}$$

In the second line the integral over f_{w} vanishes since V_{w} is an odd function in q. Substituting (5.33) into (5.44) gives

$$\begin{aligned}
-\hbar^2 \int\limits_{|q|\le q_{\mathrm{c}}/2} \mathrm{d}q\, q V_{\mathrm{w}}(x,\hbar q) &= -\frac{2}{\pi} \int_{-q_{\mathrm{c}}/2}^{q_{\mathrm{c}}/2} \mathrm{d}q\, qA(2q) \sin\left[\varphi(2q) + 2qx\right] \\
&= -\frac{1}{2\pi} \int_{-q_{\mathrm{c}}}^{q_{\mathrm{c}}} \mathrm{d}q\, qA(q) \sin\left[\varphi(q) + qx\right] \\
&= \frac{\partial}{\partial x} \frac{1}{2\pi} \int_{-q_{\mathrm{c}}}^{q_{\mathrm{c}}} \mathrm{d}q\, A(q) \cos\left[\varphi(q) + qx\right] \\
&= \frac{\partial}{\partial x} \Re\left\{ \frac{1}{2\pi} \int_{-q_{\mathrm{c}}}^{q_{\mathrm{c}}} \mathrm{d}q\, A(q) \mathrm{e}^{i\varphi(q)} \mathrm{e}^{iqx} \right\} \\
&= \frac{\partial}{\partial x} \Re\left\{ \frac{1}{2\pi} \int_{-q_{\mathrm{c}}}^{q_{\mathrm{c}}} \mathrm{d}q\, \hat{V}(q) \mathrm{e}^{iqx} \right\} \\
&= \frac{\partial}{\partial x} V_{\mathrm{cl}}(x)
\end{aligned}$$

Here we introduced the classical potential component as

$$V_{\mathrm{cl}}(x) = \frac{1}{2\pi}\int_{-q_{\mathrm{c}}}^{q_{\mathrm{c}}} \mathrm{d}q\,\hat{V}(q)\mathrm{e}^{iqx}. \tag{5.45}$$

This function is real, as can be easily shown by substituting $\hat{V}(q)$.

$$V_{\mathrm{cl}}(x) = \frac{1}{2\pi}\int_{-q_{\mathrm{c}}}^{q_{\mathrm{c}}} \mathrm{d}q \int \mathrm{d}y V(y)\mathrm{e}^{iq(x-y)} = \int dy V(y)\frac{\sin[q_{\mathrm{c}}(x-y)]}{\pi(x-y)} \tag{5.46}$$

So we have a convolution of two real functions, the potential $V(x)$ and the $\sin(x)/x$ function.

According to its definition (5.45), the classical potential component shows a smooth spatial variation, as it is composed of long-wavelength Fourier components only. Equation (5.45) motivates the following spectral decomposition of the potential profile into a slowly varying, classical component (5.45) and a rapidly varying, quantum mechanical component.

$$V(x) = V_{\mathrm{cl}}(x) + V_{\mathrm{qm}}(x) \tag{5.47}$$

When the linearization described above is introduced in the classical component, this decomposition yields a Wigner equation including both a local classical force term and a nonlocal potential operator.

$$\left(\frac{\partial}{\partial t} + \frac{p}{m}\frac{\partial}{\partial x} - \frac{\partial V_{\mathrm{cl}}(x)}{\partial x}\frac{\partial}{\partial p}\right) f_{\mathrm{w}}(x,p,t) = \int \mathrm{d}p' V_{\mathrm{w}}^{\mathrm{qm}}(x,p') f_{\mathrm{w}}(x,p-p',t) \tag{5.48}$$

The Wigner potential is calculated from the quantum mechanical potential component, $V_{\mathrm{qm}} = V - V_{\mathrm{cl}}$. The two potential components have the following properties. The classical component accommodates the applied voltage. As it is treated through a classical force term, it does not induce any quantum reflections. The quantum mechanical component vanishes at infinity and has a smooth Fourier transform.

2.9 Quantum Statistics

The density operator $\hat{\rho}_t = |\Psi_t\rangle\langle\Psi_t|$, used to obtain the Wigner function, corresponds to a system in a pure state. The state of the system is often not known exactly. Assuming that a set of possible states $\hat{\rho}_t^i$ can be occupied with probabilities γ_i, the definition (5.13) of density operator can be generalized for a mixed state:

$$\hat{\rho}_t = \sum_i \gamma_i \hat{\rho}_t^i \qquad \sum_i \gamma_i = 1, \qquad \gamma_i > 0 \tag{5.49}$$

The mean value of a given physical quantity becomes a statistical average of "averages in states i". It is easy to see that the von Neumann equation (5.18) and the expression (5.12) hold also in this case. Accordingly, the mixed state Wigner function and equation are derived from $\hat{\rho}$ and its equation of motion as in the case of a pure state. Since the derivation is reversible, one can equivalently postulate $f_w(x,p,t)$ as a definition of the state of the system. Note that if the set γ_i is known, the density matrix can be obtained from (5.49). This is for example possible in models where γ_i are defined by the boundary conditions [12]. Then the problem is reduced to a set of pure state problems. However, for more complex physical systems, containing electrons which interact with other types of quasi-particles, γ_i are not known a priori. In this case $\hat{\rho}_i$ and γ_i are obtained with the help of the basic notions (5.18) and (5.12). We note that in the latter the Hamiltonian already contains the term accounting for the interaction with the quasi-particles, so that (5.18) must be augmented accordingly. Indeed the corresponding representation of the system is given by the basis vectors $|X_i\rangle|x\rangle$ where the additional degrees of freedom X describing the quasi-particles are assumed enumerable. Of particular interest are the electron averages, so that the operator $\hat{A}$ does not affect X_i. Equation (5.12) becomes:

$$\langle\hat{A}\rangle(t) = Tr(\hat{\rho}_t\hat{A}) = \sum_i \int dx\langle x|\langle X_i|\hat{\rho}_t\hat{A}|X_i\rangle|x\rangle = \int dx\langle x|\hat{\rho}_t^e\hat{A}|x\rangle = Tr_e(\hat{\rho}_t^e\hat{A}) \quad (5.50)$$

where $\hat{\rho}_t^e = \sum_i\langle X_i|\hat{\rho}_t|X_i\rangle$ is the electron, or reduced density operator. The set of probabilities γ_i and the set of electron density operators $\hat{\rho}_t^{e,i}$ are now introduced according to:

$$\gamma_i = Tr_e(\langle X_i|\hat{\rho}_t|X_i\rangle) \geq 0, \quad \sum_i \gamma_i = 1; \qquad \hat{\rho}_t^{e,i} = \frac{\langle X_i|\hat{\rho}_t|X_i\rangle}{Tr_e(\langle X_i|\hat{\rho}_t|X_i\rangle)}, \quad Tr_e(\hat{\rho}_t^{e,i}) = 1$$

These estimates follow from the fact that $\hat{\rho}_t$ is a positively defined operator and from the conservation of the probability. Hence, in a formal consistence with (5.49), it holds

$$\hat{\rho}_t^e = \sum_i \gamma_i\hat{\rho}_t^{e,i}$$

However, in order to obtain γ_i and $\hat{\rho}_t^{e,i}$ one needs $\hat{\rho}_t$ which entails solving the evolution equation for the whole system. Usually this is not possible, moreover we are not interested in the detailed information about the state of the quasi-particles. This implies to approximate the evolution equation to a closed equation for the electron subsystem. Alternatively this can be done in terms of the Wigner functions obtained after a Wigner transform of the corresponding density operators.

With the help of (5.13) and (5.49) it is obtained:

$$f_w(x,p,t) = \sum_{m,n}\left(\sum_i \gamma_i c_n(t)c_m^*(t)\right) f_{w(m,n)}(x,p)$$

This equation introduces the off-diagonal Wigner function

$$f_{w(m,n)} = (2\pi\hbar)^{-1} W(|\phi_n\rangle\langle\phi_m|) \tag{5.51}$$

If $|\psi_{t,1}\rangle$ and $|\psi_{t,2}\rangle$ are two states, solutions of (5.8), the off-diagonal Wigner function $f_{w(1,2)} = (2\pi\hbar)^{-1} W(|\psi_{t,1}\rangle\langle\psi_{t,2}|)$ is a solution of (5.22). Furthermore if $|\psi_1\rangle$ and $|\psi_2\rangle$ are two stationary energy eigenstates, corresponding to energy eigenvalues E_1 and E_2, it holds:

$$H(x,p) * f_{w(1,2)} = E_1 f_{w(1,2)} \qquad f_{w(1,2)} * H(x,p) = E_2 f_{w(1,2)} \tag{5.52}$$

where $H(x,p) = W(\hat{H}) = p^2/2m + V(x)$.

2.10 Quantum Phase Space States

It has been shown that the laws and relations of the operator quantum mechanics can be reformulated into the language of the phase space functionals. A systematic presentation of the inverse approach is not possible within this chapter, however we provide some selected ideas which help the reader to build up an initial impression.

A basic question which must be addressed is about the identification of the admissible quantum phase space functionals. Conditions have been derived, which specify the functionals in terms of pure or mixed quantum states and the rest of non-quantum states. A phase space function is an off-diagonal pure state if it can be presented in the form (5.51) for two complex valued, normalized functions $\langle x|\phi_{m,n}\rangle$. In particular, if $m = n$ the function is just a pure state. The first necessary and sufficient condition for a pure state has been introduced by Tatarskii [4], and will be formulated later. The condition has been generalized for off-diagonal pure states [5] as follows:

If $f_w(x,p,t)$ is square-integrable, and if Z, defined as

$$Z(x,x',t) = \int dp e^{ix'p/\hbar} f_w(x,p,t) \tag{5.53}$$

satisfies the following equation

$$\frac{\partial^2 lnZ(x,x',t)}{\partial x'^2} = \left(\frac{1}{2}\right)^2 \frac{\partial^2 lnZ(x,x',t)}{\partial x^2} \tag{5.54}$$

then f_w is a phase space function of the form (5.51):

$$f_{w(1,2)}(x,p,t) = \frac{1}{2\pi\hbar} \int dy e^{-iyp/\hbar} \psi_2^* \left(x - \frac{y}{2}, t\right) \psi_1 \left(x + \frac{y}{2}, t\right) \tag{5.55}$$

where $\psi_{1,2}$ are some complex square integrable functions. If, moreover, f_w is a real function, then it is a pure state Wigner function. On the other hand, if f_w is a pure state, or an off-diagonal pure state Wigner function, then it satisfies the above differential equation.

The proof presented in [5] is short and elegant: Equation (5.54) can be viewed as a wave equation with 'time' variable x', spatial variable x, and velocity $1/2$. The general solution, known as the one-dimensional case of d'Alembert's solution, is given by two arbitrary functions which are shifted in time to the left and right with the velocity used to define the equation. Thus:

$$lnZ(x,x',t) = ln\psi_2^*\left(x-\frac{\hbar x'}{2},t\right)+ln\psi_1\left(x+\frac{\hbar x'}{2},t\right)$$

where $ln\psi_{1,2}$ are two arbitrary functions. Then the evaluation of (5.55) is straightforward. Moreover $\psi_{1,2}$ are square integrable as f_w is square integrable. Besides, if f_w is real, then ψ_1 is proportional to ψ_2^*. The normalization of ψ follows from the normalization of f_w which is a pure state. The converse result is shown by direct calculations.

Equation (5.54) provides the pure state quantum condition. Physical states are presented by its real and normalized solutions, namely the pure state Wigner functions. The non-real off-diagonal solutions are relevant for the treatment of the mixed states. An important result follows [4]: Let us assume that f_w is a solution of (5.22) and satisfies the quantum condition at the initial time. Then f_w is a solution of (5.54) for all times. Namely, the Wigner evolution preserves the pure (possible off-diagonal) quantum condition. In contrast, it can be shown that this is not true if the evolution is provided by the classical limit (5.29). Moreover, as originally shown by Tatarskii, the quantum character of the evolution is not ensured solely by the Wigner equation: the initial condition must also be an admissible quantum state. In this way the pure state condition implicitly implies the Heisenberg uncertainty relation.

The wave functions can be explicitly constructed from the knowledge of $f_{w(1,2)}$. Namely, if f_w satisfies the conditions around (5.54), it takes the form (5.51). Then with the help of (5.53) it holds:

$$\psi_1(x) = N_1 Z\left(\frac{x}{2},x\right) \quad \psi_2(x) = N_2 Z^*\left(\frac{x}{2},-x\right) \quad N_1 = \psi_2^*(0)^{-1} \quad N_2 = \psi_1(0)^{-1}$$

A shift of the arguments of Z is assumed if one of the wave functions becomes zero at zero. These expressions are valid for stationary wave functions: in the time-dependent case they introduce an arbitrary time-dependent phase. For this case an alternative formula is suggested in [5].

The following result is important: Let us assume β to be such that $\hat{A}$, defined by (5.15), is a generic linear operator. Hence $A(x,p)$, defined in (5.16) satisfies the following equations:

$$A(x,p) * f_{w(m,n)}(x,p) = a_n f_{w(m,n)}(x,p) \qquad f_{w(m,n)} * A(x,p) = a_m f_{w(m,n)}(x,p) \tag{5.56}$$

Then $f_{w(m,n)}$ is a (off-diagonal) pure state, where the associated functions ϕ_n and ϕ_m satisfy the eigenvalue equations:

$$\hat{A}\phi_n(x) = a_n\phi_n(x) \qquad \hat{A}^*\phi_m(x) = a_m^*\phi_m(x)$$

The result holds in particular for the energy eigenvalue problem.

The above considerations make it possible to establish a one to one correspondence between the space of all real pure state functions $f_w(x,p)$ defined in the phase space – the functions satisfying the conditions around (5.54) and the Hilbert space of the physical states $\psi(x)$:

$$\psi \to f_w: \quad f_w(x,p) = \frac{1}{2\pi\hbar}\int dy e^{-iyp/\hbar}\psi^*\left(x-\frac{y}{2}\right)\psi\left(x+\frac{y}{2}\right)$$

$$f_w \to \psi: \quad \psi(x) = N\int dp e^{ipx/\hbar} f_w\left(\frac{x}{2},p\right)$$

where N is defined as a normalization phase factor constant.

Similar necessary and sufficient conditions are formulated for mixed phase space quantum states [5].

These considerations illustrate how the Wigner quantum mechanics can be introduced in an independent way, and used as a formalism to re-derive the standard operator quantum mechanics.

2.11 Summary

We summarize the basic notions used in the Wigner representation of quantum mechanics by taking into account the three dimensional nature of the space. The momentum variable will be replaced by the wave vector $\mathbf{k}$, as the latter is usually preferred for modeling of carrier transport in semiconductors and devices. This allows to skip $\hbar$ in the definitions (5.20):

$$f_w(\mathbf{r},\mathbf{k},t) = \frac{1}{(2\pi)^3}\int d\mathbf{r}'\rho(\mathbf{r}+\mathbf{r}'/2,\mathbf{r}-\mathbf{r}'/2,t)e^{-i\mathbf{r}'.\mathbf{k}}, \tag{5.57}$$

and to restate the Wigner equation and the Wigner potential as follows:

$$\frac{\partial f_w(\mathbf{r},\mathbf{k},t)}{\partial t} + \frac{\hbar\mathbf{k}}{m}\cdot\nabla_{\mathbf{r}} f_w(\mathbf{r},\mathbf{k},t) = \int dk' V_w(\mathbf{r},\mathbf{k}-\mathbf{k}')f_w(\mathbf{r},\mathbf{k}',t) \tag{5.58}$$

$$V_w(\mathbf{r},\mathbf{k}) = \frac{1}{i\hbar(2\pi)^3}\int d\mathbf{r}' e^{-i\mathbf{r}'\mathbf{k}}(V(\mathbf{r}+\mathbf{r}'/2)-V(\mathbf{r}-\mathbf{r}'/2)) \tag{5.59}$$

If one is interested in the properties of the system along a desired direction, in the general case the relevant Wigner function becomes (5.57), integrated over the

obsolete variables. It is a special case when the task is separable into transversal and longitudinal modes: $\rho = \rho_x \rho_\perp$. Then (5.57) can be reduced to the single-dimensional definition after an integration over the transversal variables. It is also possible to consider a Wigner function of the type $f_x(x, k_x, \mathbf{k}_\perp)$ where the longitudinal variables come from the single-dimensional definition, imposed e.g. by the fact that the potential depends only on x, while the transversal variables are introduced by other parts of the Hamiltonian accounting e.g. for phonons.

2.12 The Bound-States Problem

If the state $\psi_n(\mathbf{r},t) = \psi_n(\mathbf{r},0)\exp(-E_n t/\hbar)$ of the physical system is a given energy eigenstate, the density matrix is time-independent, $\rho_{nn}(\mathbf{r}_1,\mathbf{r}_2,t) = \psi_n^*(\mathbf{r}_1,0)\,\psi_n(\mathbf{r}_2,0)$. In this case the system Hamiltonian and the density operator commute, and the von Neumann equation (5.18) reduces to

$$i\hbar\frac{\partial\hat{\rho}}{\partial t} = [\hat{H},\hat{\rho}]_- = 0\,. \tag{5.60}$$

This equation does not contain the system Hamiltonian any longer, and cannot determine the bound-state density matrix, since any given bound-state density matrix, being time-independent, will satisfy this equation. Similar arguments hold for the Wigner equation, linked to (5.60) by the Weyl transform. As it has been shown in [14], bound states cannot be obtained from the ballistic Wigner equation (5.58).

The harmonic oscillator is an example clearly demonstrating this problem. If the potential is a quadratic function of position, $V(\mathbf{r}) = m^*\omega^2|\mathbf{r}|^2/2$, the Wigner equation (5.58) reduces to the collisionless Boltzmann equation, the three dimensional version of (5.30), with $F(\mathbf{r}) = -m^*\omega^2\mathbf{r}$ being the classical force. The equation propagates an initial distribution classically. This demonstrates that, in the spirit of Sect. 2.10, the single equation (5.58) is not completely equivalent to the Schrödinger equation. Two alternative solutions of this problem can be pursued.

The solutions of the Wigner equation have to be subjected to a necessary and sufficient condition which selects an allowed class of Wigner distributions describing quantum-mechanical pure states. The condition preceding (5.54) originally formulated [4] in terms of the density matrix is:

$$\nabla_{\mathbf{r}_1}\nabla_{\mathbf{r}_2}\ln\rho(\mathbf{r}_1,\mathbf{r}_2) = 0 \tag{5.61}$$

$$\rho(\mathbf{r}_1,\mathbf{r}_2) = \int f_{\mathrm{w}}\left(\mathbf{k},\frac{\mathbf{r}_1+\mathbf{r}_2}{2}\right)\mathrm{e}^{i\mathbf{k}\cdot(\mathbf{r}_1-\mathbf{r}_2)}\,\frac{d\mathbf{k}}{(2\pi)^3} \tag{5.62}$$

This restriction holds also for the initial condition, responsible for the correct physical foundation of the computational task. Thus bound states enter externally, via the initial establishment of the task. The system Hamiltonian does not provide further

information via the Wigner equation: the only property of the latter is that a bound state remains unaffected during the evolution. For example, in the case of the harmonic oscillator, the quantization condition for the energy does not follow from the Wigner equation, but from a supplementary condition.

The alternative way is to incorporate bound states as a part of the computational task. Carruthers and Zachariasen [14] start from the Schrödinger equation and derive an adjoint Wigner equation. If this adjoint equation is considered in addition, the usual Schrödinger eigenvalue problem can be reconstructed from the two Wigner equations. The adjoint equation is obtained with the help of the anti-commutator [14],

$$[\hat{H},\hat{\rho}]_+ = \hat{H}\hat{\rho} + \hat{\rho}\hat{H} = 2E\hat{\rho},$$

and takes a form, consistent with (5.52) and (5.56):

$$\begin{aligned} &\frac{\hbar^2}{2m^*}\left(|\mathbf{k}|^2 - \frac{1}{4}\nabla_{\mathbf{r}}^2\right) f_{w(m,n)}(\mathbf{k},\mathbf{r}) - \int \widetilde{V}_{\mathrm{w}}(\mathbf{k}-\mathbf{k}',\mathbf{r})\, f_{w(m,n)}(\mathbf{k}',\mathbf{r})\, d\mathbf{k}' \\ &\quad = \frac{E_m + E_n}{2} f_{w(m,n)}(\mathbf{k},\mathbf{r}) \qquad (5.63) \\ &\widetilde{V}_{\mathrm{w}}(\mathbf{q},\mathbf{r}) = \frac{1}{2i\hbar}\int \left\{V\left(\mathbf{r}+\frac{\mathbf{s}}{2}\right) + V\left(\mathbf{r}-\frac{\mathbf{s}}{2}\right)\right\} \mathrm{e}^{-i\mathbf{q}\cdot\mathbf{s}}\, \frac{d^3s}{(2\pi)^3} \end{aligned}$$

For $m = n$ one obtains the bound-state Wigner functions, which are real valued. The case $m \neq n$ gives the off-diagonal functions (5.51). The entire set of $f_{w(m,n)}(\mathbf{k},\mathbf{r})$ form a complete orthonormal basis.

The fact that the Wigner equation alone cannot provide the bound-states of a closed system has some implications for the numerical solution methods. Consider a system in which quasi-bound states of long life time exist. In this case the energy levels have very little broadening, which indicates that the system is almost closed. Such a system would be a double barrier structure realized by a semiconductor heterostructure. The spacing between resonance energies is typically in the 10^{-2} eV range. For thick barriers the broadening of the resonances can be in the 10^{-9} eV range. To resolve such a resonance a highly non-uniform energy grid with extremely small spacing around the resonance peaks would be needed. The discrete Fourier transform utilized by a numerical Wigner equation solver, on the other hand, permits only equi-distant grids in momentum space. With such a grid the extremely narrow resonances cannot be resolved in practice, and the discrete Wigner equation would become ill-conditioned. From this discussion one can conclude that a numerical Wigner function approach is applicable only to sufficiently open systems, i.e., to systems with not too narrow resonances.

The bound state problem is inherent to the coherent picture imposed by the ballistic Wigner transport. Bound states can be equally well treated in the more realistic picture which accounts for de-coherence processes of interaction with the environment, introduced in the next section.

3 Wigner–Boltzmann Equation

3.1 Introduction

The Wigner function approach allows to handle open-boundary systems, (carrier exchange with the environment is actually the basic characteristic of an operating electronic device), under stationary, small signal, or transient conditions, in a natural way [15]. Early works investigate the theoretical and numerical properties of the coherent Wigner equation, appropriate for ballistic transport [4, 12, 16]. At that time it has been recognized that dissipative processes are not only a part of the world of device physics, but that neglecting the interplay between coherent and de-coherence phenomena may lead to unphysical behavior of the modeled system [17]. The reason for such behavior are quasi-bound, or 'notch' states which may be charged properly by the boundary conditions only via a dissipation mechanism.

Dissipative interactions have been approached by means of phenomenological models based on the relaxation time approximation, [15, 18, 19] and also by introducing an actual Boltzmann-like collision operator [17, 20]. The phonon collision operator acting upon the Wigner distribution has been initially suggested as an a priory assumption that 'is an adequate approximation at some level' [17]. Can the classical Boltzmann scattering operator and the quantum Wigner-potential operator reside in a common equation? The answer is not trivial: derivations from first principles and analysis of the assumptions and approximations have been provided only recently for interactions with ionized impurities [21] and with phonons [22]. Moreover the two approaches are very different.

Consider for instance the short-range Coulomb potential created by an ionized impurity $e^2 \exp(-\beta |\mathbf{r} - \mathbf{r}_i|)/4\pi\varepsilon |\mathbf{r} - \mathbf{r}_i|$, where ε is the semiconductor permittivity and β is the screening factor in the static screening approximation. The demonstration starts with the derivation of the Wigner potential associated with this Coulomb potential, from which a quantum evolution term is derived. After some tedious but straightforward calculations, considering a large number of dopants and within the fast collision approximation, the electron–impurity collision term finally takes exactly the same form as commonly derived for the Boltzmann collision operator with continuous doping density [21].

The semiclassical phonon collision is derived from the equation for the generalized Wigner function [23, 24]. Along with the electron coordinates, the function depends on the occupation number of the phonon states in the system. Of interest is the electron, or reduced, Wigner function obtained from the generalized Wigner function by a trace over the phonon coordinates. A closed equation for the reduced Wigner function can be derived after a hierarchy of approximations, which includes the weak scattering limit and assumes that the phonon system is in equilibrium [22]. They concern the interaction with the phonons, while the potential operator remains exact. The phonon interaction in the resulting equation, being nonlocal in both space and time is yet quantum. The Wigner–Boltzmann equation is obtained after a classical limit in the phonon term, leading to the instantaneous, local in position Boltzmann collision operator.

The effects neglected by this limit can be studied from the homogeneous form of the equation for the reduced Wigner function. In this case the latter reduces to the Levinson equation [25], or equivalently to the Barker–Ferry equation, [26] with infinite electron lifetime. It should be noted that the inclusion of a finite lifetime requires a refined set of approximations in the generalized Wigner equation [27].

Effects of time dependent collisional broadening (CB) and retardation of phonon replicas have been investigated theoretically and experimentally in homogeneous semiconductors [28–32]. These effects are related to the lack of energy conservation and the memory character of the electron–phonon dynamics, and are due to the finite duration of the interaction process. The effect of the action of the electric field during the process of collision – the intra-collisional field effect (ICFE) – has attracted the scientific attention for quite some time [33–35]. Numerical studies demonstrate the CB, CR and ICFE effects in the case of ultrafast and/or high field transport in semiconductors and insulators [24,36–40] and in the case of photo-excited semiconductors [31, 32]. The solutions of the Levinson equation show the establishment of the classical, energy conserving delta function for long times. Semiclassically forbidden states are occupied at early evolution times [22, 32]. The first experimental evidence of memory effects and energy non-conserving transitions in the relaxation of hot carrier distributions have been reported a decade ago [29]. At higher times, which are above few hundred femtoseconds for GaAs, the Boltzmann limit dominates in the carrier evolution. A theoretical analysis [41] supports this result: the classical limit and the first order correction of the equation have been derived by using a small parameter. The latter requires that the product of the time scale and the phonon frequency scale to become much larger than unity, which gives rise to coarse graining in time. Thus, for long evolution times, the quantum effects in the electron–phonon interaction can be neglected. Consequently, the intra-collisional field effect is not important in stationary high field transport in semiconductors [38]. Rather, the effect must be sought in the time domain of the early time evolution, which precedes the formation of the classical energy conserving δ-function [39, 42]. We note that the above considerations hold in the weak collision limit, where the next interaction begins well after the completion of the current one.

The above considerations show that the inclusion of the Boltzmann collision operator in the Wigner equation requires that the dwell time of the carriers inside the device, and hence the device itself, must be sufficiently large. On the contrary, the application of the Wigner potential operator is reasonable for small device domains, where the potential changes over a region comparable with the coherence length of the electron. These requirements are not contradictory, since common devices are composed by an active quantum domain attached to large contact regions.

3.2 Electron–Phonon Interaction

We consider the dynamics of a single electron, subject to the action of the electric potential and interacting with the lattice vibrations. The description of the system

is provided by both electron and phonon coordinates. The Wigner function and the Wigner equation for such a coupled electron–phonon system are defined as follows. The Hamiltonian of the system is given by

$$\begin{aligned} H &= H_0 + V + H_p + H_{e-p} \\ &= -\frac{\hbar^2}{2m}\nabla_{\mathbf{r}} + V(\mathbf{r}) + \sum_{\mathbf{q}} b_{\mathbf{q}}^{\dagger} b_{\mathbf{q}} \hbar\omega_{\mathbf{q}} + i\hbar \sum_{\mathbf{q}} C(\mathbf{q})(b_{\mathbf{q}} e^{i\mathbf{qr}} - b_{\mathbf{q}}^{\dagger} e^{-i\mathbf{qr}}) \end{aligned} \quad (5.64)$$

where the free electron part is H_0, the structure potential is $V(\mathbf{r})$, the free-phonon Hamiltonian is given by H_p and the electron–phonon interaction is H_{e-p}. In the above expressions $b_{\mathbf{q}}^{\dagger}$ and $b_{\mathbf{q}}$ are the creation and annihilation operators for the phonon mode $\mathbf{q}$, $\omega_{\mathbf{q}}$ is the energy of that mode and $\mathscr{C} = i\hbar C(\mathbf{q})$ is the electron–phonon coupling element, which depends on the type of phonon scattering analyzed. The state of the phonon subsystem is presented by the set $\{n_{\mathbf{q}}\}$ where $n_{\mathbf{q}}$ is the occupation number of the phonons in mode $\mathbf{q}$. Then the representation is given by the vectors $|\{n_{\mathbf{q}}\}, \mathbf{r}\rangle = |\{n_{\mathbf{q}}\}\rangle|\mathbf{r}\rangle$. The generalized Wigner function [23] is defined by:

$$f_w(\mathbf{r}, \mathbf{k}, \{n_{\mathbf{q}}\}, \{n_{\mathbf{q}}\}', t) = \frac{1}{(2\pi)^3} \int d\mathbf{r}' e^{-i\mathbf{kr}'} \langle \mathbf{r} + \mathbf{r}'/2, \{n_{\mathbf{q}}\}|\hat{\rho}_t|\{n_{\mathbf{q}}\}', \mathbf{r} - \mathbf{r}'/2\rangle$$

The equation of motion of f_w is derived [43] with the help of (5.18):

$$\frac{\partial f_w(\mathbf{r}, \mathbf{k}, \{n_{\mathbf{q}}\}, \{n_{\mathbf{q}}\}', t)}{\partial t} = \frac{1}{i\hbar} \int d\mathbf{r}' e^{-i\mathbf{kr}'} \langle \mathbf{r} + \mathbf{r}'/2, \{n_{\mathbf{q}}\}|[H, \hat{\rho}_t]_-|\{n_{\mathbf{q}}\}', \mathbf{r} - \mathbf{r}'/2\rangle$$

The right hand side of this equation is shortly denoted by $WT(H)$. In the following we evaluate $WT(H)$ for each term of the Hamiltonian (5.64). $WT(H_0 + V(\mathbf{r}))$ can be readily evaluated by using the steps applied after (5.18). The free phonon term is evaluated as:

$$WT(H_p) = \frac{1}{i\hbar}\left(\varepsilon(\{n_{\mathbf{q}}\}) - \varepsilon(\{n'_{\mathbf{q}}\})\right) f_w(\mathbf{r}, \mathbf{k}, \{n_{\mathbf{q}}\}, \{n_{\mathbf{q}}\}', t)$$

where $\varepsilon(\{n_{\mathbf{q}}\}) = \sum_{\mathbf{q}} n_{\mathbf{q}} \hbar\omega_{\mathbf{q}}$. The transform $WT(H_{e-p})$ gives rise to four terms. By inserting $\int d\mathbf{r}''|\mathbf{r}'' >< \mathbf{r}''|$ in the first one it is obtained:

$$\begin{aligned} &\int d\mathbf{r}' \int d\mathbf{r}'' e^{-i\mathbf{kr}'} \left\langle \mathbf{r} + \frac{\mathbf{r}'}{2}, \{n_{\mathbf{q}}\}|b_{\mathbf{q}'} e^{i\mathbf{q}'\mathbf{r}''}|\mathbf{r}''\right\rangle \left\langle \mathbf{r}''|\hat{\rho}_t|\{n'_{\mathbf{q}}\}, \mathbf{r} - \mathbf{r}'/2\right\rangle \\ &= \sqrt{n_{\mathbf{q}'} + 1} \int d\mathbf{r}' e^{-i\mathbf{kr}'} e^{i\mathbf{q}'(\mathbf{r} + \mathbf{r}'/2)} \left\langle \mathbf{r} + \frac{\mathbf{r}'}{2}, \{n_1, \ldots, n_{\mathbf{q}'} + 1, \ldots\}|\hat{\rho}_t|\{n'_{\mathbf{q}}\}, \mathbf{r} - \frac{\mathbf{r}'}{2}\right\rangle \\ &= \sqrt{n_{\mathbf{q}'} + 1} e^{i\mathbf{q}'\mathbf{r}} f_w\left(\mathbf{r}, \mathbf{k} - \frac{\mathbf{q}'}{2}, \{n_1, \ldots, n_{\mathbf{q}'} + 1, \ldots\}, \{n'_{\mathbf{q}}\}, t\right) \end{aligned}$$

where the ortho-normality relation $\langle \mathbf{r}|\mathbf{r}'\rangle = \delta(\mathbf{r} - \mathbf{r}')$ has been used along with the fact that $b_{\mathbf{q}}$ becomes a creation operator when operating to the left. The remaining terms are evaluated in a similar way.

We are now ready to formulate the generalized Wigner equation:

$$\begin{aligned}
&\left(\frac{\partial}{\partial t}+\frac{\hbar\mathbf{k}}{m}\cdot\nabla_{\mathbf{r}}\right) f_w(\mathbf{r},\mathbf{k},\{n_{\mathbf{q}}\},\{n'_{\mathbf{q}}\},t)\\
&\quad=\frac{1}{i\hbar}\left(\varepsilon(\{n_{\mathbf{q}}\})-\varepsilon(\{n'_{\mathbf{q}}\})\right) f_w(\mathbf{r},\mathbf{k},\{n_{\mathbf{q}}\},\{n'_{\mathbf{q}}\},t)\\
&\qquad+\int \mathrm{d}\mathbf{k}' V_w(\mathbf{r},\mathbf{k}-\mathbf{k}') f_w(\mathbf{r},\mathbf{k}',\{n_{\mathbf{q}}\},\{n'_{\mathbf{q}}\},t)+\sum_{\mathbf{q}'} C(\mathbf{q}')\\
&\qquad\times\left\{\mathrm{e}^{i\mathbf{q}'\mathbf{r}}\sqrt{n_{\mathbf{q}'}+1}\, f_w\left(\mathbf{r},\mathbf{k}-\frac{\mathbf{q}'}{2},\{n_{\mathbf{q}}\}^{+}_{\mathbf{q}'},\{n'_{\mathbf{q}}\},t\right)\right.\\
&\qquad\quad-\mathrm{e}^{-i\mathbf{q}'\mathbf{r}}\sqrt{n_{\mathbf{q}'}}\, f_w\left(\mathbf{r},\mathbf{k}+\frac{\mathbf{q}'}{2},\{n_{\mathbf{q}}\}^{-}_{\mathbf{q}'},\{n'_{\mathbf{q}}\},t\right)\\
&\qquad\quad-\mathrm{e}^{i\mathbf{q}'\mathbf{r}}\sqrt{n'_{\mathbf{q}'}}\, f_w\left(\mathbf{r},\mathbf{k}+\frac{\mathbf{q}'}{2},\{n_{\mathbf{q}}\},\{n'_{\mathbf{q}}\}^{-}_{\mathbf{q}'},t\right)\\
&\qquad\quad\left.+\mathrm{e}^{-i\mathbf{q}'\mathbf{r}}\sqrt{n'_{\mathbf{q}'}+1}\, f_w\left(\mathbf{r},\mathbf{k}-\frac{\mathbf{q}'}{2},\{n_{\mathbf{q}'}\},\{n'_{\mathbf{q}}\}^{+}_{\mathbf{q}'},t\right)\right\}
\end{aligned}\tag{5.65}$$

where we denoted by $\{n_{\mathbf{q}}\}^{+}_{\mathbf{q}'}$ ($\{n_{\mathbf{q}}\}^{-}_{\mathbf{q}'}$) the states of the phonon subsystem, obtained from $\{n_{\mathbf{q}}\}$ by increasing (decreasing) the number of phonons in the mode $\mathbf{q}'$ by unity. Furthermore we observe that the last two terms in the curly brackets can be obtained from the first ones by the following rule: (a): the argument of the exponent changes its sign; (b): the phonon number in the mode determined by the summation index ($\mathbf{q}'$) is changed in the right state instead in the left state; (c): in the square roots $n_{\mathbf{q}'}$ is replaced by $n'_{\mathbf{q}'}$. In what follows we denote the last two terms by *i.c.*.

The generalized Wigner equation couples an element $f_w(\ldots,\{n\},\{m\},t)$ to four neighborhood elements for any phonon mode $\mathbf{q}$. For any such mode $n_{\mathbf{q}}$ can be any integer between 0 and infinity and the sum over $\mathbf{q}$ couples all modes.

In accordance with Sect. 2.9 and (5.50) of interest is the reduced Wigner function, which is obtained from the generalized Wigner function by taking the trace over the phonon states. An exact equation for the reduced Wigner function can not be obtained since the trace operation does not commute with the electron–phonon interaction Hamiltonian. In what follows we derive a model, which approximates the generalized Wigner equation, but is closed with respect to the reduced Wigner function. The model is general enough to account for the quantum character of the interaction with the phonons. The electron-device potential part of the transport is treated on a rigorous quantum level. A classical limit in the electron–phonon operators gives rise to the Wigner–Boltzmann equation. The derivation introduces a consistent hierarchy of assumptions and simplifications.

3.2.1 Weak Coupling

We begin with the assumptions which simplify (5.65) towards a model equation set for the electron Wigner function. Of interest are the diagonal elements of the

generalized WF. The evolution of an initial state of the system defined at time $t = 0$ is considered. The state is assumed diagonal with respect to the phonon coordinates, which corresponds to the evolution process of an initially decoupled electron–phonon system.

$$\left(\frac{\partial}{\partial t}+\frac{\hbar\mathbf{k}}{m}\cdot\nabla_{\mathbf{r}}\right)f_w(\mathbf{r},\mathbf{k},\{n_{\mathbf{q}}\},\{n_{\mathbf{q}}\},t)=\int \mathrm{d}\mathbf{k}' V_w(\mathbf{r},\mathbf{k}-\mathbf{k}')f_w(\mathbf{r},\mathbf{k}',\{n_{\mathbf{q}}\},\{n_{\mathbf{q}}\},t)$$
$$+\sum_{\mathbf{q}'}C(\mathbf{q}')\left\{\mathrm{e}^{i\mathbf{q}'\mathbf{r}}\sqrt{n_{\mathbf{q}'}+1}f_w\left(\mathbf{r},\mathbf{k}-\frac{\mathbf{q}'}{2},\{n_{\mathbf{q}}\}^{+}_{\mathbf{q}'},\{n_{\mathbf{q}}\},t\right)\right.$$
$$\left.-\mathrm{e}^{-i\mathbf{q}'\mathbf{r}}\sqrt{n_{\mathbf{q}'}}f_w\left(\mathbf{r},\mathbf{k}+\frac{\mathbf{q}'}{2},\{n_{\mathbf{q}}\}^{-}_{\mathbf{q}'},\{n_{\mathbf{q}}\},t\right)+i.c.\right\} \tag{5.66}$$

A diagonal element is linked to so called first-off-diagonal elements, which are diagonal in all modes but the current mode $\mathbf{q}'$ of the summation. In this mode the four neighbors of $n_{\mathbf{q}'}, n_{\mathbf{q}'}$ namely $n_{\mathbf{q}'}\pm 1, n_{\mathbf{q}'}$ and $n_{\mathbf{q}'}, n_{\mathbf{q}'}\pm 1$ are concerned. This is schematically presented on Fig. 5.1.

The auxiliary equation for the first-off-diagonal element in (5.66) is obtained by the help of (5.65):

$$\left(\frac{\partial}{\partial t}+\frac{\hbar(\mathbf{k}-\frac{\mathbf{q}'}{2})}{m}\cdot\nabla_{\mathbf{r}}\right)f_w\left(\mathbf{r},\mathbf{k}-\frac{\mathbf{q}'}{2},\{n_{\mathbf{q}}\}^{+}_{\mathbf{q}'},\{n_{\mathbf{q}}\},t\right)$$
$$=-i\omega_{\mathbf{q}'}f_w\left(\mathbf{r},\mathbf{k}-\frac{\mathbf{q}'}{2},\{n_{\mathbf{q}}\}^{+}_{\mathbf{q}'},\{n_{\mathbf{q}}\},t\right)$$

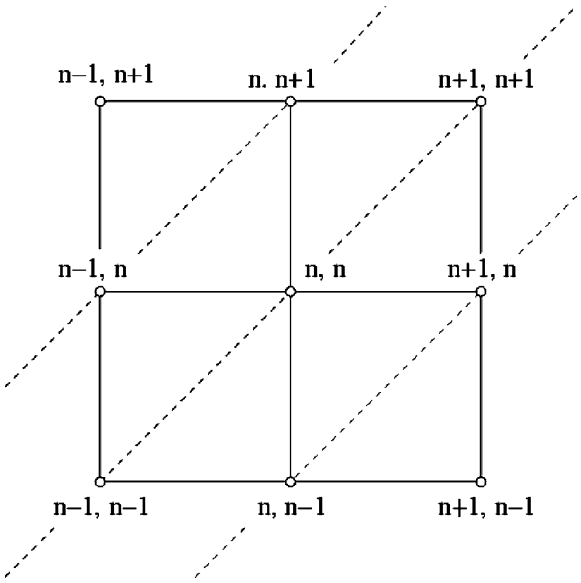

Fig. 5.1 Diagonal and first-off-diagonal elements

$$+\int \mathrm{d}\mathbf{k}' V_w(\mathbf{r},\mathbf{k}-\mathbf{k}') f_w\left(\mathbf{r},\mathbf{k}-\frac{\mathbf{q}'}{2},\{n_\mathbf{q}\}^+_{\mathbf{q}'},\{n_\mathbf{q}\},t\right)+\sum_{\mathbf{q}''} C(\mathbf{q}'')$$

$$\times\left\{\mathrm{e}^{i\mathbf{q}''\mathbf{r}}\sqrt{n_{\mathbf{q}''}+1}\, f_w\left(\mathbf{r},\mathbf{k}-\frac{\mathbf{q}'}{2}-\frac{\mathbf{q}''}{2},\{\{n_\mathbf{q}\}^+_{\mathbf{q}'}\}^+_{\mathbf{q}''},\{n_\mathbf{q}\},t\right)\right.$$

$$-\mathrm{e}^{-i\mathbf{q}''\mathbf{r}}\sqrt{n_{\mathbf{q}''}} f_w\left(\mathbf{r},\mathbf{k}-\frac{\mathbf{q}'}{2}+\frac{\mathbf{q}''}{2},\{\{n_\mathbf{q}\}^+_{\mathbf{q}'}\}^-_{\mathbf{q}''},\{n_\mathbf{q}\},t\right)$$

$$-\mathrm{e}^{i\mathbf{q}''\mathbf{r}}\sqrt{n_{\mathbf{q}''}} f_w\left(\mathbf{r},\mathbf{k}-\frac{\mathbf{q}'}{2}+\frac{\mathbf{q}''}{2},\{n_\mathbf{q}\}^+_{\mathbf{q}'},\{n_\mathbf{q}\}^-_{\mathbf{q}''},t\right)$$

$$\left.+\,\mathrm{e}^{-i\mathbf{q}''\mathbf{r}}\sqrt{n_{\mathbf{q}''}+1}\, f_w\left(\mathbf{r},\mathbf{k}-\frac{\mathbf{q}'}{2}-\frac{\mathbf{q}''}{2},\{n_\mathbf{q}\}^+_{\mathbf{q}'},\{n_\mathbf{q}\}^+_{\mathbf{q}''},t\right)\right\} \quad (5.67)$$

Accordingly, the first-off-diagonal elements are linked to elements which in general are placed further away from the diagonal ones by increasing or decreasing the phonon number in a second mode, $\mathbf{q}''$, by unity. These are the second-off-diagonal elements. The only exception is provided by two contributions which recover diagonal elements. They are obtained when the running index $\mathbf{q}''$ coincides with $\mathbf{q}'$ due to: (a): $(\{\{n_\mathbf{q}\}^+_{\mathbf{q}'}\}^-_{\mathbf{q}''},\{n_\mathbf{q}\})$ in the term in the fifth row of (5.67). We note that in this case $n''_\mathbf{q}=n'_\mathbf{q}+1$ in the square root in front of f_w. (b): $(\{n_\mathbf{q}\}^+_{\mathbf{q}'},\{n_\mathbf{q}\}^+_{\mathbf{q}''})$ in the last row of (5.67).

Next we observe that each link of two elements corresponds to a multiplication by the factor C. Thus the next assumption is that C is a small quantity. While the first-off-diagonal elements give contributions to (5.66) by order of C^2, the second-off-diagonal elements give rise to higher order contributions and are neglected. The physical meaning of the assumption is that the interaction with a phonon in mode $\mathbf{q}'$ which begins from a diagonal element completes at a diagonal element by another interaction with the phonon in the same mode, without any interference with phonons of other modes. The assumption allows to truncate the considered elements to those between the two lines parallel to the main diagonal on Fig. 5.1. As a next step we need to solve the truncated equation, which can be done explicitly after further approximations related to the Wigner potential. For this it is sufficient to consider the classical force according (5.30). Such a model is able to account for correlations between electric field and scattering – the ICFE. As we aim at derivation of a Boltzmann type of collisions, we entirely neglect the Wigner potential term:

$$\left(\frac{\partial}{\partial t}+\frac{\hbar\left(\mathbf{k}-\frac{\mathbf{q}'}{2}\right)}{m}\cdot\nabla_\mathbf{r}+i\omega_{\mathbf{q}'}\right) f_w\left(\mathbf{r},\mathbf{k}-\frac{\mathbf{q}'}{2},\{n_\mathbf{q}\}^+_{\mathbf{q}'},\{n_\mathbf{q}\},t\right)$$

$$=C(\mathbf{q}')\mathrm{e}^{-i\mathbf{q}'\mathbf{r}}\sqrt{n_{\mathbf{q}'}+1}\left(-f_w\left(\mathbf{r},\mathbf{k},\{n_\mathbf{q}\},\{n_\mathbf{q}\},t\right)+f_w\left(\mathbf{r},\mathbf{k}-\mathbf{q}',\{n_\mathbf{q}\}^+_{\mathbf{q}'},\{n_\mathbf{q}\}^+_{\mathbf{q}'},t\right)\right) \quad (5.68)$$

We consider the trajectory

$$\mathbf{k}(t') = \mathbf{k} - \frac{\mathbf{q}'}{2}; \qquad \mathbf{R}(t', \mathbf{q}') = \mathbf{r} - \int_{t'}^{t} d\tau \frac{\hbar \mathbf{k}(\tau)}{m} = \mathbf{r} - \frac{\hbar(\mathbf{k} - \mathbf{q}'/2)}{m}(t - t'); \quad (5.69)$$

initialized at time t by $\mathbf{k} - \frac{\mathbf{q}'}{2}$, $\mathbf{r}$ and the function

$$f_w(\mathbf{R}(t', \mathbf{q}'), \mathbf{k}(t'), \{n_{\mathbf{q}}\}^{+}_{\mathbf{q}'}, \{n_{\mathbf{q}}\}, t) e^{i\omega'_{\mathbf{q}} t'} \quad (5.70)$$

The total time derivative of this function, taken at time $t' = t$ gives the left hand side of (5.68). Then we consider a form of this equation, obtained by a parameterization by t' with the help of (5.69), and a multiplication by the exponent. A final integration in the time interval $0, t$ gives rise to:

$$f_w\left(\mathbf{r}, \mathbf{k} - \frac{\mathbf{q}'}{2}, \{n_{\mathbf{q}}\}^{+}_{\mathbf{q}'}, \{n_{\mathbf{q}}\}, t\right) = C(\mathbf{q}') \int_0^t dt' \mathrm{e}^{-i\omega_{\mathbf{q}'}(t-t')} \mathrm{e}^{-i\mathbf{q}'\mathbf{R}(t', \mathbf{q}')} \sqrt{n_{\mathbf{q}'} + 1}$$

$$\left(f_w(\mathbf{R}(t', \mathbf{q}'), \mathbf{k} - \mathbf{q}', \{n_{\mathbf{q}}\}^{+}_{\mathbf{q}'}, \{n_{\mathbf{q}}\}^{+}_{\mathbf{q}'}, t') - f_w(\mathbf{R}(t', \mathbf{q}'), \mathbf{k}, \{n_{\mathbf{q}}\}, \{n_{\mathbf{q}}\}, t')\right) \quad (5.71)$$

where we used the fact that the initial condition is zero due to the assumption for an initially decoupled system.

The corresponding equation for the second first-off-diagonal element is obtained in the same fashion:

$$f_w\left(\mathbf{r}, \mathbf{k} + \frac{\mathbf{q}'}{2}, \{n_{\mathbf{q}}\}^{-}_{\mathbf{q}'}, \{n_{\mathbf{q}}\}, t\right) = C(\mathbf{q}') \int_0^t dt' \mathrm{e}^{i\omega_{\mathbf{q}'}(t-t')} \mathrm{e}^{i\mathbf{q}'\mathbf{R}(t', -\mathbf{q}')} \sqrt{n_{\mathbf{q}'}}$$

$$\left(f_w(\mathbf{R}(t', -\mathbf{q}'), \mathbf{k}, \{n_{\mathbf{q}}\}, \{n_{\mathbf{q}}\}, t') - f_w(\mathbf{R}(t', -\mathbf{q}'), \mathbf{k} + \mathbf{q}', \{n_{\mathbf{q}}\}^{-}_{\mathbf{q}'}, \{n_{\mathbf{q}}\}^{-}_{\mathbf{q}'}, t')\right) \quad (5.72)$$

The remaining two elements, which compose the *i.c.* term in (5.66) give rise to two integral equations which are complex conjugate to the first two. In this way the relevant information is provided by (5.66), (5.71) and (5.72), which can be unified as follows:

$$\left(\frac{\partial}{\partial t} + \frac{\hbar \mathbf{k}}{m} \cdot \nabla_{\mathbf{r}}\right) f_w(\mathbf{r}, \mathbf{k}, \{n_{\mathbf{q}}\}, \{n_{\mathbf{q}}\}, t) = \int \mathrm{d}\mathbf{k}' V_w(\mathbf{r}, \mathbf{k} - \mathbf{k}') f_w(\mathbf{r}, \mathbf{k}', \{n_{\mathbf{q}}\}, \{n_{\mathbf{q}}\}, t)$$

$$+2Re \sum_{\mathbf{q}'} C^2(\mathbf{q}') \int_0^t dt' \left\{ (n_{\mathbf{q}'} + 1) \mathrm{e}^{i \frac{\varepsilon(\mathbf{k}) - \varepsilon(\mathbf{k} - \mathbf{q}') - \hbar\omega_{\mathbf{q}'}}{\hbar}(t - t')} \right.$$

$$\left(f_w(\mathbf{R}(t', \mathbf{q}'), \mathbf{k} - \mathbf{q}', \{n_{\mathbf{q}}\}^{+}_{\mathbf{q}'}, \{n_{\mathbf{q}}\}^{+}_{\mathbf{q}'}, t') - f_w(\mathbf{R}(t', \mathbf{q}'), \mathbf{k}, \{n_{\mathbf{q}}\}, \{n_{\mathbf{q}}\}, t')\right)$$

$$- n_{\mathbf{q}'} \mathrm{e}^{i \frac{\varepsilon(\mathbf{k}) - \varepsilon(\mathbf{k} + \mathbf{q}') + \hbar\omega_{\mathbf{q}'}}{\hbar}(t - t')} \left(f_w(\mathbf{R}(t', -\mathbf{q}'), \mathbf{k}, \{n_{\mathbf{q}}\}, \{n_{\mathbf{q}}\}, t')\right.$$

$$\left. \left. - f_w(\mathbf{R}\ (t', -\mathbf{q}'), \mathbf{k} + \mathbf{q}', \{n_{\mathbf{q}}\}^{-}_{\mathbf{q}'}, \{n_{\mathbf{q}}\}^{-}_{\mathbf{q}'}, t')\right) \right\} \quad (5.73)$$

where we have used the equalities:

$$\pm\mathbf{q}'\mathbf{r} \mp \omega_{\mathbf{q}'}(t-t') \mp \mathbf{q}'\mathbf{R}(t',\pm\mathbf{q}') = \frac{\varepsilon(\mathbf{k}) - \varepsilon(\mathbf{k}\mp\mathbf{q}') \mp \hbar\omega_{\mathbf{q}'}}{\hbar}(t-t')$$

The model involves only diagonal elements, so that the double counting of the phonon coordinates becomes obsolete and one set of phonon numbers may be omitted.

3.2.2 Equilibrium Phonons

The obtained equation set (5.73) is still infinite with respect to the phonon coordinates, which are to be eliminated by the trace operation. The next assumption is that the phonon system is a thermostat for the electrons, i.e. the phonon distribution remains in equilibrium during the evolution:

$$P(n_{\mathbf{q}},t') = \int \mathrm{d}\mathbf{r} \int \mathrm{d}\mathbf{k} \sum_{\{n_{\mathbf{q}'}\}}{}' f_w(\mathbf{r},\mathbf{k},\{n_{\mathbf{q}'}\},\{n_{\mathbf{q}'}\},t') = P_{eq}(n_{\mathbf{q}}) = \frac{e^{-\hbar\omega_{\mathbf{q}}n_{\mathbf{q}}/kT}}{n(\mathbf{q})+1} \quad (5.74)$$

Here $P(n_{\mathbf{q}},t')$ is the probability for finding $n_{\mathbf{q}}$ phonons in mode $\mathbf{q}$ at time t', the $\sum'$ denotes summation over all phonon coordinates but the one in mode $\mathbf{q}$, and n($\mathbf{q}$) is the mean equilibrium phonon number (Bose distribution):

$$n(\mathbf{q}) = \sum_{n_{\mathbf{q}}=0}^{\infty} n_{\mathbf{q}} P_{eq}(n_{\mathbf{q}}) = \frac{1}{e^{\hbar\omega_{\mathbf{q}}/kT}-1}; \qquad \sum_{n_{\mathbf{q}}=0}^{\infty} P_{eq}(n_{\mathbf{q}}) = 1 \quad (5.75)$$

The condition (5.74) is equivalent to the assumption that at any time $0 \le t' \le t$ it holds

$$f_w(\mathbf{r},\mathbf{k},\{n_{\mathbf{q}}\},\{n_{\mathbf{q}}\},t') = f(\mathbf{r},\mathbf{k},t')\prod_{\mathbf{q}} P_{eq}(n_{\mathbf{q}}) \quad (5.76)$$

where $f(\mathbf{r},\mathbf{k},t')$ reduced or electron Wigner function. Accordingly, the four terms in the curly brackets of (5.73) become dependent on the phonon coordinates by the following factors:

$$(n_{\mathbf{q}'}+1)P_{eq}(n_{\mathbf{q}'}+1)\prod_{\mathbf{q}}{}' P_{eq}(n_{\mathbf{q}}); \qquad (n_{\mathbf{q}'}+1)P_{eq}(n_{\mathbf{q}'})\prod_{\mathbf{q}}{}' P_{eq}(n_{\mathbf{q}})$$
$$n_{\mathbf{q}'}P_{eq}(n_{\mathbf{q}'})\prod_{\mathbf{q}}{}' P_{eq}(n_{\mathbf{q}}); \qquad n_{\mathbf{q}'}P_{eq}(n_{\mathbf{q}'}-1)\prod_{\mathbf{q}}{}' P_{eq}(n_{\mathbf{q}}) \quad (5.77)$$

Now the trace operation, namely the sum over $n_{\mathbf{q}}$ for all modes $\mathbf{q}$, can be readily done with the help of (5.75) and the following equalities [44]:

$$n(\mathbf{q}) = \sum_{n_{\mathbf{q}}}(n_{\mathbf{q}}+1)P_{eq}(n_{\mathbf{q}}+1); \quad n(\mathbf{q})+1 = \sum_{n_{\mathbf{q}}} n_{\mathbf{q}} P_{eq}(n_{\mathbf{q}}-1);$$

The factors depending on the phonon coordinates are replaced by the following numbers:

$$n(\mathbf{q}'); \qquad (n(\mathbf{q}')+1); \tag{5.78}$$

$$n(\mathbf{q}'); \qquad (n(\mathbf{q}')+1) \tag{5.79}$$

This is an important step which allows to close the equation set for the electron Wigner function, transforming it into a single equation.

However, it is important to clarify what the physical side of the formal assumption (5.76) is. The peculiarities of the model (5.73) in conjunction with (5.76) can be conveniently analyzed from the integral form of the equation set, written for a homogeneous system, where the space dependence appears due to the initial condition only, which is of a decoupled electron–phonon system. The integral form is obtained within the following steps: $\mathbf{R}(t',\pm\mathbf{q}')$ is replaced from (5.69), introduced is another trajectory, initialized by $\mathbf{r},\mathbf{k},T$,

$$\mathbf{k}_T(t)=\mathbf{k}; \qquad \mathbf{R}_T(t)=\mathbf{r}-\int_t^T d\tau\frac{\hbar\mathbf{k}_T(\tau)}{m}=\mathbf{r}-\frac{\hbar\mathbf{k}}{m}(T-t); \tag{5.80}$$

where T now becomes the evolution time. $\mathbf{k},\mathbf{r}$ are replaced on both sides of (5.73) by $\mathbf{k}_T(t),Rv_T(t)$ and the equation is integrated on t in the limits $0,T$. The initial condition in the form (5.76) appears explicitly:

$$\begin{aligned}
f_w(\mathbf{r},\mathbf{k},\{n_\mathbf{q}\},T)&=f(\mathbf{r},\mathbf{k},0)\prod_\mathbf{q}P_{eq}(n_\mathbf{q})\\
&+2Re\sum_{\mathbf{q}'}C^2(\mathbf{q}')\int_0^T dt\int_0^t dt'\Bigg\{(n_{\mathbf{q}'}+1)\mathrm{e}^{i\frac{\varepsilon(\mathbf{k})-\varepsilon(\mathbf{k}-\mathbf{q}')-\hbar\omega_{\mathbf{q}'}}{\hbar}(t-t')}\\
&\Bigg(f_w(\mathbf{R}_T(t)-\frac{\hbar(\mathbf{k}-\mathbf{q}'/2)}{m}(t-t'),\mathbf{k}-\mathbf{q}',\{n_\mathbf{q}\}^+_{\mathbf{q}'},t')\\
&-f_w(\mathbf{R}_T(t)-\frac{\hbar(\mathbf{k}-\mathbf{q}'/2)}{m}(t-t'),\mathbf{k},\{n_\mathbf{q}\},t')\Bigg)-n_{\mathbf{q}'}\mathrm{e}^{i\frac{\varepsilon(\mathbf{k})-\varepsilon(\mathbf{k}+\mathbf{q}')+\hbar\omega_{\mathbf{q}'}}{\hbar}(t-t')}\\
&\Bigg(f_w(\mathbf{R}_T(t)-\frac{\hbar(\mathbf{k}+\mathbf{q}'/2)}{m}(t-t'),\mathbf{k},\{n_\mathbf{q}\},t')\\
&-f_w\ (\mathbf{R}_T(t)-\frac{\hbar(\mathbf{k}+\mathbf{q}'/2)}{m}(t-t'),\mathbf{k}+\mathbf{q}',\{n_\mathbf{q}\}^-_{\mathbf{q}'},t')\Bigg)\Bigg\}
\end{aligned} \tag{5.81}$$

The phonon system can be at any state with certain set of numbers $\{n_\mathbf{q}\}$, however now the initial condition assigns a probability to this set. A replacement of the equation into itself presents the solution as consecutive iterations of the initial condition. We fix a set of numbers $\{n_\mathbf{q}\}$, corresponding to the phonon state of interest, and consider the first iteration of the term in the third row of (5.81). Until time t' the arguments of the initial condition are $\mathbf{r}_{t'}=\mathbf{R}_T(t)-\frac{\hbar(\mathbf{k}-\mathbf{q}'/2)}{m}(t-t'),\mathbf{k}_{t'}=\mathbf{k}-\mathbf{q}'$ which we may think as coordinates of a given particle, and the phonon system is

in another state with an extra phonon in mode $\mathbf{q}'$ which contributes to the state of interest. At time t' the interaction begins by absorption of the half of the wave vector of a phonon in mode $\mathbf{q}'$, so that the particle appears with a wave vector $\mathbf{k}-\mathbf{q}'/2$, and moves along a trajectory determined by $\mathbf{r}_{t'}+\frac{\hbar(\mathbf{k}-\mathbf{q}'/2)}{m}(t-t')$ At time t the second half of the phonon is absorbed. The particle coordinates become $\mathbf{R}_T(t)$, $\mathbf{k}$ – exactly the right ones, which will bring it to $\mathbf{r},\mathbf{k}$ at time T. It contributes to the function on the left by the real part of the initial condition value at the starting point, multiplied by the pre factor in front of the considered term. The process corresponds to real absorption of a phonon: the phonons at the initial state are reduced by one. The next term describes a virtual process: the particle at $\mathbf{r}_{t'},\mathbf{k}$ first emits half of the wave vector of a phonon in mode $\mathbf{q}'$, but then, at time t it is absorbed back. Thus the initial phonon state does not change at the end of the interaction. The rest of the terms can be explained in the same way. We also note that the origin of the ICFE is the acceleration of the model particle along the trajectories.

The important message from this picture is the finite duration of the interaction process. We also expect the usual for a physical point of view existence of a mean interval with vanishing probabilities for large deviations from the mean. By recalling the fact that given interaction completes before another initiates, it follows that for a given evolution interval there is only a finite number of involved phonons. In accordance, the assumption for a thermostat means that the number of phonons is so huge that a given phonon mode can be involved only once in the interaction. A quantitative analysis can be found in [27].

3.2.3 Closed Model

The assumption for equilibrium allows to eliminate the phonon degrees of freedom from (5.73), which are now replaced by the numbers (5.79). The equation can be conveniently rewritten by relying on the symmetry of C, $n_{\mathbf{q}}$ and $\omega_{\mathbf{q}}$ with respect to the change the sign of the wave vector. We change the sign of $\mathbf{q}$ in the last two rows and introduce the variable $\mathbf{k}'=\mathbf{k}-\mathbf{q}'$.

$$\left(\frac{\partial}{\partial t}+\frac{\mathbf{k}}{m}\cdot\nabla_{\mathbf{r}}\right)f_w(\mathbf{r},\mathbf{k},t)=\int \mathrm{d}\mathbf{k}'\left\{V_w(\mathbf{r},\mathbf{k}-\mathbf{k}')f_w(\mathbf{r},\mathbf{k}',t)\right.$$
$$\left.+\int_0^t \mathrm{d}t'\left(S(\mathbf{k}',\mathbf{k},t,t')f_w(\mathbf{R}(t',\mathbf{q}'),\mathbf{k}',t')-S(\mathbf{k},\mathbf{k}',t,t')f_w(\mathbf{R}(t',\mathbf{q}'),\mathbf{k},t')\right)\right\} \quad (5.82)$$

$$S(\mathbf{k}',\mathbf{k},t,t')=\frac{2VC_{\mathbf{q}}^2}{(2\pi)^3}\left(n(\mathbf{q})cos(\Omega(\mathbf{k}',\mathbf{k},t,t'))+(n(\mathbf{q})+1)cos(\Omega(\mathbf{k},\mathbf{k}',t,t'))\right)$$
$$\Omega(\mathbf{k},\mathbf{k}',t,t')=\frac{\varepsilon(\mathbf{k})-\varepsilon(\mathbf{k}')+\hbar\omega_{\mathbf{q}}}{\hbar}(t-t');\quad \mathbf{q}=\mathbf{k}-\mathbf{k}'$$

The phonon interaction in this equation bears quantum character despite all simplifying assumptions. No approximations are introduced for the coherent part of the transport process: if the phonon interaction is neglected, the common Wigner

equation for an electron in a potential field is recovered. The analysis of the physical processes involved is the same as for (5.81). The main peculiarity is the non-locality in the real space. The Boltzmann distribution function in point $\mathbf{r},\mathbf{k}$ at time t collects contributions only from the past of the real space part of the trajectory passing through this point. Since the finite duration of the phonon interaction, the solution of (5.83) can collect contributions from all points in the phase space and thus gives rise to a spatial non-locality. There is a lack of energy conservation even in the most simple homogeneous case, where the electric field is zero. The energy conserving delta function in the Boltzmann type of interaction is obtained after a limit which neglects the duration of the collision process.

3.2.4 Classical Limit: General Form of the Equation

We consider the classical limit of the electron–phonon interaction. The time integral in (5.83) is of the form:

$$\int_0^t \mathrm{d}\tau \mathrm{e}^{\frac{i}{\hbar}\varepsilon\tau}\phi(\tau) \tag{5.83}$$

The following formal limit holds in terms of generalized functions:

$$\lim_{\hbar\to 0}\frac{1}{\hbar}\int_0^\infty \mathrm{d}\tau \mathrm{e}^{\frac{i}{\hbar}\varepsilon\tau}\phi(\tau) = \phi(0)\left\{\pi\delta(\varepsilon) + i\mathscr{P}\frac{1}{\varepsilon}\right\} \tag{5.84}$$

The actual meaning of the process of encouraging a constant to approach zero is that the product of the energy and time scales becomes much larger than $\hbar$. The mathematical aspects of the derivation are considered in [41]. As applied to the right hand side of (5.83) the limit (5.84) leads to cancellation of all principal values $\mathscr{P}$. This is in accordance with the fact that (5.83) contains only real quantities. The energy and momentum conservation laws are incorporated in the obtained equation. We note that the time argument of the integrant is zero, which implies $t = t'$ and thus $\mathbf{R}(t',\mathbf{q}') = \mathbf{r}$.

The general form of the obtained Wigner–Boltzmann equation is

$$\left(\frac{\partial}{\partial t} + \frac{\mathbf{k}}{m}\cdot\nabla_{\mathbf{r}}\right) f_w(\mathbf{r},\mathbf{k},t) = \int \mathrm{d}\mathbf{k}' V_w(\mathbf{r},\mathbf{k}-\mathbf{k}') f_w(\mathbf{r},\mathbf{k}',t') + \int \mathrm{d}\mathbf{k}' \left(f_w(\mathbf{r},\mathbf{k}',t)S(\mathbf{k}',\mathbf{k}) - f_w(\mathbf{r},\mathbf{k},t)S(\mathbf{k},\mathbf{k}')\right) \tag{5.85}$$

with the particular for the electron–phonon interaction scattering rate S:

$$S(\mathbf{k}',\mathbf{k}) = \frac{2\pi}{\hbar}\frac{V}{(2\pi)^3}\Big\{|\mathscr{C}(\mathbf{q})|^2\delta(\varepsilon(\mathbf{k}) - \varepsilon(\mathbf{k}') - \hbar\omega_{\mathbf{q}})n(\mathbf{q}) + |\mathscr{C}(\mathbf{q})|^2\delta(\varepsilon(\mathbf{k}) - \varepsilon(\mathbf{k}') + \hbar\omega_{\mathbf{q}})(n(\mathbf{q})+1)\Big\}$$

where $\mathbf{q} = \mathbf{k} - \mathbf{k}'$, and C has been replaced by the electron–phonon matrix element $\mathscr{C}$: $C^2 = |\mathscr{C}|^2/(\hbar)^2$.

The interaction with phonons is now treated classically while the interaction with the Wigner potential is considered on a rigorous quantum level. We conclude by noting that a classical limit in the potential term recovers the Boltzmann equation.

3.3 Electron–Impurity Interaction

Let us now see in more detail, as was already mentioned above, how the short-range scattering by ionized impurities may be included into the Wigner transport equation. For an assembly of dopant atoms j of position $\mathbf{r}_j$ the short-range interaction potential with electrons may be written in the form of a screened Coulomb potential

$$V_{e-ii} = \sum_j \frac{e^2 \exp\left(-\beta \left|\mathbf{r}-\mathbf{r}_j\right|\right)}{4\pi\varepsilon \left|\mathbf{r}-\mathbf{r}_j\right|} \tag{5.86}$$

where ε and β are the dielectric constant and the screening factor, respectively. The corresponding Wigner potential simply writes

$$\begin{aligned} V_w(\mathbf{r},\mathbf{k}) &= \frac{i}{\hbar(2\pi)^3}\frac{e^2}{4\pi\varepsilon}\sum_j \int d\mathbf{r}' e^{-i\mathbf{k}\mathbf{r}'}\left(\frac{e^{-\beta\left|\mathbf{r}-\frac{\mathbf{r}'}{2}-\mathbf{r}_j\right|}}{\left|\mathbf{r}-\frac{\mathbf{r}'}{2}-\mathbf{r}_j\right|}-\frac{e^{-\beta\left|\mathbf{r}+\frac{\mathbf{r}'}{2}-\mathbf{r}_j\right|}}{\left|\mathbf{r}+\frac{\mathbf{r}'}{2}-\mathbf{r}_j\right|}\right) \\ &= \frac{i}{\hbar(2\pi)^3}\frac{e^2}{4\pi\varepsilon}\sum_j\left(2^3\left(e^{-2i\mathbf{k}\left(\mathbf{r}-\mathbf{r}_j\right)}-e^{2i\mathbf{k}\left(\mathbf{r}-\mathbf{r}_j\right)}\right)\int d\mathbf{r}''\frac{e^{-2i\mathbf{k}\mathbf{r}''}e^{-\beta\left|\mathbf{r}''\right|}}{\left|\mathbf{r}''\right|}\right) \\ &= \frac{i}{\hbar(\pi)^3}\frac{e^2}{\varepsilon}\sum_j\left(\left(e^{-2i\mathbf{k}\left(\mathbf{r}-\mathbf{r}_j\right)}-e^{2i\mathbf{k}\left(\mathbf{r}-\mathbf{r}_j\right)}\right)\frac{1}{4\mathbf{k}^2+\beta^2}\right) \end{aligned} \tag{5.87}$$

which leads to the quantum evolution term

$$\begin{aligned} Q f_w(\mathbf{r},\mathbf{k}) = \frac{i}{\hbar(\pi)^3}\int d\mathbf{k}' f_w\left(\mathbf{r},\mathbf{k}'\right)\frac{e^2}{\varepsilon} \\ \times\sum_j\left(\left(e^{-2i\left(\mathbf{k}-\mathbf{k}'\right)\left(\mathbf{r}-\mathbf{r}_j\right)}-e^{2i\left(\mathbf{k}-\mathbf{k}'\right)\left(\mathbf{r}-\mathbf{r}_j\right)}\right)\frac{1}{4(\mathbf{k}-\mathbf{k}')^2+\beta^2}\right) \end{aligned} \tag{5.88}$$

In this section, we assume as a simplification the external field to be zero. It is in accordance with the similar assumption that was used in the previous section regarding electron–phonon scattering. Over a trajectory initialized by $\mathbf{r}(t)=\mathbf{r},\mathbf{k},t$, where the notation implies the meaning of a usual change of variables,

$$\mathbf{r}(t) = \mathbf{R}\left(t'\right)+\frac{\hbar\mathbf{k}}{m}\left(t-t'\right)$$

in the Wigner transport equation (5.58), the left hand side term $\frac{\partial f_w(\mathbf{r},\mathbf{k},t')}{\partial t'} + \frac{\hbar\mathbf{k}}{m}\frac{\partial f_w(\mathbf{r},\mathbf{k},t')}{\partial \mathbf{r}}$ simplifies into $(\frac{\partial f_w(\mathbf{R}(t'),\mathbf{k},t')}{\partial t'})_{\mathbf{R}(t')}$. By taking (5.88) into account, the Wigner transport equation thus becomes

$$\left(\frac{\partial f_w\left(\mathbf{R}\left(t'\right),\mathbf{k},t'\right)}{\partial t'}\right)_{\mathbf{R}(t')} = \frac{i}{\hbar\left(\pi\right)^3}\int d\mathbf{k}' f_w\left(\mathbf{R}\left(t'\right),\mathbf{k}'\right)\frac{e^2}{\varepsilon}$$
$$\times\sum_j\left(\left(e^{-2i\left(\mathbf{k}-\mathbf{k}'\right)\left(\mathbf{R}\left(t'\right)-\mathbf{r}_j\right)} - e^{2i\left(\mathbf{k}-\mathbf{k}'\right)\left(\mathbf{R}\left(t'\right)-\mathbf{r}_j\right)}\right)\frac{1}{4\left(\mathbf{k}-\mathbf{k}'\right)^2+\beta^2}\right),$$

which may be integrated into

$$f_w\left(\mathbf{r},\mathbf{k}',t\right) = ic + \frac{e^2}{\varepsilon}\frac{i}{\hbar\left(\pi\right)^3}\int_0^t dt'\int d\mathbf{k}'' f_w\left(\mathbf{R}'\left(t'\right),\mathbf{k}'',t'\right)$$
$$\times\sum_j\left[\left(e^{-2i\left(\mathbf{k}'-\mathbf{k}''\right)\left(\mathbf{R}'\left(t'\right)-\mathbf{r}_j\right)} - e^{2i\left(\mathbf{k}'-\mathbf{k}''\right)\left(\mathbf{R}'\left(t'\right)-\mathbf{r}_j\right)}\right)\frac{1}{4\left(\mathbf{k}-\mathbf{k}'\right)^2+\beta^2}\right] \tag{5.89}$$

where the prime of R prompts that the trajectory is now initialized by the arguments $\mathbf{r},\mathbf{k}',t$ of the left hand side of the equation. By choosing a time origin far enough from time t, the initial condition term vanishes. Substituting (5.89) into (5.88) leads to

$$Q\,f_w\left(\mathbf{r},\mathbf{k},t\right) = -\frac{1}{\hbar^2\left(\pi\right)^6}\frac{e^4}{\varepsilon^2}\int_0^t dt'\int d\mathbf{k}'\int d\mathbf{k}'' f_w\left(\mathbf{R}'\left(t'\right),\mathbf{k}'',t'\right)$$
$$\times\sum_j\left[\left(e^{-2i\left(\mathbf{k}-\mathbf{k}'\right)\left(\mathbf{r}-\mathbf{r}_j\right)} - e^{2i\left(\mathbf{k}-\mathbf{k}'\right)\left(\mathbf{r}-\mathbf{r}_j\right)}\right)\right.$$
$$\times\left(e^{-2i\left(\mathbf{k}'-\mathbf{k}''\right)\left(\mathbf{R}'\left(t'\right)-\mathbf{r}_j\right)} - e^{2i\left(\mathbf{k}'-\mathbf{k}''\right)\left(\mathbf{R}'\left(t'\right)-\mathbf{r}_j\right)}\right)$$
$$\left.\times\left(4\left(\mathbf{k}-\mathbf{k}'\right)^2+\beta^2\right)^{-1}\left(4\left(\mathbf{k}'-\mathbf{k}''\right)^2+\beta^2\right)^{-1}\right] \tag{5.90}$$

By developing the product of exponential functions, the non-cross terms give

$$S_1 = \left(4\left(\mathbf{k}-\mathbf{k}'\right)^2+\beta^2\right)^{-1}\left(4\left(\mathbf{k}'-\mathbf{k}''\right)^2+\beta^2\right)^{-1}$$
$$\times\sum_j e^{-2i\left(\mathbf{k}-\mathbf{k}'\right)\left(\mathbf{r}-\mathbf{r}_j\right)}e^{-2i\left(\mathbf{k}'-\mathbf{k}''\right)\left(\mathbf{R}'\left(t'\right)-\mathbf{r}_j\right)} + cc \tag{5.91}$$

$$S_1 = \left(4\left(\mathbf{k}-\mathbf{k}'\right)^2+\beta^2\right)^{-1}\left(4\left(\mathbf{k}'-\mathbf{k}''\right)^2+\beta^2\right)^{-1}$$
$$\times e^{-2i\left(\mathbf{k}-\mathbf{k}'\right)\left(\mathbf{r}\right)}\,e^{-2i\left(\mathbf{k}'-\mathbf{k}''\right)\left(\mathbf{r}-\frac{\hbar\mathbf{k}'}{m}\left(t-t'\right)\right)}\sum_j e^{2i\left(\mathbf{k}-\mathbf{k}''\right)\left(\mathbf{r}_j\right)} \tag{5.92}$$

If the number of doping atoms in density N_D is assumed to be large enough the discrete sum in (5.90) can be replaced by an integral that takes the form

$$\sum_j e^{2i\left(\mathbf{k}-\mathbf{k}''\right)\mathbf{r}_j} \approx N_D \int d\,\mathbf{r}_j e^{2i\left(\mathbf{k}-\mathbf{k}''\right)\mathbf{r}_j} = N_D(2\pi)^3 \delta\left(2\left(\mathbf{k}-\mathbf{k}''\right)\right) \tag{5.93}$$

and then,

$$\begin{aligned} S_1 \approx & \left(4\left(\mathbf{k}-\mathbf{k}'\right)^2+\beta^2\right)^{-1}\left(4\left(\mathbf{k}'-\mathbf{k}''\right)^2+\beta^2\right)^{-1} e^{-2i\left(\mathbf{k}-\mathbf{k}'\right)(\mathbf{r})} \\ & \times e^{-2i\left(\mathbf{k}'-\mathbf{k}''\right)\left(\mathbf{r}-\frac{\hbar\mathbf{k}'}{m}\left(t-t'\right)\right)}\,\pi^3 N_D\,\delta\left(\mathbf{k}-\mathbf{k}''\right) \end{aligned} \tag{5.94}$$

$$S_1 \approx \pi^3\left[\frac{4}{4(\mathbf{k}-\mathbf{k}')^2+\beta^2}\right]^2 e^{-2i\left(\mathbf{k}'-\mathbf{k}\right)\left(-\frac{\hbar\mathbf{k}'}{m}\left(t-t'\right)\right)} N_D\,\delta\left(\mathbf{k}-\mathbf{k}''\right) \tag{5.95}$$

Similarly, the cross terms of the product of exponential functions in (5.90) may be written as

$$S_2 \approx \pi^3\left[\frac{1}{(\mathbf{k}-\mathbf{k}'')^2+\beta^2}\right]^2 e^{\frac{2i}{4}\left(\mathbf{k}-\mathbf{k}''\right)\left(-\frac{\hbar\left(\mathbf{k}+\mathbf{k}''\right)}{m}\left(t-t'\right)\right)} N_D\,\delta\left(\mathbf{k}-2\mathbf{k}'+\mathbf{k}''\right)+cc \tag{5.96}$$

Substituting (5.95) and (5.96) into (5.90) yields

$$\begin{aligned} Q f_w(\mathbf{r},\mathbf{k},t) = -\frac{e^4 N_D}{\hbar^2\pi^3\varepsilon^2}\int_0^t dt' \Bigg\{ & \int d\,\mathbf{k}' f_w\left(\mathbf{R}'(t'),\mathbf{k},t'\right) e^{-2i\left(\mathbf{k}'-\mathbf{k}\right)\left(-\frac{\hbar\mathbf{k}'}{m}\left(t-t'\right)\right)} \\ & \times\left(4\left(\mathbf{k}-\mathbf{k}'\right)^2+\beta^2\right)^{-2}+cc \\ & -\int d\mathbf{k}'' f_w\left(\mathbf{R}'(t'),\mathbf{k}'',t'\right) e^{2i\left(\mathbf{k}^2-\mathbf{k}''^2\right)\left(\frac{\hbar}{m}\left(t-t'\right)\right)} \\ & \left(\left(\mathbf{k}-\mathbf{k}''\right)^2+\beta^2\right)^{-2}+cc\Bigg\} \end{aligned} \tag{5.97}$$

The change of variable $2\mathbf{k}' = \mathbf{k}+\mathbf{k}''$ in the first integral of (5.97) leads to

$$\begin{aligned} Q f_w(\mathbf{r},\mathbf{k},t) = -\frac{e^4 N_D}{\hbar^2(2\pi)^3\varepsilon^2}\int_0^t dt' \Bigg\{ & \int d\mathbf{k}''\left(\left(\mathbf{k}-\mathbf{k}''\right)^2+\beta^2\right)^{-2} \\ & \Big[f_w\left(\mathbf{R}'(t'),\mathbf{k},t'\right)\, e^{2i\frac{1}{4}\left(\mathbf{k}^2-\mathbf{k}''^2\right)\left(\frac{\hbar}{m}\left(t-t'\right)\right)} \\ & -f_w\left(\mathbf{R}'(t'),\mathbf{k}'',t'\right) e^{2i\frac{1}{4}\left(\mathbf{k}^2-\mathbf{k}''^2\right)\left(\frac{\hbar}{m}\left(t-t'\right)\right)}\Big]+cc\Bigg\} \end{aligned} \tag{5.98}$$

In the limit of fast collisions, as seen for electron–phonon scattering in (5.84), we finally find:

$$\left[\frac{\partial}{\partial t}+\frac{\hbar\mathbf{k}}{m}\frac{\partial}{\partial\mathbf{r}}\right]f_w(\mathbf{r},\mathbf{k},t)=\frac{e^4N_D}{\hbar\,(2\pi)^2\,\varepsilon^2}\times\int d\,\mathbf{k}''\left\{\left(\left(\mathbf{k}-\mathbf{k}''\right)^2+\beta^2\right)^{-2}\right.$$
$$\left.\times\,\delta\left(E\left(\mathbf{k}\right)-E\left(\mathbf{k}''\right)\right)\,\left[f_w\left(\mathbf{r},\mathbf{k}'',t\right)-f_w\left(\mathbf{r},\mathbf{k},t\right)\right]\right\} \tag{5.99}$$

This equation is of the form of (5.85), and is exactly the same, as the one commonly used to model the electron/ionized impurity scattering in the Boltzmann equation (see e.g. [45] (4.24)). Once again the Wigner function allows modeling of this scattering in an intuitive and familiar way that is ideal for electron device simulation.

4 Numerical Approaches: Particle Algorithms

The first applications of the Wigner function in computational electronics are already more than two decades old. Coherent transport in one-dimensional (1D) structures have been successfully approached within deterministic methods [16]. Addressed have been issues related to the correct impose of the boundary conditions which ensure the convergency of the method as well as the discretization scheme. Latter deterministic approaches [12, 15]. have been refined towards self-consistent schemes which take into account the Poisson equation, and dissipation processes have been included by using the relaxation time approximation. The importance of the dissipative processes for the correct distribution of the charge across the device has very soon turned the attention towards the Boltzmann collision term [17]. The three dimensional space of the before- and after- scattering wave vectors has been reduced with the help of an assumption for overall transversal equilibrium to wave vector components along the transport direction.

At that time it has been recognized that an extension of the deterministic approaches to more dimensions is prohibited by the enormous increase of the memory requirements, a fact which remains true even for today's computers. Indeed, despite the progress of the deterministic Boltzmann simulators which nowadays can consider even 3D problems, the situation with Wigner model remains unchanged. The reason is that, in contrast to the Boltzmann scattering matrix, which is relatively sparse due to the δ-functions introduced by the conservation laws, the counterpart provided by the Wigner potential operator is dense.

One of the main difficulty in the implementation of the deterministic solution comes from the discretization of the diffusion term $\nabla_{\mathbf{r}}f_w$ because of the typically rapid variations of the Wigner function in the phase-space. Though a second order discretization scheme is widely used, it has been shown that first, second, third and

fourth order schemes lead to very different $I-V$ characteristics of RTDs [46]. In the case of nano-transistors, the third order is required to provide good results in subthreshold regime [47, 48].

A basic property of the stochastic methods is that they turn the memory requirements of the deterministic counterparts into computation time requirements. The efforts towards development of stochastic methods for Wigner transport begun almost two decades ago [23, 49–51]. As based on the formal analogy between the Wigner and Boltzmann equations, they have been inspired by the success of the classical device Monte Carlo methods, and thus brought the idea of numerical quantum particles.

Particle models are developed for computation of physical quantities in the framework of different kinetic theories. Actually, numerical particles emerged in the field due to the probabilistic transparency of the Boltzmann equation: the numerical concepts of the device Monte Carlo simulators are developed in accordance with the underlying physics of the transport of classical carriers. The most simple version of these simulators is built up on the free electron quasi-particle concepts of effective mass and energy dispersion. Expansions of the physical concepts with respect to the band structure, scattering mechanisms, Pauli exclusion principle etc, retain the picture of developing particles.

Further particle models are already introduced by numerical approaches. Sometimes these introduced for numerical purposes models can be used to interpret and explain the underlying physics even of pure quantum phenomena such as tunneling and interference.

Below we summarize some particle models starting with the direct application of the classical picture.

The smoothed effective potential approach, [52] utilizes classical particles to account for quantum mechanical size quantization effects. The effective potential is a smoothing of the real classical potential due to the finite size of the electron wave packet. It has been shown that the classical trajectories resulting from the effective potential have important details in common with the corresponding Bohm trajectories [53]. A further generalization of the approach replaces the action of the Hamiltonian on the wave function by the action of a classical Hamiltonian on particles with an appropriately modified potential. A set of coupled equations is obtained for the inhomogeneous equilibrium distribution function in the device and its first order correction. The effective potential, defined in terms of a pseudo-differential operator acting on the device potential, becomes also a function of the momenta of the classical particles [54, 55].

Ultrafast phenomena in photo-excited semiconductors are described by a set of coupled equations where the distributions of the electrons and holes and the inter-band polarization are treated as independent dynamical variables. If interaction processes are treated on a semiclassical level, so that all transition functions become positive, the set of equations has the structure of rate equations which can be solved by a Monte Carlo method [56]. The remarkable fact that a particle model is associated with the evolution of the inter-band polarization, a complex quantity

responsible for the coherence in the photo-generation processes, shows how the method has evolved beyond the understanding of a computer experiment which emulates natural processes.

Furthermore the positiveness of the transition functions is not a necessary condition for a Monte Carlo approach. It has been shown that the action of the Wigner potential, which is an antisymmetric quantity, gives rise to a Markov process which can be regarded as a scattering of a particle between consecutive points in the phase space [57].

Wigner trajectories have been defined by modified Hamilton equations, formulated with the help of a quantum force [50]. The latter is manifestly nonlocal in space and is expressed through the Wigner potential and function, and its derivative with respect to the momentum coordinate. The quantum force has singularities at the points where the momentum derivative of the Wigner function becomes zero. At these points trajectories can be created or destroyed [50]. Due to this Wigner trajectories can merely provide a pictorial explanation of the evolution of the quantum system and in particular nicely illustrate tunneling processes [58, 59].

In general, Wigner trajectories remain an auxiliary tool for modeling of quantum transport, unless the Wigner function in the quantum force term is assumed to be known. An appropriate approximation for a nearly equilibrium system is a displaced Maxwell–Boltzmann distribution function. It can be shown that such an assumption corresponds to the zeroth order correction in the effective potential approach. In this case the quantum force is defined everywhere except at the phase-space origin, and gives rise to an effective lowering of the peaks of the potential barriers [49]. The increase of the particle flow observed through the barriers is associated with tunneling processes.

Another particle model is introduced by Wigner paths [24, 37, 60]. It has been shown that a ballistic evolution of a δ-like contribution to the Wigner function carries its value following a classical trajectory [36]. The action of the Wigner potential operator is interpreted as scattering, which, along with the scattering by the phonons, links pieces of classical trajectories to Wigner paths. We note that, in this model, the phonon interaction is treated fully quantum mechanically according to the first-principle equation (5.65). That is, the scattering with phonons begins with exchange of half of the phonon momentum and completes after a finite time. During this time, an arbitrary number of interactions with other phonons can be initiated and/or completed. In comparison, Levinson's equation considers a single interaction with finite duration while Boltzmann scattering is instantaneous, so that the trajectory changes with the full phonon momentum. During the evolution particles accumulate a numerical quantity called weight, which carries the quantum information for the system. The weight is taken into account in the computation of the physical averages.

Next we introduce two particle models for solving the Wigner–Boltzmann equation. They unify classical and quantum regions within a single transport picture where the scattering occurs in the full wave vector space, and two dimensional devices can be considered [61–63].

Since it can take negative values in some regions of the phase space, it may look nonsensical to represent the Wigner function with particles which cannot have a "negative presence". Classically, electrons either do or do not exist. To solve this apparent inconsistency with a view to developing a statistical particle approach to the solution of the Wigner–Boltzmann equation it is necessary to give simulated particles the strange property to carry negative contributions. With this in mind, it has been suggested to describe the Wigner function as a sum of Dirac excitations still localized in the phase-space but weighted by an amplitude, called affinity in [64,65]. The particle affinities contain all the information on the quantum state of the electron system. They evolve continuously according to the local quantum evolution term of the Wigner–Boltzmann equation generated by the potential and can take negative values which are taken into account as weights in the reconstruction of the Wigner function and in the computation of all physical averages.

An alternative particle approach interprets the Wigner equation, with a Boltzmann scattering term as a Boltzmann equation with a generation term. The interaction with the Wigner potential gives rise to generation of particle pairs with opposite sign. The sign is the basic property which outlines the introduced numerical particles from classical quasi-particles. It is an important property, since positive and negative particles annihilate one another. The negative values of the Wigner function in certain phase space regions can be explained in a natural way by the accumulation of negative particles in these regions. The Wigner–Boltzmann transport process corresponds to drift, scattering, generation and annihilation of these particles.

These models present the state of the art in the field and will be described in detail in the rest of this section.

4.1 The Affinity Method

4.1.1 Principles

In this approach, the Wigner function is represented as a sum of Dirac excitations of the form

$$f_w(\mathbf{r},\mathbf{k},t) = \sum_j \delta(\mathbf{r}-\mathbf{r}_j(t))\ \delta(\mathbf{k}-\mathbf{k}_j(t))\ A_j(t) \tag{5.100}$$

In contrast to classical particles, these excitations are weighted by an amplitude A_j, called affinity, which evolves continuously under the action of the quantum evolution term of the Wigner–Boltzmann equation (5.58) which describes the non-local effect of the potential. Since the Wigner function can take negative values in the presence of quantum transport effects, the affinity may be negative too. Consistently with the Heisenberg inequalities, such excitations of negative weight cannot represent physical particles and will be called pseudo-particles. They should be considered as mathematical objects useful to solve the Wigner transport equation.

Let's remember the quantum evolution term of this equation, which writes by introducing the associated operator Q as

$$Q f_w(\mathbf{r},\mathbf{k},t) = \int d\mathbf{k}'\, V_w\left(\mathbf{r},\mathbf{k}-\mathbf{k}',t\right) f_w\left(\mathbf{r},\mathbf{k}',t\right) \tag{5.101}$$

with the Wigner potential defined by (5.59). Compared to the semi-classical Monte Carlo algorithm, one of the main changes consists of adding, at each time step, the update of the Wigner function and of the particle affinities. In a mesh of the phase-space $M(\mathbf{r},\mathbf{k})$ the quantum evolution term $Q f_w$ induces the change of the affinity of particles in the mesh according to

$$\sum_{i\in M(x,k)} \frac{dA_i}{dt} = Q f_w(\mathbf{r},\mathbf{k}) \tag{5.102}$$

which means that at each time step the affinity of all pseudo-particles in a mesh of the phase-space is updated according to the value of $Q f_w$ in this mesh. The non-local effect of the potential is thus fully applied to the affinity evolution, in contrast to the semi-classical case where the local effect of the potential gradient induces the change of wave vector. The simple idea on which is based this quantum simulation method now appears clearly. Along its trajectory a pseudo-particle scatter as a classical particle, and during a free flight the coordinates of the j-th particle obey, in the effective mass approximation,

$$\frac{d}{dt}\mathbf{r}_j = \frac{\hbar}{m}\mathbf{k}_j \tag{5.103}$$

$$\frac{d}{dt}\mathbf{k}_j = 0 \tag{5.104}$$

The wave vector of each pseudo-particle is thus constant during a free flight and can take a new value only after scattering. However, if the potential may be separated into slowly and rapidly varying parts, the slowly varying part may be treated semi-classically through the evolution of the particle wave vector under the influence of electric field while only the rapidly varying part is taken into account in the computation of the Wigner potential and in the affinity (5.102).

In the semi-classical limit, i.e. if the full potential is treated as a slowly varying quantity, the quantum evolution term $Q f_w$ is zero and the particle affinity is constant. The method turns out to be equivalent to the semi-classical Monte Carlo algorithm. It should be noted that the strong similarity and even compatibility of this technique with the conventional Monte Carlo solution of the Boltzmann equation is one of its highest advantage, which will be illustrated later.

We now detail some important specific features of the numerical implementation of the affinity method. Additional discussion may be found in [66]. Though so far the algorithm has been implemented for 1D transport problems only, i.e. with phase-space coordinates of the Wigner function reduced to (x,k), the discussion below is made in the general case of the full phase space (r, k).

4.1.2 Conservation of Affinity and Pseudo-Particle Injection

First of all, it should be reminded that in semi-classical device simulation with Ohmic contacts, the only condition of particle injection is the neutrality of real-space meshes adjacent to the Ohmic contacts. After each time step, if particles are missing in some "Ohmic" meshes with respect to the charge neutrality, the appropriate number of carriers (of affinity equal to 1) is injected in these meshes to recover the neutrality. Assuming these "Ohmic" regions to be in thermal equilibrium, an equilibrium distribution is used to select randomly their wave vector components. In this way the consistence between the distribution of potential and the average number and the distribution of particles in the device is reached. Obviously, this condition of particle injection should still be used in Wigner simulation of Ohmic contacts if the transport in the contact region is assumed to be essentially semi-classical. However, it is not enough to ensure the conservation of total affinity and charge within an algorithm in which the particle affinity evolves continuously.

Indeed, one of the most important difficulties in this MC method lies in the fact that even a particle with zero affinity may gain finite affinity through the quantum evolution term $Q f_w$ according to (5.102). It means that if there is no particle in a particular region of the phase space where the affinity should evolve, a significant error may occur with possible non-conservation of charge since the contribution of each particle to the total charge in the device is weighted by its affinity. This problem is very important for device simulation and should be fixed by implementing an appropriate algorithm to inject particles of convenient affinity.

The correct approach consists in filling the phase-space with pseudo-particles of zero affinity as follows. After each time step the quantum evolution term $Q f_w(\mathbf{r},\mathbf{k})$ is calculated in the full phase-space. If in a mesh $M(\mathbf{r},\mathbf{k})$ of the phase-space, even inside the device, the quantity $|Q f_w(\mathbf{r},\mathbf{k})|$ is finite, a pseudo-particle of zero affinity is injected in the mesh [65]. In summary, it is necessary to combine the "semi-classical injection" of particles of affinity equal to 1 at Ohmic contacts to guarantee the electrical neutrality near the contacts and the "quantum injection" of pseudo-particles of 0 affinity in all regions of the phase-space where particles are missing and where $Q f_w$ takes significant values.

4.1.3 Computation of the Wigner Potential and of the Affinity Evolution

A fundamental problem lies in the choice of the limits of integration for the calculation of the Wigner potential (5.59). There are two possible approaches depending on whether the contacts are assumed to be coherent or non-coherent. In the former case the integration is cut at a maximum size from the contact corresponding to the "coherence length" beyond which no quantum effect may occur [67], which raises the question of the relevant choice of the coherence length in the contact. In the latter case, the integration should be limited to positions $\mathbf{r}'$ such that both $\mathbf{r}-\mathbf{r}'/2$ and $\mathbf{r}+\mathbf{r}'/2$ belong to the device [68]. This approach is used in the model we have developed. However, we have checked that in the devices considered in the application

section (RTD, MOSFET), all limits of integration larger than that corresponding to the hypothesis of decoherent contacts yield the same results. This insensitivity is certainly due to the fact that in these cases contact regions, or access regions, have a semi-classical behavior dominated by scattering.

To describe the time evolution of pseudo-particle affinities, a very stable discretization scheme is required. Indeed, we observed that due to the noise inherent to the technique, the MC simulation acts as a stiff problem, which tends to make the solution of (5.102) unstable. In our model, an implicit Backward Euler scheme was finally implemented:

$$A_i(t+dt) - A_i(t) = \frac{1}{N} dt \times Q f_w(\mathbf{r}, \mathbf{k}, t+dt) \tag{5.105}$$

where N is here the number of pseudo-particles in the mesh $M(\mathbf{r}, \mathbf{k})$ of the phase space. This backward Euler scheme is implicit. It may be implemented by matrix inversion of the quantum evolution operator Q, or by using a predictor/corrector technique of high order, at least fourth order. The two techniques give the same results but the predictor/corrector one is faster. All higher precision schemes were proved to be detrimental to the simulation stability and required longer simulation time to obtain good average quantities. In particular Cayley's scheme, known to be the best technique for the evaluation of the time derivative in the deterministic solution of the Wigner–Boltzmann equation, leads to unstable results in MC simulation.

4.2 The Particle Generation Method

Monte Carlo algorithms can be devised based on the notion that the terms on right hand side of the Wigner–Boltzmann equation represent gain and loss terms for the phase space density. To introduce the ideas we consider the semiclassical Boltzmann equation.

$$\left(\frac{\partial}{\partial t} + \mathbf{v}(\mathbf{k}) \cdot \nabla_{\mathbf{r}} + \frac{1}{\hbar} \mathbf{F}(\mathbf{r}) \cdot \nabla_{\mathbf{k}}\right) f(\mathbf{r}, \mathbf{k}, t) = \int d\mathbf{k}' f(\mathbf{r}, \mathbf{k}', t) S(\mathbf{k}', \mathbf{k}) - \lambda(\mathbf{k}) f(\mathbf{r}, \mathbf{k}, t) \tag{5.106}$$

$S(\mathbf{k}, \mathbf{k}')$ denotes the transition rate from initial state $\mathbf{k}'$ to final state $\mathbf{k}$, induced by the physical scattering processes, and λ is the total scattering rate.

$$\lambda(\mathbf{k}) = \int d\mathbf{k}' S(\mathbf{k}, \mathbf{k}') \tag{5.107}$$

We note that the positive term on the RHS of (5.106) is an integral operator representing a particle gain term. In a Monte Carlo algorithm transitions from state $\mathbf{k}'$ to $\mathbf{k}$ are selected randomly from the normalized transition probability $S(\mathbf{k}, \mathbf{k}')/\lambda(\mathbf{k}')$.

The negative term on the RHS of (5.106) is local in **k**-space. In a Monte Carlo algorithm the term $-\lambda f$ gives rise to the exponential distribution for the carrier free flight time.

The Wigner–Boltzmann equation has the same structure as (5.106). We use (5.48) and augment it by a Boltzmann scattering operator.

$$\left(\frac{\partial}{\partial t} + \mathbf{v}(\mathbf{k}) \cdot \nabla_{\mathbf{r}} + \frac{1}{\hbar}\, \mathbf{F}_{\mathrm{cl}}(\mathbf{r}) \cdot \nabla_{\mathbf{k}}\right) f_{\mathrm{w}}(\mathbf{r},\mathbf{k},t) = \int d\,\mathbf{k}'\, \Gamma(\mathbf{k},\mathbf{k}')\mu(\mathbf{k}') f_{\mathrm{w}}(\mathbf{r},\mathbf{k}',t) - \mu(\mathbf{k}) f_{\mathrm{w}}(\mathbf{r},\mathbf{k},t) \tag{5.108}$$

The integral kernel Γ in this equation has the form

$$\Gamma(\mathbf{r},\mathbf{k},\mathbf{k}') = \frac{1}{\mu(\mathbf{r},\mathbf{k}')}\left[S(\mathbf{k}',\mathbf{k}) + V_{\mathrm{w}}(\mathbf{r},\mathbf{k}-\mathbf{k}') + \alpha(\mathbf{k},\mathbf{r})\,\delta(\mathbf{k}-\mathbf{k}')\right], \tag{5.109}$$

$$\mu(\mathbf{r},\mathbf{k}') = \lambda(\mathbf{r},\mathbf{k}') + \alpha(\mathbf{r},\mathbf{k}'), \tag{5.110}$$

where μ is the normalization factor. It holds

$$\int d\,\mathbf{k}'\, \Gamma(\mathbf{k},\mathbf{k}',\mathbf{r}) = 1. \tag{5.111}$$

In (5.109) a fictitious scattering mechanism

$$S_{\mathrm{self}}(\mathbf{k}',\mathbf{k}) = \alpha(\mathbf{r},\mathbf{k})\delta(\mathbf{k}-\mathbf{k}') \tag{5.112}$$

is introduced, referred to as self-scattering [69]. Mathematically, the related contributions in the gain and loss terms simply cancel and have no effect. Physically, because of the δ-function, this mechanism does not change the state of the electron and hence does not alter the free-flight trajectory. The choice of α offers a degree of freedom in the construction of a Monte Carlo algorithm, as shown below.

4.2.1 Integral Form of the Wigner–Boltzmann Equation

Equation (5.108) can be transformed into a path integral equation [70]. The adjoint integral equation, which will give rise to forward Monte Carlo algorithms, has the following integral kernel.

$$P(\mathbf{k}_f,t_f|\,\mathbf{k}_i,t_i) = \Gamma[\mathbf{k}_f,\mathbf{K}(t_f)]\;\mu[\mathbf{K}(t_f)]\exp\left\{-\int_{t_i}^{t_f}\mu[\mathbf{K}(\tau)]\,\mathrm{d}\tau\right\} \tag{5.113}$$

The kernel represents a transition consisting of a free flight starting at time t_i with initial state $\mathbf{k}_i$, followed by a scattering process to the final state $\mathbf{k}_f$ at time t_f. For the sake of brevity the **r**-dependences of Γ and μ are omitted in the following. In a

Monte Carlo simulation, the time of the next scattering event, t_f, is generated from the exponential distribution appearing in (5.113):

$$p_{\mathrm{t}}(t_f, t_i, \mathbf{k}_i) = \mu[\mathbf{K}(t_f)] \exp\left\{-\int_{t_i}^{t_f} \mu[\mathbf{K}(\tau)]\, \mathrm{d}\tau\right\} \tag{5.114}$$

We denote by $\mathbf{k}'$ the state at the end of the free flight, $\mathbf{k}' = \mathbf{K}(t_f)$. A transition from the trajectory end point $\mathbf{k}'$ to the final state $\mathbf{k}_f$ is realized using the kernel Γ. In contrast to the classical case, where P would represent a transition probability, such an interpretation is not possible in the case of the Wigner equation because P is not positive semidefinite. The problem originates from the Wigner potential, which assumes positive and negative values.

Because of its antisymmetry with respect to $\mathbf{q}$, the Wigner potential can be reformulated in terms of one positive function V_{w}^{+}

$$V_{\mathrm{w}}^{+}(\mathbf{r}, \mathbf{q}) = \max(0, V_{\mathrm{w}}(\mathbf{r}, \mathbf{q})) \tag{5.115}$$

$$V_{\mathrm{w}}(\mathbf{r}, \mathbf{q}) = V_{\mathrm{w}}^{+}(\mathbf{r}, \mathbf{q}) - V_{\mathrm{w}}^{+}(\mathbf{r}, -\mathbf{q}) \tag{5.116}$$

Then, the kernel Γ is rewritten as a sum of the following conditional probability distributions.

$$\Gamma(\mathbf{k}, \mathbf{k}') = \frac{\lambda}{\mu} s(\mathbf{k}, \mathbf{k}') + \frac{\alpha}{\mu} \delta(\mathbf{k}' - \mathbf{k}) + \frac{\gamma}{\mu} \left[w(\mathbf{k}, \mathbf{k}') - w^*(\mathbf{k}, \mathbf{k}')\right], \tag{5.117}$$

$$s(\mathbf{k}', \mathbf{k}) = \frac{S(\mathbf{k}', \mathbf{k})}{\lambda(\mathbf{k}')}, \qquad w(\mathbf{k}, \mathbf{k}') = \frac{V_{\mathrm{w}}^{+}(\mathbf{k} - \mathbf{k}')}{\gamma}, \qquad w^*(\mathbf{k}, \mathbf{k}') = w(\mathbf{k}', \mathbf{k}) \tag{5.118}$$

The normalization factor for the Wigner potential is

$$\gamma(\mathbf{r}) = \int d\,\mathbf{q} V^{+}(\mathbf{r}, \mathbf{q}). \tag{5.119}$$

In the following, different variants of generating the final state $\mathbf{k}_f$ from the kernel Γ will be discussed.

4.2.2 The Markov Chain Method

We have now to decompose the kernel P into a transition probability p and the remaining function P/p. More details on the Markov chain method can be found in [71, 72]. With respect to (5.113), one could use the absolute value of Γ as a transition probability. Practically, it is more convenient to use the absolute values of the components of Γ, giving the following transition probability.

$$p(\mathbf{k}_f, \mathbf{k}') = \frac{\lambda}{\nu} s(\mathbf{k}_f, \mathbf{k}') + \frac{\alpha}{\nu} \delta(\mathbf{k}_f - \mathbf{k}') + \frac{\gamma}{\nu} w(\mathbf{k}_f, \mathbf{k}') + \frac{\gamma}{\nu} w^*(\mathbf{k}_f, \mathbf{k}') \tag{5.120}$$

The normalization factor is

$$\nu = \int d\,\mathbf{k} f\, p(\mathbf{k}_f, \mathbf{k}') = \lambda + \alpha + 2\gamma. \tag{5.121}$$

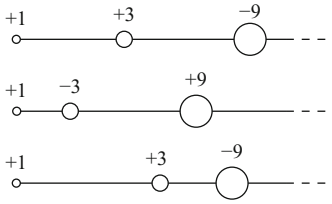

Fig. 5.2 With the Markov chain method, the number of numerical particles is conserved. The magnitude of the particle weight increases with each event, and the sign of the weight changes randomly according to a given probability distribution

In the first method considered here, the free-light time is generated from the exponential distribution (5.114). To generate the final state $\mathbf{k}_f$ for the given trajectory endpoint $\mathbf{k}'$, one of the four terms in (5.120) is selected with the associated probabilities λ/ν, α/ν, γ/ν, and γ/ν, respectively. Apparently, these probabilities sum up to one. If classical scattering is selected, $\mathbf{k}_f$ is generated from s. If self-scattering is selected, the state does not change and $\mathbf{k}_f = \mathbf{k}'$ holds. If the third or fourth term are selected, the particle state is changed by scattering from the Wigner potential and $\mathbf{k}_f$ is selected from w or w^*, respectively. The particle weight has to be multiplied by the ratio

$$\frac{\Gamma}{p} = \pm\frac{\nu}{\mu} = \pm\left(1 + \frac{2\gamma}{\lambda+\alpha}\right), \tag{5.122}$$

where the minus sign applies if $\mathbf{k}_f$ has been generated from w^*. For instance, for a quantum mechanical system, where the classical scattering rate λ is less than the Wigner scattering rate γ, the self-scattering rate α can be chosen such that $\lambda + \alpha = \gamma$. Then, the multiplier (5.122) evaluates to ± 3. An ensemble of particles would evolve as shown schematically in Fig. 5.2. As the multiplier (5.122) is always greater than one, the absolute value of the particle weight will inevitably grow with the number of transitions on the trajectory.

4.2.3 Pair Generation Method

To solve the problem of growing particle weights, one can split particles. In this way, an increase in particle weight is transformed to an increase in particle number. The basic idea of splitting is refined so as to avoid fractional weights. Different interpretations of the kernel are presented, that conserve the magnitude of the particle weight [73]. Choosing the initial weight to be $+1$, all generated particles will have weight $+1$ or -1. This is achieved by interpreting the potential operator in the Wigner–Boltzmann equation as a generation term of positive and negative particles. We consider the kernel (5.117).

$$\Gamma(\mathbf{k}_f, \mathbf{k}') = \frac{\lambda}{\mu} s(\mathbf{k}_f, \mathbf{k}') + \frac{\alpha}{\mu}\delta(\mathbf{k}_f - \mathbf{k}') + \frac{\gamma}{\mu}\left[w(\mathbf{k}_f, \mathbf{k}') - w^*(\mathbf{k}_f, \mathbf{k}')\right] \tag{5.123}$$

If the Wigner scattering rate γ is larger than the classical scattering rate λ, the self-scattering rate α has to be chosen large enough to satisfy the inequality $\gamma/\mu \leq 1$. Typical choices are $\mu = \mathrm{Max}(\lambda, \gamma)$ or $\mu = \lambda + \gamma$. These expressions also hold for the less interesting case $\gamma < \lambda$, where quantum interference effects are less important than classical scattering effects. In the following, we discuss the case $\gamma > \lambda$, where quantum effects are dominant. We choose the self-scattering rate equal to $\alpha = \gamma$ and regroup the kernel as

$$\Gamma(\mathbf{k}_f, \mathbf{k}') = \frac{\lambda}{\mu} s(\mathbf{k}_f, \mathbf{k}') + \left(1 - \frac{\lambda}{\mu}\right) \left[\delta(\mathbf{k}_f - \mathbf{k}') + w(\mathbf{k}_f, \mathbf{k}') - w^*(\mathbf{k}_f, \mathbf{k}')\right]. \quad (5.124)$$

As in the classical Monte Carlo method, the distribution of the free-flight duration is given by the exponential distribution (5.114). At the end of a free flight, classical scattering is selected with probability $p_s = \lambda/\mu$. With the complementary probability, $1 - p_s$, a self-scattering event and a pair generation event occur. The weight of the state generated from w^* is multiplied by -1. The weights of the states generated from w and from self-scattering do not change. Therefore, the magnitude of the initial particle weight is conserved, as shown in Fig. 5.3. In this algorithm, classical scattering and pair generation are complementary events and thus cannot occur at the same time, as shown in Fig. 5.4. Different choices of the self-scattering rate α result in different variants of the Monte Carlo algorithm. A more detailed discussion can be found in [73].

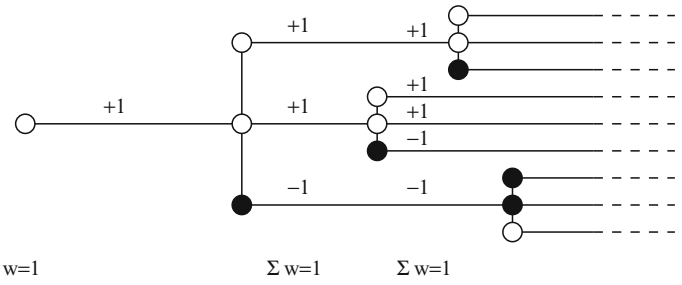

Fig. 5.3 With the pair generation method the magnitude of the particle weight is conserved, but one initial particle generates a cascade of numerical particles. At all times mass is exactly conserved

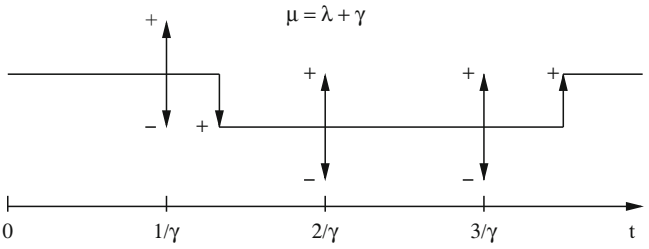

Fig. 5.4 Trajectory in k-space of a sample particle resulting from the pair-generation method. Discontinuities in the main trajectory indicate semi-classical scattering events, whereas *arrows* indicate instances when particle pairs are generated

In the pair-generation method described, the weights of the generated particles are ± 1, because the generation rate used equals 2γ (generation of one pair at a rate of γ). If a generation rate larger than 2γ or a fixed time-step less than $(2\gamma)^{-1}$ were used, the magnitude of the generated weight would be less than one. The resulting fractional weights are referred to as affinities. On the other hand, a generation rate less than 2γ would result in an under-sampling of the physical process. Then, the magnitude of the generated weights would be generally greater than one.

Instead of using $V_w^+(\mathbf{r},\mathbf{q})$ to generate the momentum transfer $\hbar\mathbf{q}$, one can construct a Monte Carlo algorithm which uses the amplitude of the Fourier transform, $A(\mathbf{q})$ in (5.33). The advantage is that the numerical representation of $A(\mathbf{q})$ only requires a discretization of the momentum coordinate, whereas for the Wigner potential $V_{\mathrm{w}}^+(\mathbf{q},\mathbf{r})$ both momentum and spatial coordinates need to be discretized.

We start with the potential operator (5.58) defined in the three-dimensional $\mathbf{k}$-space, change variables $\mathbf{q}=\mathbf{k}'-\mathbf{k}$ and $\mathbf{q}=\mathbf{k}-\mathbf{k}'$, and build a symmetrized expression.

$$Qf_{\mathrm{w}}(\mathbf{r},\mathbf{k}) = \frac{1}{2}\int d\,\mathbf{q} V_{\mathrm{w}}(\mathbf{r},\mathbf{q})\left[f_{\mathrm{w}}(\mathbf{r},\mathbf{k}-\mathbf{q}) - f_{\mathrm{w}}(\mathbf{r},\mathbf{k}+\mathbf{q})\right]. \tag{5.125}$$

Expressing the Wigner potential through the three-dimensional Fourier transform of the potential,

$$V_{\mathrm{w}}(\mathbf{r},\mathbf{q}) = \frac{2}{\hbar\pi^3} A(2\mathbf{q}) \sin\left[\varphi(2\mathbf{q}) + 2\mathbf{q}\cdot\mathbf{r}\right], \tag{5.126}$$

the potential operator (5.125) can be rewritten as

$$Qf_{\mathrm{w}}(\mathbf{r},\mathbf{k}) = \frac{1}{\hbar}\int \frac{d\,\mathbf{q}}{(2\pi)^3} A(\mathbf{q}) \sin\left[\varphi(\mathbf{q}) + \mathbf{q}\cdot\mathbf{r}\right]\left[f_{\mathrm{w}}\left(\mathbf{r},\mathbf{k}-\frac{\mathbf{q}}{2}\right) - f_{\mathrm{w}}\left(\mathbf{r},\mathbf{k}+\frac{\mathbf{q}}{2}\right)\right] \tag{5.127}$$

An advantage of this formulation is that no discretization of the spatial variable $\mathbf{r}$ is needed. The expression can be evaluated at the actual position $\mathbf{r}$ of a particle. The structure of (5.127) suggests the usage of a rejection technique. The normalization factor γ now is larger than the actual pair generation rate.

$$\gamma = \frac{1}{\hbar}\int \frac{d\,\mathbf{q}}{(2\pi)^3} A(\mathbf{q}) \tag{5.128}$$

The rate of γ is used as in the algorithms described above to randomly generate the times between two particle pair-generation events. From the distribution $A(\mathbf{q})$ one generates randomly the momentum transfer $\mathbf{q}$. Then the sine function is evaluated at the actual particle position $\mathbf{r}$.

$$s = \sin\left[\varphi(\mathbf{q}) + \mathbf{q}\cdot\mathbf{r}\right] \tag{5.129}$$

With probability $|s|$ the pair-generation event is accepted, otherwise a self-scattering event is performed. In the former case, two particle states are generated with momenta $\mathbf{k}_1 = \mathbf{k}-\mathbf{q}/2$ and $\mathbf{k}_2 = \mathbf{k}+\mathbf{q}/2$ and statistical weights $w_1 = w_0\mathrm{sign(s)}$ and $w_2 = -w_1$, respectively, where w_0 is the statistical weight of the initial particle.

4.2.4 The Negative Sign Problem

In the following, we analyze the growth rates of particle weights and particle numbers associated with the different Monte Carlo algorithms. In the Markov chain method discussed in Sect. 4.2.2, the weight increases at each scattering event by the multiplier (5.122). The growth rate of the weight can be estimated for the case of constant coefficients γ and μ. Because free-flight times are generated with rate μ, the mean free-flight time will be $1/\mu$. During a given time interval t, on average $n = \mu t$ scattering events will occur. The total weight is then estimated asymptotically for $t \gg 1/\mu$.

$$|W(t)| = \left(1 + \frac{2\gamma}{\mu}\right)^n = \left(1 + \frac{2\gamma t}{n}\right)^n \simeq \exp(2\gamma t) \tag{5.130}$$

This expression shows that the growth rate is determined by the Wigner scattering rate γ independently of the classical and the self-scattering rates. The growth rate 2γ is equal to the L_1 norm of the Wigner potential.

In the pair generation method, the potential operator

$$Qf_{\mathrm{w}}(\mathbf{k}) = \int d\,\mathbf{q}\, V^{+}(\mathbf{q}) \left[f_{\mathrm{w}}(\mathbf{k}-\mathbf{q}) - f_{\mathrm{w}}(\mathbf{k}+\mathbf{q})\right] \tag{5.131}$$

is interpreted as a generation term. It describes the creation of two new states, $\mathbf{k}-\mathbf{q}$ and $\mathbf{k}+\mathbf{q}$. The pair generation rate is equal to γ. When generating the second state, the sign of the statistical weight is changed. It should be noted that the Wigner–Boltzmann equation strictly conserves mass, as can be seen by taking the zeroth order moment of (5.108):

$$\frac{\partial n}{\partial t} + \operatorname{div} \mathbf{J} = 0 \tag{5.132}$$

Looking at the number of particles regardless of their statistical weights, that is, counting each particle as positive, would correspond to using the following potential operator:

$$Q^{*} f_{\mathrm{w}}(\mathbf{k}) = \int d\,\mathbf{q}\, V_{\mathrm{w}}^{+}(\mathbf{q}) \left[f_{\mathrm{w}}(\mathbf{k}-\mathbf{q}) + f_{\mathrm{w}}(\mathbf{k}+\mathbf{q})\right] \tag{5.133}$$

Using (5.133), a continuity equation for numerical particles is obtained as

$$\frac{\partial n^{*}}{\partial t} + \operatorname{div} \mathbf{J}^{*} = 2\gamma(\mathbf{r}) n^{*} \tag{5.134}$$

Assuming a constant γ, the generation rate in this equation will give rise to an exponential increase in the number of numerical particles N^{*}.

$$N^{*}(t) = N^{*}(0) \exp(2\gamma t) \tag{5.135}$$

This discussion shows that the appearance of an exponential growth rate is independent of the details of the particular Monte Carlo algorithm. It is a fundamental consequence of the non-positive kernel.

4.2.5 Particle Annihilation

The discussed particle models are instable, because either the particle weight or the particle number grows exponentially in time. Using the Markov chain method, it has been demonstrated that tunneling can be treated numerically by means of a particle model [74]. However, because of the exponentially increasing particle weight at the very short timescale $(2\gamma)^{-1}$, application of this algorithm turned out to be restricted to single-barrier tunneling and small barrier heights only. This method can be useful for devices where quantum effects are weak, and the potential operator is a small correction to the otherwise classical transport equation.

A stable Monte Carlo algorithm can be obtained by combining one of the particle generation methods with a method to control the particle number. One can assume that two particles of opposite weight and a sufficiently small distance in phase space annihilate each other. The reason is that the motions of both particles are governed by the same equation. Therefore, when they come close to each other at some time instant, the two particles have approximately the same initial condition. They can be considered a super particle of total weight zero, which indeed needs not be considered further in the simulation. In an ensemble Monte Carlo method, a particle removal step should be performed at given time steps. During the time step, the ensemble is allowed to grow to a certain limit, then particles are removed and the initial size of the ensemble is restored.

For a stationary transport problem a one-particle Monte Carlo method can be devised which annihilates numerical particles at the same rate as they are generated. For this purpose a phase space mesh can be utilized [75]. In the following we describe an algorithm which traces only one branch of the trajectory tree originating from a single particle injected at the contact.

After each generation event one has to deal with three particle states, namely the initial state $\mathbf{k}$ and the two generated states, $\mathbf{k}_1$ and $\mathbf{k}_2$. In a first step the weights of all three particles are stored on the annihilation mesh, that is, the statistical weight of each particle is added to a counter associated with the mesh element. Then one has to decide which of the three states is used to continue the trajectory. One may choose the weight of the continuing particle to have the same sign as the incoming one (Fig. 5.5). In this way the statistical weight along one trajectory does not change,

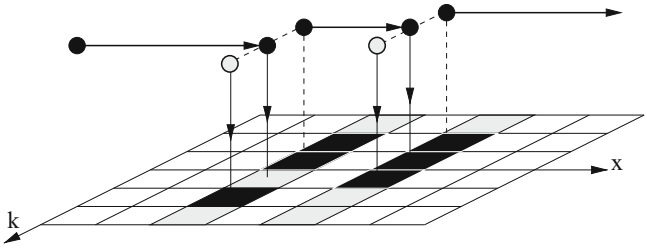

Fig. 5.5 The particle annihilation strategy attempts to minimize the weights stored in the mesh elements. The weights of the initial and continuing particle have the same sign to ensure current continuity. Particles and mesh elements carrying a positive weight are in *black*, the ones carrying a negative weight are in *grey*

which results in exact current conservation [76]. Note that because of the pair-wise generation of particles with weights ± 1 the algorithm also ensures exact mass conservation. If the initial state has a positive statistical weight, out of the three mesh elements the one with the largest stored weight is selected. Continuing from that element will reduce the weight of the element. Conversely, a negative trajectory is to be continued from the element with the smallest stored weight. A certain fraction of negative trajectories needs to be constructed in order to resolve the negative parts of the Wigner function. This rule for selecting the continuing particle is an attempt to minimize the weights stored in the three elements after each pair-generation event. The repeated execution of this rule in the Monte Carlo main loop results in a minimization of the stored weight on the whole annihilation mesh. Particle annihilation takes place when positive and negative particles are alternately stored in the same mesh element. Note that because of the mass conservation property of the transport equation and of the associated particle model, no net-charge can build up on the annihilation mesh. The weights stored on the mesh sum up to zero. The local weights on the mesh have to be kept small, as they are a measure for the numerical error of the method. This can be controlled by the fraction of negative trajectories, which has to be specified by the user.

5 Applications

For many years, the RTD was certainly the device operating at room temperature in which the wave-like behavior of electrons played the most prominent role. Thanks to the control of tunneling through the resonant state of a quantum well coupled to two electrodes via tunnel barriers, the RTD provides a negative differential resistance (NDR) in the $I-V$ characteristics. Since the pioneering works of Tsu and Esaki [77] and the first experimental evidence for NDR effect in an RTD at low temperature [78] and at room temperature [79], an intense research effort has been devoted to this fascinating device. Beyond its high potential of applications [80], the RTD is also an incomparable "toy" for fundamental physics and quantum device physics, in particular to understand the quantum features of shot noise, as in [81–87]. It is also a useful test device for new materials in which quantum transport is likely to occur, as [88–90]. Here, the RTD has been used to develop and validate the affinity technique of Wigner–Boltzmann Monte Carlo simulation. Some typical results are presented in Sect. 5.1. This device has been used also to study the impact of scattering on quantum transport and to discuss the physics of de-coherence, as reported in Sect. 5.2.

The model is then applied to the simulation of an ultra-short double-gate Metal-oxide-semiconductor Field-effect transistor (DG-MOSFET) in Sect. 5.3.

Among the new silicon-on-insulator (SOI) device architectures based on thin undoped channel controlled by multiple gates which are currently developed and envisioned to be the future of CMOS technology [91, 92], the double-gate planar configuration is one of the most promising [93] to overcome the limitations

of conventional bulk-device towards further scaling, in particular the limitations linked with the multiple sources of leakage and variability [94–97]. Compared to the single-gate SOI transistor, a second back-gate is "introduced" underneath the channel [98–101] thanks to the molecular bonding of two substrates. The electrostatics of this architecture is excellent [102]. Its main issue is the self-alignment of both gates which is required for optimized performance [98, 103]. This challenge has been recently taken up by including metal gates, high-κ dielectrics, metallic source/drain with gate length down to 6 nm [104].

5.1 Application to Resonant Tunneling Diodes

As shown schematically in Fig. 5.6 the simulated GaAs/GaAlAs RTD consists of a 5 nm-thick quantum well sandwiched between two AlGaAs barriers 0.3 eV high and 3 nm wide. The quantum well, the barriers, and 9.5 nm-thick buffer regions surrounding the barriers are slightly doped to $10^{16}\,\mathrm{cm}^{-3}$. The 50 nm-long access regions are doped to $10^{18}\,\mathrm{cm}^{-3}$. The temperature is 300 K. The scattering mechanisms considered are those due to polar optical phonons, acoustic phonons and ionized impurities, in a single Γ band with effective mass of 0.06 m_0. The transport algorithm is self-consistently coupled with the 1D Poisson equation.

Current–voltage characteristics are plotted in Fig. 5.7. The result obtained from the Wigner–Boltzmann model including scattering (circles, solid line) is compared with that given by the ballistic simulation for which scattering mechanisms have been artificially deactivated (squares, solid line) and with that obtained using a well-established ballistic Green's function technique self-consistently coupled to Poisson's equation [87]. An excellent agreement was found between both ballistic results, which suggests that the Wigner–Boltzmann Monte Carlo approach correctly handles the quantum transport effects including the resonance on a quasi-bound state. It is also clearly seen here that scattering effects dramatically reduce the peak-to-valley ratio. It is thus essential to consider them properly for room-temperature simulation of RTDs.

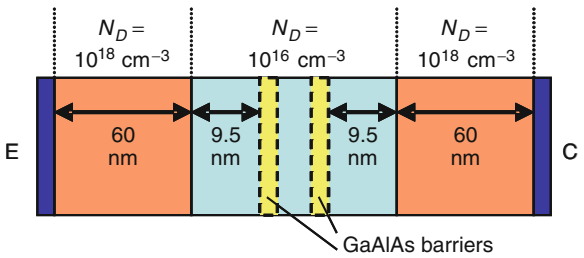

Fig. 5.6 Schematic cross-section of the simulated RTD. The GaAlAs barriers and the GaAs quantum well are 3 nm- and 5 nm-thick, respectively

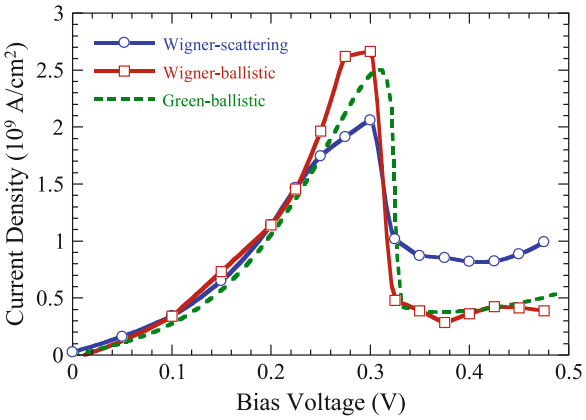

Fig. 5.7 $I-V$ characteristics of the RTD schematized in Fig. 5.6 obtained using Wigner MC simulation with scattering mechanisms activated (*circles, solid line*) or artificially deactivated (*squares, solid line*) and using ballistic Green's function simulation (*dashed line*)

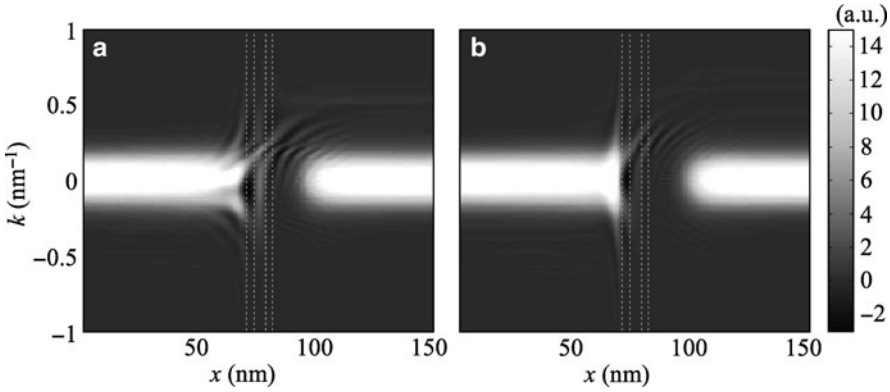

Fig. 5.8 Cartography in phase-space of the Wigner function computed (**a**) for a resonant state ($V = 0.3\,\mathrm{V}$) and (**b**) a non-resonant state ($V = 0.475\,\mathrm{V}$)

It is instructive to examine the cartography in phase-space of the Wigner function displayed in Fig. 5.8. Near the contacts, i.e. for $x < 40\,\mathrm{nm}$ and $x > 120\,\mathrm{nm}$, the Wigner function appears to be very close to a displaced Maxwellian function. The transport may be thus considered to be semi-classical in these regions. In contrast, the situation is very different in the quantum well. For the resonant state, i.e. $V = 0.3\,\mathrm{V}$ (Fig. 5.8a), between the barriers schematized by dashed lines one can see a peak (a spot) centered on $k = 0$ similar to that obtained for the Wigner function associated with the first energy level of a quantum well. This peak is due to the contribution of electrons crossing the double-barrier through the resonant state in the well. For a non-resonant state (Fig. 5.8b) this peak vanishes and becomes almost

invisible. It should also be noted that, in both cases, the oscillations of the Wigner function give rise to some negative values in small part of the phase-space (darkest shaded areas), which is the signature of quantum coherence.

The conduction band profiles plotted in Fig. 5.9 highlight the importance of the self-consistence for RTD simulation. In particular, when scattering is included a potential drop appears in the emitter region while the conduction band is flat in the ballistic case. This potential drop may induce an energy spreading of electrons, which modifies the resonant condition at $V = 0.3\,\mathrm{V}$ for electrons reaching the double barrier and contributes to the suppression of current peak at the resonance.

As shown in Fig. 5.10, a peak of electron density appears in the quantum well under resonant bias ($V = 0.3\,\mathrm{V}$), which is in accordance with the spot observed on

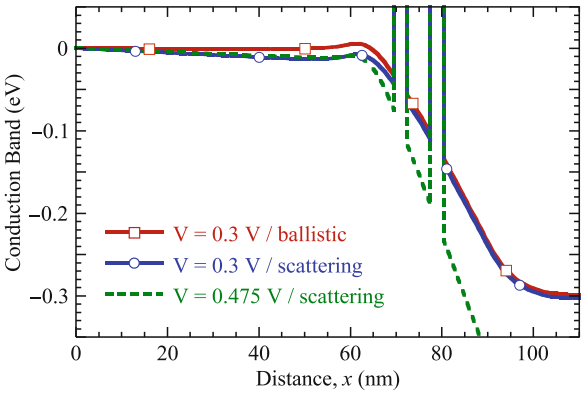

Fig. 5.9 Conduction band profile obtained by Wigner simulation, at peak ($V = 0.3\,\mathrm{V}$, *solid line, circles*) and valley ($V = 0.475\,\mathrm{V}$, *dashed line*) biases from simulation with scattering, and at peak bias (*solid line, squares*) from ballistic simulation

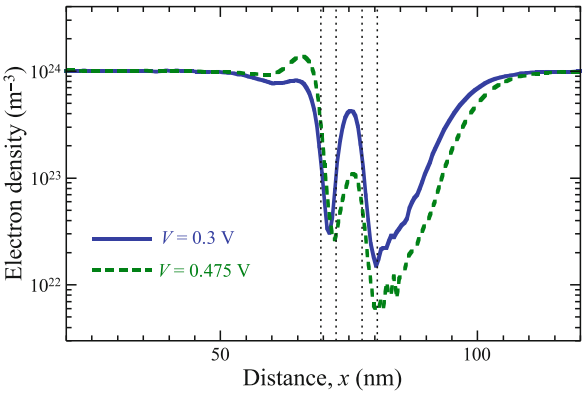

Fig. 5.10 Electron density in the RTD, obtained simulation at peak ($V = 0.3\,\mathrm{V}$, *solid line*) and valley ($V = 0.475\,\mathrm{V}$, *dashed line*) voltages from Wigner simulation with scattering

the Wigner function map (Fig. 5.8a). In off-resonance bias $V = 0.475\,\mathrm{V}$, this peak suppresses and an electron accumulation is formed in front of the double-barrier as a consequence of its weak transparency.

Finally, it should be noted that the peak-to-valley ratio obtained for typical GaAlAs/GaAs RTDs at room temperature and 77 K have been found in good agreement with experimental data [65], which suggests this MC technique is actually able to provide realistic simulation results for nano-devices exhibiting quantum transport effects with significant rates of scattering.

5.2 *Interpretation of Device Behavior Through De-Coherence Theory*

Understanding quantum transport in the presence of scattering has always been a difficult problem. Originally, there were limited available models to approach this question in electron devices, where scattering is ubiquitous. Now, with the progress of Wigner function based models – as we have seen – and of the Green's function formalism, powerful simulation tools are starting to emerge, including relatively detailed physics of scattering. However, the interpretation of their results remains difficult. This is because we are tied in our vision to the collision-less picture of quantum mechanisms that is traditionally taught in introductory quantum mechanism class. To understand device quantum physics better, a novel point of view would be therefore highly desirable.

It is thus insightful to look in fields more tightly linked to quantum mechanics than electron devices for inspiration. Particularly, in atomic physics and quantum optics, de-coherence theory has been widely successful to understand the effect of an environment (source of scattering) on a quantum system. De-coherence theory studies how the intrication between a quantum system and its environment may emerge from their interaction. This tends to lead to a separation of the system states: two different system states can intricate differently with the environment. If the system was initially in a superposition of these two states, interference between them becomes impossible after intrication with the environment. This thus leads to a suppression of some coherence effects – and to the occurrence of a more classical behavior for the system since interference may vanish. With this point of view we can even see a sort of competition between quantum coherence, and scattering leading to classical behaviors. Many more details may be found in recent excellent textbooks like [105]. It is a good lead to see if this theory highly successful in atomic physics may apply to electron devices.

The Wigner function and the density matrix are used very often in atomic physics to study de-coherence. Besides, it is encouraging to realize that our derivation of the impact of phonon scattering in Sect. 3.2 is analogous to the models commonly used for de-coherence problems. Indeed, we considered a full system consisting of the system of interest (an electron) and its environment (a phonon mode). We performed advanced derivation on the full system and then went to a reduced Wigner function

for the electron system only through a trace on the environment states (phonon numbers). It is thus very natural to look for phonon-induced de-coherence effects using our model.

In practical de-coherence studies, the density matrix is usually complementary to the Wigner function. Although our model computes a Wigner function, it is easy to switch from one formalism to another by appropriate Fourier transform. The emergence of semi-classical behaviors is very clear on the Wigner function due to the continuity between this formalism and Boltzmann's formalism. Quantum coherence is however more clearly identified in the density matrix elements.

5.2.1 Study of the Free Evolution of a Wave Packet in GaAs: Scattering-Induced De-Coherence

To understand how de-coherence occurs in electron devices we may start with a simple case: the propagation of a free wave packet. In collision-less quantum mechanics, wave packets tend to spread infinitely when propagating, becoming always more de-localized spatially, as seen in many textbooks. Is it the case in an electron device?

To answer this question we consider a simple Gaussian wave-packet

$$\psi(x) = N \exp\left[-\frac{(x-x_0)^2}{2\sigma^2}\right] \exp\left[ik_0 x\right] \tag{5.136}$$

the Wigner function of which is written

$$f_w(x,k) = N' \exp\left[-\frac{(x-x_0)^2}{\sigma^2}\right] \exp\left[-(k-k_0)^2\sigma^2\right] \tag{5.137}$$

where N and N' are normalization constants. Figures 5.11a and b show the cartography of the Wigner function and the density matrix (DM), respectively, associated with the initial state defined by $k_0 = 4 \times 10^8\,\mathrm{m}^{-1}$, $\sigma = 10\,\mathrm{nm}$. Figures 5.11c and e display the Wigner function of the wave packet after 130 fs of ballistic (no coupling with phonons) and diffusive (with phonon coupling) propagation, respectively. Phonon scattering tends to widespread the Wigner function over smaller wave vector and displacement values (Figs. 5.11e) than in the purely coherent case (Figs. 5.11c).

The density matrix allows us to analyze the situation in a smarter way. The DM associated with Wigner functions of Figs. 5.11c and e are plotted in Figs. 5.11d and f, respectively. In the ballistic case (Fig. 5.11d) all diagonal and off-diagonal elements grow from the initial state according to the natural coherent extension of the wave packet, as described in many textbooks of quantum mechanics. When including interactions with phonons (Fig. 5.11f), the result is very different. The diagonal elements still grow similarly but they extend over a larger range, as indicated by the

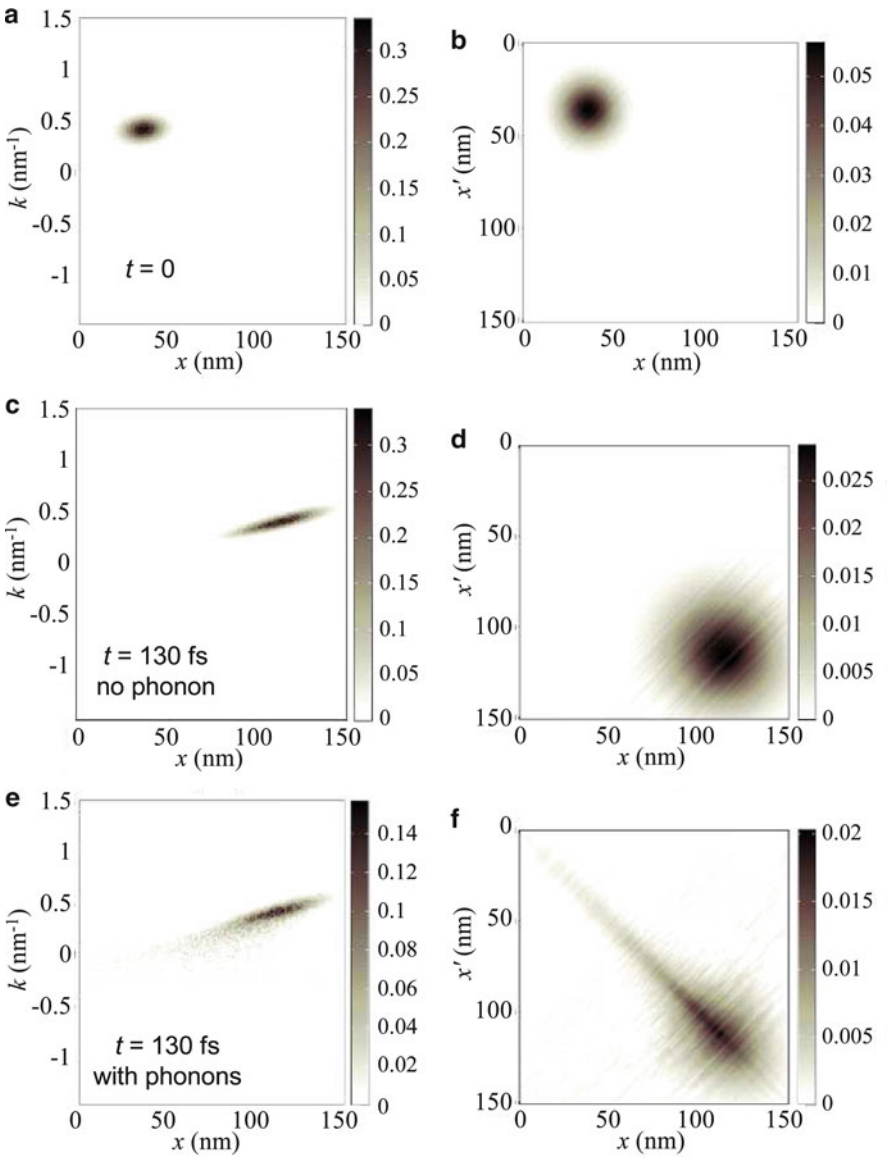

Fig. 5.11 Evolution of a free Gaussian wave packet coupled or uncoupled with a phonon bath at room temperature in GaAs. (**a**) Wigner function (WF) and (**b**) modulus of density matrix (DM) elements of the initial pure state. Simulated WF and DM after 130 fs without (**c**, **d**) or with (**e**, **f**) coupling to the phonon bath. DM elements are expressed in nm^{-1}

distribution tail at small x values. However, the off-diagonal elements do not extend as in the coherent case. They actually reduce as a function of time. It seems that actually the wave packet does not extend but splits into different wave packets which are not more de-localized than in the initial state. The quantum extension of the wave

packet is inhibited by interactions with phonons. In other words, phonon scattering prevent the wave packet from de-localizing as in the case of free propagation. Many more details may be found in [10].

5.2.2 Reinterpretation of the RTD Behavior: De-Coherence and Quantum/Semi-Classical Transition

After this academic study of wave packets, we may turn to the simulation of the RTD presented in the previous section, including the same phonon and impurity scattering mechanisms.

Figure 5.8 shows the Wigner function of the RTD operating at peak voltage ($V = 0.3\,\mathrm{V}$). In a large part of access regions ($x < 30\,\mathrm{nm}$ and $x > 120\,\mathrm{nm}$) the transport is essentially semi-classical and the Wigner function matches very well a semi-classical distribution function represented by a displaced Maxwellian function. Inside the quantum well the Wigner function around $k = 0$ is similar to that of the Wigner function of the first bound state in a square potential [106]. In the overall active region of the device, oscillations of the Wigner function reveal the presence of spatial coherence. Hence, there is apparently a transition between coherent quantum and semi-classical regions within the device. To understand better this behavior and the de-coherence effect, it is insightful to analyze the density matrix associated with the Wigner function for different strengths of electron–phonon scattering.

Accordingly, the density matrix is displayed in Figs. 5.12a–c for three different scattering situations. In Fig. 5.12a the transport is fully ballistic in the active region, which means that phonon scattering has been artificially switched off. In Fig. 5.12b standard scattering rates were used as for the Wigner function plotted in Fig. 5.8. In Fig. 5.12c phonon scattering rates have been artificially multiplied by five.

In the ballistic case a strong coherence is observed between electrons in the quantum well and in the emitter region. The amplitude of off-diagonal elements is even significant between electrons in collector and emitter regions, which is a clear indication of a coherent transport regime. When including standard scattering rates the off-diagonal elements are strongly reduced. When phonon scattering rates are artificially multiplied by five, the off-diagonal elements of the density matrix vanish, i.e. the coherence between electrons on left and right sides almost disappears. The process of double barrier tunneling is thus no longer fully resonant. Electrons can be seen as entering and leaving the quasi-bound state in distinct processes, with the possibility of energy exchange with the phonons. This illustrates the well-known coherent versus sequential tunneling situation.

This phonon-induced transition between coherent and sequential tunneling regimes manifests itself in the current–voltage characteristics of the RTD plotted in Fig. 5.13 for the three scattering situations. Phonon scattering tends to suppress the resonant tunneling peak while the valley current increases to such a point that the negative differential conductance effect almost disappears. The device tends to behave as two incoherent tunneling resistances connected in series for which a semi-classical-type description could be accurate enough.

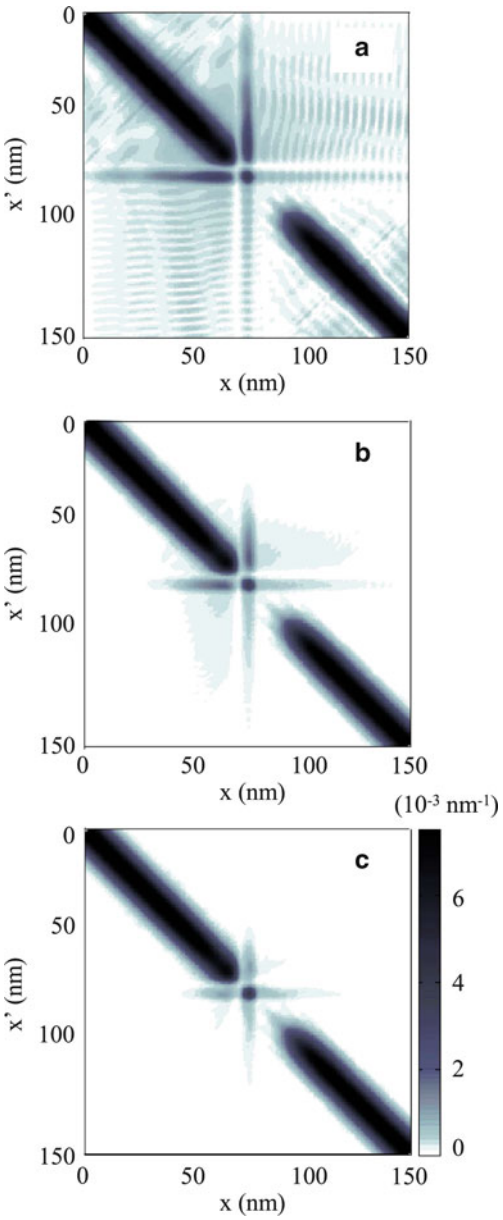

Fig. 5.12 Density matrix of a RTD operating at peak voltage for three: (**a**) no scattering, (**b**) standard phonon scattering rates, (**c**) standard rates multiplied by 5

All these considerations give a clear view of how electrons are de-localized in the active part of the device and become more localized in the access region. As already observed from the Wigner function displayed in Fig. 5.8, this suggests a transition from "quantum" to "semiclassical" transport from the active region to the access ones. More advanced considerations about this transition may be found in [10].

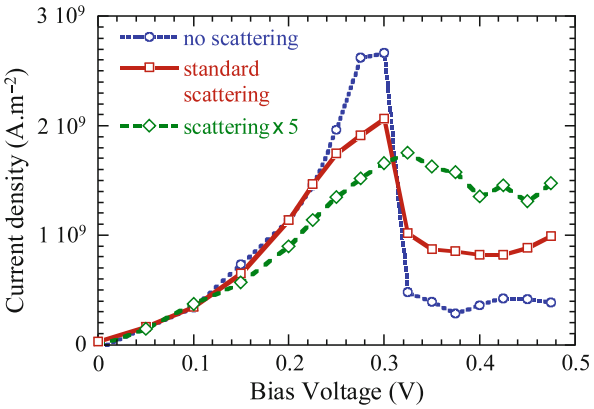

Fig. 5.13 $I-V$ characteristics for the RTD obtained from Wigner simulation, with scattering artificially deactivated (*empty circles*), with standard scattering (*squares*), and scattering rates artificially multiplied by 5 (*diamonds*)

5.3 Application to Nano-Scale Transistors

As a last illustration of application of the Wigner–Boltzmann MC method, we present here some results obtained for the ultra-small MOSFET with self-aligned double-gate, schematized in Fig. 5.14. It is inspired by the recommendations of the 2005 and 2007 ITRS Edition for the High-Performance 16 nm technology node [93] scheduled to be available in 2019. This DG-MOSFET structure is typical of a possible design for implementation in standard CMOS technology in the future.

The gate length is $L_G = 6\,\text{nm}$, the silicon film thickness is $T_{Si} = 3\,\text{nm}$ and the equivalent gate oxide thickness is aggressively scaled to $EOT = 0.5\,\text{nm}$. The source and drain access are 15 nm long and doped to $5 \times 10^{19}\,\text{cm}^{-3}$. The gate metal work function is 4.36 eV and the supply voltage is $V_{DD} = 0.7\,\text{V}$. The tunneling through gate oxide layers is not considered here. It is assumed indeed that silicon oxide may be replaced by high-κ material of same EOT and higher physical thickness to control this effect without degrading the interface quality. All simulations were performed at room temperature.

The DG-MOSFET is simulated here in the multi-sub-band mode-space approximation which decouples the gate-to-gate z direction and the xy plane parallel to interfaces. Assuming the potential V to be y-independent, the formation of uncoupled sub-bands may be simply deduced from the effective 1D Schrödinger's equation to be solved at each position x_i in the channel self-consistently with 2D Poisson's equation. Each resulting sub-band profile $E_n(x)$ is used as potential energy for the particle transport along the source-to-drain axis in the sub-band. The transport can be treated either semi-classically using the Boltzmann algorithm or in a quantum way using the Wigner–Boltzmann method. In this approach, the sub-bands

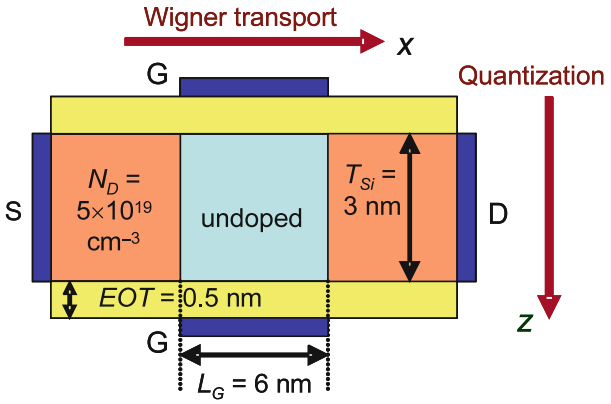

Fig. 5.14 Schematic cross-section of the simulated DG-MOSFET structure

are assumed to be independent and coupled only by scattering mechanisms. In its semi-classical form this technique has been developed in several groups [107–110].

To treat the 2D electron gas, the MC procedure makes use here of scattering rates calculated according to the envelope functions whose dependence on time and position generates an additional difficulty. In contrast to the case of standard Monte Carlo simulation, it is no longer possible to store the scattering rates in a look-up table prior to the simulation. They have to be regularly updated throughout the simulation. Phonon and ionized impurity scattering rates are derived as in [111] where 2D electron mobility in Si/SiGe heterostructures was calculated in good agreement with experimental data. The oxide interface roughness scattering rate is calculated by considering both the classical effect of electrostatic potential fluctuations [112] and the quantum effect on eigen-energies [113] which becomes significant for Si film thickness smaller than 5 nm [114]. Standard parameters, i.e. root-mean-square $\Delta_m = 0.5$ nm and correlation length $L_C = 1.5$ nm, are used to characterize the surface roughness.

5.3.1 Quantum Transport Effects

First of all, we look at the current–voltage characteristics of the transistor. The transfer characteristics $I_D - V_{GS}$ obtained at room temperature are plotted in Figs. 5.15 and 5.16 for low and high drain bias, respectively. In these figures the Wigner simulation results are systematically compared with that of two other mode-space approaches: (i) the comparison with the semi-classical Boltzmann MC model (triangles, solid lines) which includes scattering will show the impact of quantum transport and (ii) the comparison with a quantum ballistic model based on the non-equilibrium Green's function formalism (NEGF) (circles, dashed lines) [115] will show the impact of scattering.

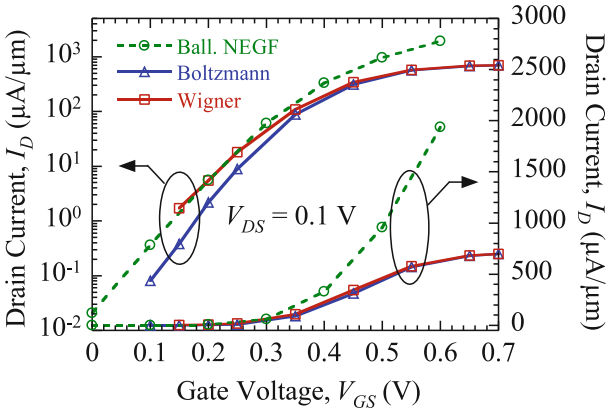

Fig. 5.15 Transfer characteristics obtained at $V_{DS} = 0.1$ V using three types of mode-space simulation, i.e. Wigner MC (*squares, solid lines*) Boltzmann MC (*triangles, solid lines*) and ballistic Green's function (*circles, dashed lines*). Both MC simulations include scattering. Results are displayed in both log and linear scale. $T = 300$ K

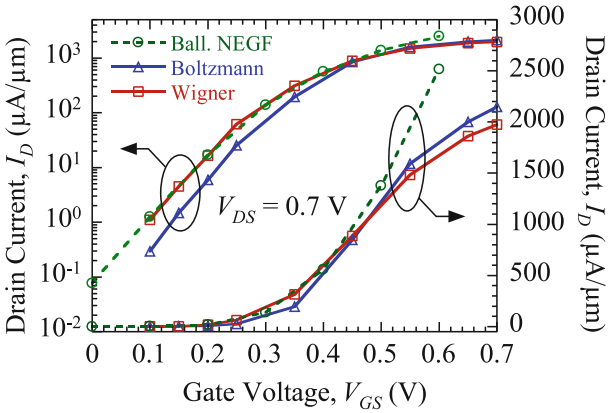

Fig. 5.16 Transfer characteristics obtained at $V_{DS} = 0.7$ V using three types of mode-space simulation, i.e. Wigner MC (*squares, solid lines*) Boltzmann MC (*triangles, solid lines*) and ballistic Green's function (*circles, dashed lines*). $T = 300$ K

Let us first consider the results obtained at low V_{GS} (subthreshold regime) and low V_{DS} (see Fig. 5.15). Wigner and Boltzmann curves are very different in this regime. The semi-classical simulation gives a better subthreshold slope than the quantum approach (70 mV dec^{-1} vs 80 mV dec^{-1}) and an off-state current I_{OFF} (extrapolated at $V_{GS} = 0$ V) five times smaller. The subthreshold current is thus strongly influenced by quantum transport at this ultra-small gate length, which may be easily understood. The additional current is nothing but a tunneling current of electrons flowing from the source to the drain through the gate-induced potential barrier.

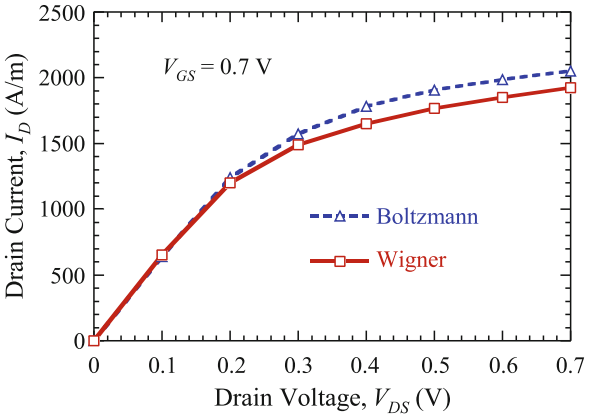

Fig. 5.17 Drain current as a function of drain voltage obtained at $V_{GS} = 0.7\,\mathrm{V}$ using Wigner MC (*squares, solid lines*) and Boltzmann MC (*triangles, dashed lines*) simulation

Since the source-drain tunneling current is especially strong in the subthreshold regime, it is interesting to compare quantum models, i.e. Wigner MC and ballistic NEGF results. It is remarkable that they coincide closely, which confirms that scattering mechanisms have a very small impact in this regime.

The situation is dramatically different at high gate voltage. One observes in Figs. 5.15 and 5.16 that Wigner and Green simulations provide very different results, which means that scattering has an important influence on the current, both at low V_{DS} (Ohmic regime) and at high V_{DS} (saturation regime). In contrast, the Wigner current becomes quite close to the Boltzmann one and even similar at low V_{DS}. Surprisingly enough, by looking at the currents obtained at high V_{DS} (Fig. 5.16), one can observe that beyond a given gate voltage the Wigner current becomes smaller than the Boltzmann current [62]. To understand this behavior the $I_D - V_{DS}$ characteristics obtained at $V_{GS} = V_{DD} = 0.7\,\mathrm{V}$ from both Wigner and Boltzmann models are plotted in Fig. 5.17.

As already remarked just above, both currents are very similar at low V_{DS}, which suggests that quantum transport effects are negligible in Ohmic regime. At higher drain voltage two quantum effects compete. In one hand the tunneling source-drain current tends to enhance the total drain current, but on the other hand quantum reflections may occur at high drain bias due to the sharp potential drop at the drain-end of the channel, which contributes to reducing the drain current. Actually, the height of the gate-induced barrier being small in this regime the contribution of the tunneling current becomes quite weak, which makes the reflection effect significant. More details on this effect may be found in [62].

To illustrate these quantum effects the phase-space cartography of the Wigner function in the first sub-band is compared to that of the Boltzmann function in Fig. 5.18 at given bias $V_{GS} = 0.45\,\mathrm{V}$ and $V_{DS} = 0.7\,\mathrm{V}$. Both functions are very similar in the source region. The main feature of the Boltzmann function in the channel is the stream of hot electrons which forms the ballistic peak (Fig. 5.18a). In contrast,

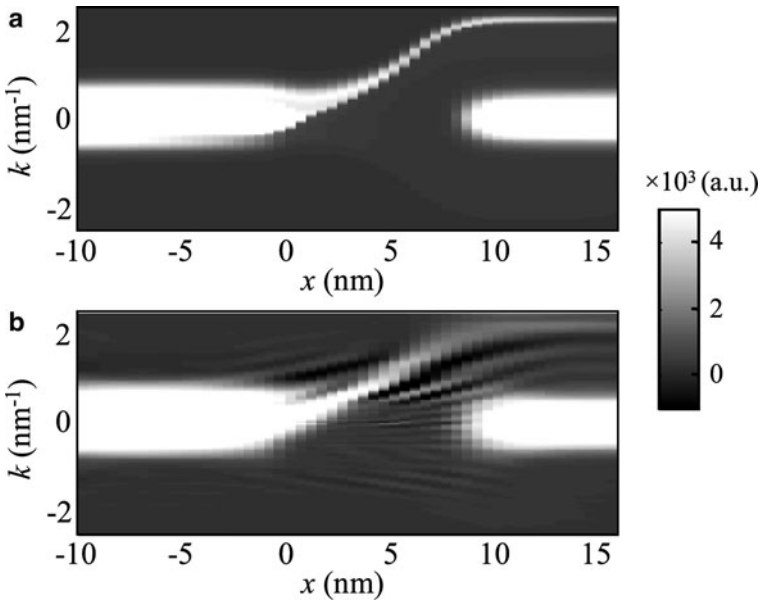

Fig. 5.18 Cartography of (**a**) Boltzmann and (**b**) Wigner functions of the first sub-band for VGS = 0.45 V and VDS = 0.7 V. The gated part of the channel extends from x = 0 to x = 6 nm

though this peak is still visible on the Wigner function (Fig. 5.18b), strong positive/negative oscillations of the Wigner function are observed where the quantum reflections occur, i.e. in the part of the channel falls abruptly, between the top of the barrier and the drain-end.

5.3.2 Impact of Scattering

We now examine the impact of scattering on device performance and operation above threshold voltage since it has been shown to be important at high gate voltage V_{GS}. In conventional MOSFET with long gate, the current is proportional to the carrier mobility in the channel. It is thus strongly dependent on scattering in the channel. In nano-transistors the channel resistance is reduced and may become comparable to that in the access regions. Hence, scattering in the access might have a significant influence on the device characteristics.

To understand the overall impact of scattering in the different parts of the device, transfer characteristics are compared in Fig. 5.19. Results of three types of simulation are plotted: (a) Ballistic Green's function method ("Ball. NEGF"), with ballistic transport in both access regions and in channel, (b) Wigner MC with scattering everywhere ("Wigner") and (c) Wigner MC with scattering activated in the access regions but deactivated in the channel ("Wigner–Ball. Channel").

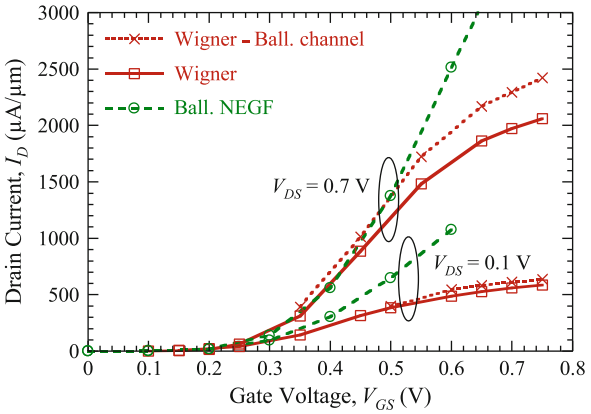

Fig. 5.19 Transfer characteristics for $V_{DS} = 0.1\,\mathrm{V}$ and $V_{DS} = 0.7\,\mathrm{V}$. The results are shown for three types of simulation: ballistic NEGF, Wigner MC and Wigner MC with all scattering mechanisms deactivated in the gated part of the channel

In Ohmic regime, i.e. at low V_{DS}, the current is strongly limited by access resistances for $V_{GS} > 0.5\,\mathrm{V}$. For $V_{GS} = 0.6\,\mathrm{V}$ the Wigner drain current is two times smaller than in the NEGF simulation. The source access resistance reaches $140\,\Omega\,\mu\mathrm{m}$ while the target value of ITRS 2005 was $60\,\Omega\,\mu\mathrm{m}$ only. This problem is critical in ultra-thin structures where T_{Si} is reduced to control short-channel effects. However, it should be noted that in the 2007 edition the ITRS target for HP16 node is raised to $145\,\Omega\,\mu\mathrm{m}$, i.e. close to the simulated value.

At high V_{DS} the impact of scattering is less pronounced but still important. The transconductance $g_m = \partial I_D / \partial V_{GS}$ is frequently used as factor of merit to assess the transistor performance. Ballistic NEGF simulation strongly overestimates g_m which appears to be limited by scattering occurring both in the access and in the channel. With ballistic channel and scattering only in access regions, the transconductance is improved by 18% with respect to standard Wigner simulation ($7090\,\mu\mathrm{A}\,\mu\mathrm{m}^{-1}$ instead of $5970\,\mu\mathrm{A}\,\mu\mathrm{m}^{-1}$) and the ON-current I_{ON} is enhanced by 16% ($2290\,\mu\mathrm{A}\,\mu\mathrm{m}^{-1}$ instead of $1970\,\mu\mathrm{A}\,\mu\mathrm{m}^{-1}$). Thus, in spite of the strong part of ballistic transport in ultra-short MOSFET [116], scattering still has a significant influence, both in the channel and the highly-doped source access region. When artificially enhancing the scattering rates in DG-MOSFET, the detailed analysis of de-coherence has shown that scattering plays an important role in the emergence of the semi-classical behavior at longer gate length, i.e. of the localization of electrons [21].

Acknowledgments This work has been partially supported by the: **European Community** through Projects PULLNANO (FP6-IST-026828), SINANO (FP6-IST-506844) and NANOSIL (FP7-ICT-216171); **French Agence Nationale de la Recherche** through Project MODERN (ANR-05-NANO-02); **Austrian Science Fund** through Projects FWF-P21685, P17285-N02 and F2509 (SFB 025 IR-ON).

References

1. H. Weyl, "Quantenmechanik und Gruppentheorie," *Zeitschrift fr Physik*, vol. 46, pp. 1–46, 1927.
2. E. Wigner, "On the quantum corrections for thermodynamic equilibrium," *Physical Review*, vol. 40, pp. 749–759, 1932.
3. J. E. Moyal, "Quantum mechanics as a statistical theory," *Proceedings of the Cambridge Philosophical Society*, vol. 45, pp. 99–124, 1949.
4. V. I. Tatarskii, "The Wigner Representation of Quantum Mechanics," *Sov. Phys. Usp.*, vol. 26, pp. 311–327, 1983.
5. N. C. Dias and J. N. Prata, "Admissible states in quantum phase space," *Annals of Physics*, vol. 313, pp. 110–146, 2004.
6. D. K. Ferry, R. Akis, and J. P. Bird, "Einselection in action: decoherence and pointer states in open quantum dots," *Physical Review Letters*, vol. 93, p. 026803, 2004.
7. I. Knezevic, "Decoherence due to contacts in ballistic nanostructures," *Physical Review B*, vol. 77, p. 125301, 2008.
8. F. Buscemi, P. Bordone, and A. Bertoni, "Simulation of decoherence in 1D systems, a comparison between distinguishable- and indistinguishable-particle collisions," *Physica Status Solidi (c)*, vol. 5, pp. 139–142, 2008.
9. F. Buscemi, E. Cancellieri, P. Bordone, A. Bertoni, and C.Jacoboni, "Electron decoherence in a semiconductor due to electron-phonon scattering," *Physica Status Solidi (c)*, vol. 5, pp. 52–55, 2008.
10. D. Querlioz, J. Saint-Martin, A. Bournel, and P. Dollfus, "Wigner Monte Carlo simulation of phonon induced electron decoherence in semiconductor nanodevices," *Physical Review B*, vol. 78, p. 165306, 2008.
11. R. Balescu, *Equilibrium and Nonequilibrium Statistical Mechanics*. Wiley and Sons, 1975.
12. N. C. Kluksdahl, A. M. Kriman, D. K. Ferry, and C. Ringhofer, "Self-consistent study of resonant-tunneling diode," *Physical Review B*, vol. 39, pp. 7720–7734, 1989.
13. A. Gehring and H. Kosina, "Wigner-Function Based Simulation of Classic and Ballistic Transport in Scaled DG-MOSFETs Using the Monte Carlo Method," *Journal of Computational Electronics*, vol. 4, pp. 67–70, 2005.
14. P. Carruthers and F. Zachariasen, "Quantum Collision Theory with Phase-Space Distributions," *Rev.Mod.Phys.*, vol. 55, no. 1, pp. 245–285, 1983.
15. B. Biegel and J. Plummer, "Comparison of self-consistency iteration options for the Wigner function method of quantum device simulation," *Physical Review B*, vol. 54, pp. 8070–8082, 1996.
16. W. Frensley, "Wigner-Function Model of Resonant-Tunneling Semiconductor Device," *Physical Review B*, vol. 36, no. 3, pp. 1570–1580, 1987.
17. W. Frensley, "Boundary conditions for open quantum systems driven far from equilibrium," *Reviews of Modern Physics*, vol. 62, no. 3, pp. 745–789, 1990.
18. K. Gullapalli, D. Miller, and D. Neikirk, "Simulation of quantum transport in memory-switching double-barrier quantum-well diodes," *Physical Review B*, vol. 49, pp. 2622–2628, 1994.
19. F. A. Buot and K. L. Jensen, "Lattice Weil-Wigner Formulation of Exact-Many Body Quantum-Transport Theory and Applications to Novel Solid-State Quantum-Based Devices," *Physical Review B*, vol. 42, no. 15, pp. 9429–9457, 1990.
20. R. K. Mains and G. I. Haddad, "Wigner function modeling of resonant tunneling diodes with high peak-to-valley ratios," *Journal of Applied Physics*, vol. 64, pp. 5041–5044, 1988.
21. D. Querlioz, H. N. Nguyen, J. Saint-Martin, A. Bournel, S. Galdin-Retailleau, and P. Dollfus, "Wigner-Boltzmann Monte Carlo approach to nanodevice simulation: from quantum to semi-classical transport," *Journal of Computational Electronics*, vol. 8, pp. 324–335, 2009.
22. M. Nedjalkov, "Wigner transport in presence of phonons: Particle models of the electron kinetics," in *From Nanostructures to Nanosensing Applications, Proceedings of the International School of Physics 'Enrico Fermi'* (A. P. A. D'Amico, G. Balestrino, ed.), vol. 160, (Amsterdam), pp. 55–103, IOS Press, 2005.

23. F. Rossi, C.Jacoboni, and M.Nedjalkov, "A Monte Carlo Solution of the Wigner Transport Equation," *Semiconductor Sci. Technology*, vol. 9, pp. 934–936, 1994.
24. P. Bordone, M. Pascoli, R. Brunetti, A. Bertoni, and C. Jacoboni, "Quantum transport of electrons in open nanostructures with the Wigner-function formalism," *Physical Review B*, vol. 59, no. 4, pp. 3060–3069, 1999.
25. I. Levinson, "Translational invariance in uniform fields and the equation for the density matrix in the Wigner representation," *Soviet Phys. JETP*, vol. 30, no. 2, pp. 362–367, 1970.
26. J. R. Barker and D. K. Ferry, "Self-Scattering Path-Variable Formulation of High Field, Time-Dependent Quantum Kinetic Equations for Semiconductor Transport in the Finite-Collision-Duration Regime," *Physical Review Letters*, vol. 42, no. 26, pp. 1779–1781, 1979.
27. M. Nedjalkov, D. Vasileska, D. Ferry, C. Jacoboni, C. Ringhofer, I. Dimov, and V. Palankovski, "Wigner transport models of the electron-phonon kinetics in quantum wires," *Physical Review B*, vol. 74, pp. 035311–1–035311–18, July 2006.
28. J. Schilp, T. Kuhn, and G. Mahler, "Electron-phonon quantum kinetics in pulse-excited semiconductors: Memory and renormalization effects," *Physical Review B*, vol. 50, no. 8, pp. 5435–5447, 1994.
29. C. Fuerst, A. Leitenstorfer, A. Laubereau, and R. Zimmermann, "Quantum Kinetic Electron-Phonon Interaction in GaAs: Energy Nonconserving Scattering Events and Memory Effects," *Physical Review Letters*, vol. 78, pp. 3733–3736, 1997.
30. P. Bordone, D. Vasileska, and D. Ferry, "Collision-Duration Time for Optical-Phonon Emission in Semiconductors," *Physical Review B*, vol. 53, no. 7, pp. 3846–3855, 1996.
31. T. Kuhn and F. Rossi, "Monte Carlo Simulation of Ultrafast Processes in Photoexcited Semiconductors: Coherent and Incoherent Dynamics," *Physical Review B*, vol. 46, pp. 7496–7514, 1992.
32. F. Rossi and T. Kuhn, "Theory of Ultrafast Phenomena in Photoexcited Semiconductors," *Reviews of Modern Physics*, vol. 74, pp. 895–950, July 2002.
33. K. Thornber, "High-field electronic conduction in insulators," *Solid-State Electron.*, vol. 21, pp. 259–266, 1978.
34. J. Barker and D. Ferry, "On the Physics and Modeling of Small Semiconductor Devices–I," *Solid-State Electron.*, vol. 23, pp. 519–530, 1980.
35. M. V. Fischetti, "Monte Carlo Solution to the Problem of High-Field Electron Heating in SiO_2," *Physical Review Letters*, vol. 53, no. 3, p. 1755, 1984.
36. C. Jacoboni, A. Bertoni, P. Bordone, and R. Brunetti, "Wigner-function Formulation for Quantum Transport in Semiconductors: Theory and Monte Carlo Approach," *Mathematics and Computers in Simulations*, vol. 55, no. 1-3, pp. 67–78, 2001.
37. P. Bordone, A. Bertoni, R. Brunetti, and C. Jacoboni, "Monte Carlo simulation of quantum electron transport based on Wigner paths," *Mathematics and Computers in Simulation*, vol. 62, p. 307, 2003.
38. P. Lipavski, F. Khan, F. Abdolsalami, and J. Wilkins, "High-Field Transport in Semiconductors. I. Absence of the Intra-Collisional Field Effect," *Physical Review B*, vol. 43, no. 6, pp. 4885–4896, 1991.
39. T. Gurov, M. Nedjalkov, P. Whitlock, H. Kosina, and S. Selberherr, "Femtosecond relaxation of hot electrons by phonon emission in presence of electric field," *Physica B*, vol. 314, pp. 301–304, 2002.
40. M. Nedjalkov, D. Vasileska, E. Atanassov, and V. Palankovski, "Ultrafast Wigner Transport in Quantum Wires," *Journal of Computational Electronics*, vol. 6, pp. 235–238, 2007.
41. C. Ringhofer, M. Nedjalkov, H. Kosina, and S. Selberherr, "Semi-Classical Approximation of Electron-Phonon Scattering beyond Fermi's Golden Rule," *SIAM Journal of Applied Mathematics*, vol. 64, pp. 1933–1953, 2004.
42. M. Herbst, M. Glanemann, V. Axt, and T. Kuhn, "Electron-phonon quantum kinetics for spatially inhomogenenous excitations," *Phisical Review B*, vol. 67, pp. 195305–1–195305–18, 2003.
43. P. Bordone, A. Bertoni, R. Brunetti, and C. Jacoboni, "Monte Carlo Simulation of Quantum Electron Transport Based on Wigner Paths," *Mathematics and Computers in Simulation*, vol. 62, pp. 307–314, 2003.

44. R. Brunetti, C. Jacoboni, and F. Rossi, "Quantum theory of transient transport in semiconductors: A Monte Carlo approach," *Physical Review B*, vol. 39, pp. 10781–10790, May 1989.
45. B. K. Ridley, *Quantum processes in semiconductors*. Oxford University Press, fourth ed., 1999.
46. K.-Y. Kim and B. Lee, "On the high order numerical calculation schemes for the Wigner transport equation," *Solid-State Electronics*, vol. 43, pp. 2243–2245, 1999.
47. Y. Yamada, H. Tsuchiya, and M. Ogawa, "Quantum Transport Simulation of Silicon-Nanowire Transistors Based on Direct Solution Approach of the Wigner Transport Equation," *IEEE Trans. Electron Dev.*, vol. 56, pp. 1396–1401, 2009.
48. S. Barraud, "Phase-coherent quantum transport in silicon nanowires based on Wigner transport equation: Comparison with the nonequilibrium-Green-function formalism," *Journal of Applied Physics*, vol. 106, p. 063714, 2009.
49. H. Tsuchiya and U. Ravaioli, "Particle Monte Carlo Simulation of Quantum Phenomena in Semiconductor Devices," *J.Appl.Phys.*, vol. 89, pp. 4023–4029, April 2001.
50. R. Sala, S. Brouard, and G. Muga, "Wigner Trajectories and Liouville's theorem," *J. Chem. Phys.*, vol. 99, pp. 2708–2714, 1993.
51. P. Vitanov, M. Nedjalkov, C. Jacoboni, F. Rossi, and A. Abramo, "Unified Monte Carlo Approach to the Boltzmann and Wigner Equations," in *Advances in Parallel Algorithms* (Bl. Sendov and I. Dimov, eds.), pp. 117–128, IOS Press, 1994.
52. D. Ferry, R. Akis, and D. Vasileska, "Quantum Effect in MOSFETs: Use of an Effective Potential in 3D Monte Carlo Simulation of Ultra-Schort Channel Devices," *Int.Electron Devices Meeting*, pp. 287–290, 2000.
53. L. Shifren, R. Akis, and D. Ferry, "Correspondence Between Quantum and Classical Motion: Comparing Bohmian Mechanics with Smoothed Effective Potential Approach," *Phys.Lett.A*, vol. 274, pp. 75–83, 2000.
54. S. Ahmed, C. Ringhofer, and D. Vasileska, "An Effective Potential Aprroach to Modeling 25nm MOSFET Devices," *Journal of Computational Electronics*, vol. 2, pp. 113–117, 2003.
55. C. Ringhofer, C. Gardner, and D. Vasileska, "An Effective Potentials and Quantum Fluid Models: A Thermodynamic Approach," *Journal of High Speed Electronics and Systems*, vol. 13, pp. 771–801, 2003.
56. S. Haas, F. Rossi, and T. Kuhn, "Generalized Monte Carlo approach for the study of the coherent ultrafast carrier dynamics in photoexcited semiconductors," *Physical Review B*, vol. 53, no. 12, pp. 12855–12868, 1996.
57. M. Nedjalkov, I. Dimov, F. Rossi, and C. Jacoboni, "Convergency of the Monte Carlo Algorithm for the Wigner Quantum Transport Equation," *Journal of Mathematical and Computer Modelling*, vol. 23, no. 8/9, pp. 159–166, 1996.
58. K. L. Jensen and F. A. Buot, "The Methodology of Simulating Particle Trajectories Trough Tunneling Structures Using a Wigner Distribution Approach," *IEEE Trans.Electron Devices*, vol. 38, no. 10, pp. 2337–2347, 1991.
59. H. Tsuchiya and T. Miyoshi, "Simulation of Dynamic Particle Trajectories through Resonant-Tunneling Structures based upon Wigner Distribution Function," *Proc. 6th Int. Workshop on Computational Electronics IWCE6, Osaka*, pp. 156–159, 1998.
60. M. Pascoli, P. Bordone, R. Brunetti, and C. Jacoboni, "Wigner Paths for Electrons Interacting with Phonons," *Physical Review B*, vol. B 58, pp. 3503–3506, 1998.
61. V. Sverdlov, A. Gehring, H. Kosina, and S. Selberherr, "Quantum transport in ultra-scaled double-gate MOSFETs: A Wigner function-based Monte Carlo approach," *Solid-State Electronics*, vol. 49, pp. 1510–1515, 2005.
62. D. Querlioz, J. Saint-Martin, V. N. Do, A. Bournel, and P. Dollfus, "A Study of Quantum Transport in End-of-Roadmap DG-MOSFETs Using a Fully Self-Consistent Wigner Monte Carlo Approach," *IEEE Trans. Nanotechnology*, vol. 5, pp. 737–744, 2006.
63. D. Querlioz, J. Saint-Martin, V. N. Do, A. Bournel, and P. Dollfus, "Fully quantum self-consistent study of ultimate DG-MOSFETs including realistic scattering using a Wigner Monte-Carlo approach," *Int. Electron Device Meeting Tech. Dig. (IEDM)*, pp. 941–944, 2006.

64. L. Shifren and D. K. Ferry, "A Wigner function based ensemble Monte Carlo approach for accurate incorporation of quantum effects in device simulation," *Journal of Computational Electronics*, vol. 1, pp. 55–58, 2002.
65. D. Querlioz, P. Dollfus, V. N. Do, A. Bournel, and V. L. Nguyen, "An improved Wigner Monte-Carlo technique for the self-consistent simulation of RTDs," *Journal of Computational Electronics*, vol. 5, pp. 443–446, 2006.
66. D. Querlioz and P. Dollfus, *The Wigner Monte Carlo Method for Nanoelectronic Devices - A particle description of quantum transport and decoherence*. ISTE-Wiley, 2010.
67. M. Nedjalkov, H. Kosina, S. Selberherr, C. Ringhofer, and D. K. Ferry, "Unified particle approach to Wigner-Boltzmann transport in small semiconductor devices," *Physical Review B*, vol. 70, p. 115319, 2004.
68. A. Bertoni, P. Bordone, G. Ferrari, N. Giacobbi, and C. Jacoboni, "Proximity effect of the contacts on electron transport in mesoscopic devices," *Journal of Computational Electronics*, vol. 2, pp. 137–140, 2003.
69. C. Jacoboni and L. Reggiani, "The Monte Carlo Method for the Solution of Charge Transport in Semiconductors with Applications to Covalent Materials," *Rev.Mod.Phys.*, vol. 55, no. 3, pp. 645–705, 1983.
70. H. Kosina, "Wigner function approach to nano device simulation," *International Journal of Computational Science and Engineering*, vol. 2, no. 3/4, pp. 100 – 118, 2006.
71. S. Ermakow, *Die Monte-Carlo-Methode und verwandte Fragen*. München, Wien: R. Oldenburg Verlag, 1975.
72. J. Hammersley and D. Handscomb, *Monte Carlo Methods*. New York: John Wiley, 1964.
73. H. Kosina and M. Nedjalkov, *Handbook of Theoretical and Computational Nanotechnology*, vol. 10, ch. Wigner Function Based Device Modeling, pp. 731–763. Los Angeles: American Scientific Publishers, 2006.
74. M. Nedjalkov, R. Kosik, H. Kosina, and S. Selberherr, "Wigner Transport Through Tunneling Structures - Scattering Interpretation of the Potential Operator," in *Proc. Simulation of Semiconductor Processes and Devices*, (Kobe, Japan), pp. 187–190, Publication Office Business Center for Academic Societies Japan, 2002.
75. H. Kosina, M. Nedjalkov, and S. Selberherr, "A Monte Carlo Method Seamlessly Linking Classical and Quantum Transport Calculations," *Journal of Compuational Electronics*, vol. 2, no. 2-4, pp. 147–151, 2003.
76. H. Kosina, V. Sverdlov, and T. Grasser, "Wigner Monte Carlo Simulation: Particle Annihilation and Device Applications," in *Proc. Simulation of Semiconductor Processes and Devices*, (Monterey, CA, USA), pp. 357–360, Institute of Electrical and Electronics Engineers, Inc., Sept. 2006.
77. R. Tsu and L. Esaki, "Tunneling in a finite superlattice," *Appl. Phys. Lett.*, vol. 22, pp. 562–564, 1973.
78. L. L. Chang, L. Esaki, and R. Tsu, "Resonant tunneling in semiconductor double barriers," *Appl. Phys. Lett.*, vol. 24, pp. 593–595, 1974.
79. T. J. Shewchuk, P. C. Chapin, P. D. Coleman, W. Kopp, R. Fischer, and H. Morkoç, "Resonant Tunneling Oscillations in a GaAs-AlxGa1-xAs Heterostructure at Room-Temperature," *Appl. Phys. Lett.*, vol. 46, pp. 508–510, 1985.
80. H. Mizuta and T. Tanoue, *The physics and applications of resonant tunnelling diodes*. Cambridge University Press, 1995.
81. G. Iannaccone, G. Lombardi, M. Macucci, and B. Pellegrini, "Enhanced Shot Noise in Resonant Tunneling: Theory and Experiment," *Phys. Rev. Lett.*, vol. 80, pp. 1054–1057, 1998.
82. Y. M. Blanter and M. Büttiker, "Transition from sub-Poissonian to super-Poissonian shot noise in resonant quantum wells," *Phys. Rev. B*, vol. 59, pp. 10217–10226, 1999.
83. W. Song, E. E. Mendez, V. Kuznetsov, and B. Nielsen, "Shot noise in negative-differential-conductance devices," *Appl. Phys. Lett.*, vol. 82, pp. 1568–1570, 2003.
84. S. S. Safonov, A. K. Savchenko, D. A. Bagrets, O. N. Jouravlev, Y. V. Nazarov, E. H. Linfield, and D. A. Ritchie., "Transition from sub-Poissonian to super-Poissonian shot noise in resonant quantum wells," *Phys. Rev. Lett.*, vol. 91, p. 136801, 2003.

85. X. Oriols, A. Trois, and G. Blouin, "Self-consistent simulation of quantum shot noise in nanoscale electron devices," *Appl. Phys. Lett.*, vol. 85, pp. 3596–3598, 2004.
86. V. Y. Aleshkin, L. Reggiani, N. V. Alkeev, V. E. Lyubchenko, C. N. Ironside, J. M. L. Figueiredo, and C. R. Stanley, "Coherent approach to transport and noise in double-barrier resonant diodes," *Phys. Rev. B*, vol. 70, p. 115321, 2004.
87. V. N. Do, P. Dollfus, and V. L. Nguyen, "Transport and noise in resonant tunneling diode using self-consistent Green's function calculation," *J. Appl. Phys.*, vol. 100, p. 093705, 2006.
88. T. J. Park, Y. K. Lee, S. K. Kwon, J. H. Kwon, and J. Jang, "Resonant tunneling diode made of organic semiconductor superlattice," *Appl. Phys. Lett.*, vol. 89, p. 151114, 2006.
89. T. Kanazawa, R. Fujii, T. Wada, Y. Suzuki, M. Watanabe, and M. Asada, "Room temperature negative differential resistance of CdF2/CaF2 double-barrier resonant tunneling diode structures grown on Si(100) substrates," *Appl. Phys. Lett.*, vol. 90, p. 092101, 2007.
90. M. V. Petrychuk, A. E. Belyaev, A. M.Kurakin, S. V. Danylyuk, N. Klein, and S. A. Vitusevich, "Mechanisms of current formation in resonant tunneling AlN/GaN heterostructures," *Appl. Phys. Lett.*, vol. 91, p. 222112, 2007.
91. J.-P. Colinge, "Multiple-gate SOI MOSFETs," *Solid-State Electronics*, vol. 48, pp. 897–905, 2004.
92. J. Saint-Martin, A. Bournel, and P. Dollfus, "Comparison of multiple-gate MOSFET architectures using Monte Carlo simulation," *Solid-State Electronics*, vol. 50, pp. 94–101, 2006.
93. http://www.itrs.net/reports.html.
94. D. J. Frank, R. H. Dennard, E. Nowak, P. M. Solomon, Y. Taur, and H. S. P. Wong, "Device scaling limits of Si MOSFETs and their application dependencies," *Proc. IEEE*, vol. 89, pp. 259–288, 2001.
95. P. Dollfus, A. Bournel, S. Galdin, S. Barraud, and P. Hesto, "Effect of discrete impurities on electron transport in ultrashort MOSFET using 3-D MC simulation," *IEEE Trans. Electron Devices*, vol. 51, pp. 749–756, 2004.
96. T. Skotnicki, "Materials and device structures for sub-32 nm CMOS nodes," *Microelectronic Engineering*, vol. 84, pp. 1845–1852, 2007.
97. D. Reid, C. Millar, G. Roy, S. Roy, and A. Asenov, "Analysis of threshold voltage distribution due to random dopants: a 100 000-sample 3-D simulation study," *IEEE Trans. Electron Devices*, vol. 56, pp. 2255–2263, 2009.
98. J. Widiez, J. Lolivier, M. Vinet, T. Poiroux, B. Previtali, F. Daugé, M. Mouis, and S. Deleonibus, "Experimental evaluation of gate architecture influence on DG SOI MOSFETs performance," *IEEE Trans. Electron Devices*, vol. 52, pp. 1772–1779, 2005.
99. M. Vinet, T. Poiroux, J. Widiez, J. Lolivier, B. Previtali, C. Vizioz, B. Guillaumot, Y. L. Tiec, P. Besson, B. Biasse, F. Allain, M. Casse, D. Lafond, J.-M. Hartmann, Y. Morand, J. Chiaroni, and S. Deleonibus, "Bonded planar double-metal-gate NMOS transistors down to 10 nm," *IEEE Electron Device Lett.*, vol. 26, pp. 317–319, 2005.
100. J. Widiez, T. Poiroux, M. Vinet, M. Mouis, and S. Deleonibus, "Experimental comparison between Sub-0.1-μm ultrathin SOI single- and double-gate MOSFETs: Performance and Mobility," *IEEE Trans. Nanotechnol.*, vol. 5, pp. 643–648, 2006.
101. V. Barral, T. Poiroux, M. Vinet, J. Widiez, B. Previtali, P. Grosgeorges, G. L. Carval, S. Barraud, J.-L. Autran, D. Munteanu, and S. Deleonibus, "Experimental determination of the channel backscattering coefficient on 10-70 nm-metal-gate Double-Gate transistors," *Solid-State Electronics*, vol. 51, pp. 537–542, 2007.
102. J. Saint-Martin, A. Bournel, V. Aubry-Fortuna, F. Monsef, C. Chassat, and P. Dollfus, "Monte Carlo simulation of double gate MOSFET including multi sub-band description," *J. Computational Electronics*, vol. 5, pp. 439–442, 2006.
103. A. Bournel, V. Aubry-Fortuna, J. Saint-Martin, and P. Dollfus, "Device performance and optimization of decananometer long double gate MOSFET by Monte Carlo simulation," *Solid-State Electronics*, vol. 51, pp. 543–550, 2007.

104. M. Vinet, T. Poiroux, C. Licitra, J. Widiez, J. Bhandari, B. Previtali, C. Vizioz, D. Lafond, C. Arvet, P. Besson, L. Baud, Y. Morand, M. Rivoire, F. Nemouchi, V. Carron, and S. Deleonibus, "Self-aligned planar double-gate MOSFETs by bonding for 22-nm node, with metal gates, high-κ dielectrics, and metallic source/drain," *IEEE Electron Device Lett.*, vol. 30, pp. 748–750, 2009.
105. E. Joos, *Decoherence and the Appearance of a Classical World in Quantum Theory*. Springer-Verlag, 2003.
106. D. Querlioz, "Phnomnes quantiques et dcohrence dans les nano-dispositifs semiconducteurs : tude par une approche Wigner Monte Carlo," *PhD Dissertation, Univ. Paris-Sud, Orsay*, 2008.
107. M. V. Fischetti and S. E. Laux, "Monte Carlo study of electron transport in silicon inversion layers," *Phys. Rev. B*, vol. 48, pp. 2244–2274, 1993.
108. J. Saint-Martin, A. Bournel, F. Monsef, C. Chassat, and P. Dollfus, "Multi sub-band Monte Carlo simulation of an ultra-thin double gate MOSFET with 2D electron gas," *Semicond. Sci. Techn.*, vol. 21, pp. L29–L31, 2006.
109. L. Lucci, P. Palestri, D. Esseni, L. Bergagnini, and L. Selmi, "Multisubband Monte Carlo Study of Transport, Quantization, and Electron-Gas Degeneration in Ultrathin SOI n-MOSFETs," *IEEE Trans. Electron Devices*, vol. 54, pp. 1156–1164, 2007.
110. D. Querlioz, J. Saint-Martin, K. Huet, A. Bournel, V. Aubry-Fortuna, C. Chassat, S. Galdin-Retailleau, and P. Dollfus, "On the Ability of the Particle Monte Carlo Technique to Include Quantum Effects in Nano-MOSFET Simulation," *IEEE Trans. Electron Devices*, vol. 54, pp. 2232–2242, 2007.
111. F. Monsef, P. Dollfus, S. Galdin-Retailleau, H. J. Herzog, and T. Hackbarth, "Electron transport in Si/SiGe modulation-doped heterostructures using Monte Carlo simulation," *J. Appl. Phys.*, vol. 95, pp. 3587–3593, 2004.
112. S. M. Goodnick, D. K. Ferry, C. W. Wilmsen, Z. Liliental, D. Fathy, and O. L. Krivanek, "Surface roughness at the Si(100)-SiO2 interface," *Phys. Rev. B*, vol. 32, pp. 8171–8186, 1985.
113. H. Sakaki, T. Noda, K. Hirakawa, M. Tanaka, and T. Matsusue, "Interface roughness scattering in GaAs/AlAs quantum wells," *Appl. Phys. Lett.*, vol. 51, pp. 1934–1936, 1987.
114. D. Esseni, A. Abramo, L. Selmi, and E. Sangiorgi, "Physically based modeling of low field electron mobility in ultrathin single- and double-gate SOI n-MOSFETs," *IEEE Trans. Electron Devices*, vol. 50, pp. 2445–2455, 2003.
115. V. N. Do, "Modelling and simulation of quantum electronic transport in semiconductor nanometer devices," *PhD Dissertation, Univ. Paris-Sud, Orsay*, 2007.
116. J. Saint-Martin, A. Bournel, and P. Dollfus, "On the ballistic transport in nanometer-scaled DG MOSFETs," *IEEE Trans. Electron Devices*, vol. 51, pp. 1148–1155, 2004.